A METHOD FOR PROBABILISTIC SEISMIC HAZARD ANALYSIS OF EARTHQUAKE MAGNITUDE TO BE USED IN A LIQUEFACTION POTENTIAL ASSESSMENT

A THESIS SUBMITTED TO
THE GRADUATE SCHOOL OF NATURAL AND APPLIED SCIENCES
OF
MIDDLE EAST TECHNICAL UNIVERSITY

BY

BATUHAN AYDOĞAN

IN PARTIAL FULFILLMENT OF THE REQUIREMENTS
FOR
THE DEGREE OF MASTER OF SCIENCE
IN
EARTHQUAKE STUDIES

JANUARY 2025

Approval of the thesis:

A METHOD FOR PROBABILISTIC SEISMIC HAZARD ANALYSIS OF EARTHQUAKE MAGNITUDE TO BE USED IN A LIQUEFACTION POTENTIAL ASSESSMENT

submitted by **BATUHAN AYDOĞAN** in partial fulfillment of the requirements for the degree of **Master of Science** i**n Earthquake Studies, Middle East Technical University** by,

Prof. Dr. Naci Emre Altun
Dean, **Graduate School of Natural and Applied Sciences** _____

Prof. Dr. Ayşegül Askan GÜNDOĞAN
Head of the Department, **Earthquake Studies** _____

Prof. Dr. Bahadır Sadık BAKIR
Supervisor, **Civil Engineering, METU** _____

Assoc. Prof. Dr. Mustafa Tolga YILMAZ
Co-Supervisor, **Engineering Sciences, METU** _____

Examining Committee Members:

Prof. Dr. Ayşegül Askan GÜNDOĞAN
Civil Engineering, METU _____

Prof. Dr. Bahadır Sadık BAKIR
Civil Engineering, METU _____

Assoc. Prof. Dr. Mustafa Tolga YILMAZ
Engineering Sciences, METU _____

Prof. Dr. Murat Altuğ ERBERİK
Civil Engineering, METU _____

Assoc. Prof. Dr. Özkan KALE
Civil Engineering, TED University _____

Date: 10.01.2025

I hereby declare that all information in this document has been obtained and presented in accordance with academic rules and ethical conduct. I also declare that, as required by these rules and conduct, I have fully cited and referenced all material and results that are not original to this work.

Name Last name : Batuhan Aydoğan

Signature :

ABSTRACT

A METHOD FOR PROBABILISTIC SEISMIC HAZARD ANALYSIS OF EARTHQUAKE MAGNITUDE TO BE USED IN A LIQUEFACTION POTENTIAL ASSESSMENT

Aydoğan, Batuhan
Master of Science, Earthquake Studies
Supervisor : Prof. Dr. Bahadır Sadık Bakır
Co-Supervisor: Assoc. Prof. Dr. Mustafa Tolga Yılmaz

January 2025, 95 pages

Cyclic stresses during earthquakes cause shear strain accumulation and excess pore water pressure, leading to soil liquefaction in extreme cases. In 1975, Seed and colleagues suggested that seismic demand on liquefiable soils could be modeled by a series of uniform shear-stress cycles normalized by the effective stress on the shearing plane. Later, the seismic demand was related to earthquake magnitude and peak ground acceleration. In this study, a method to estimate the magnitude to be considered in liquefaction potential assessment is suggested. The impact of earthquake magnitudes on seismic demand for liquefaction is represented by a relationship between the number of uniform shearing cycles and earthquake magnitudes. This relationship is developed by using the magnitude scaling factor suggested by Youd et al. in 2001, later implemented in 2018 Seismic Code of Türkiye as a benchmark. A logarithmic model between liquefaction resistance and number of cycles is applied on 234 acceleration time histories to regress the relationship, such that the model coefficients yield a conditional mean consistent with this benchmark. Then, it was possible to develop an empirical prediction equation for cyclic stress ratio corrected for the event magnitude. This prediction

equation was based on the functional form of Akkar and Bommer (2010). The study concludes with a seismic hazard analysis, applying the developed GMPE for generic faults to calculate the seismic stress ratio to be exceeded with a specific probability within a given time frame, so that the final effect of event magnitude can be calculated.

Keywords: Liquefaction, magnitude scaling factor, equivalent number of cycles, ground motion prediction equation, seismic hazard analysis

ÖZ

SIVILAŞMA POTANSİYELİ ANALİZİNDE KULLANILACAK DEPREM BÜYÜKLÜĞÜ İÇİN BİR SİSMİK TEHLİKE ANALİZİ YÖNTEMİ

Aydoğan, Batuhan
Yüksek Lisans, Deprem Çalışmaları
Tez Yöneticisi: Prof. Dr. Bahadır Sadık Bakır
Ortak Tez Yöneticisi: Prof. Dr. Mustafa Tolga Yılmaz

Ocak 2025, 95 sayfa

Depremler sırasında meydana gelen çevrimsel gerilmeler, kesme deformasyonu birikimine ve aşırı boşluk suyu basıncına yol açarak aşırı durumlarda zemin sıvılaşmasına neden olur. 1975 yılında Seed ve çalışma arkadaşları, sıvılaşabilir zeminler üzerindeki sismik talebin, kayma düzlemindeki efektif gerilme ile normalize edilmiş bir dizi uniform kayma gerilmesi çevrimi ile modellenebileceğini öne sürmüştür. Daha sonra, bu sismik talep deprem büyüklüğü ve maksimum yer ivmesi ile ilişkilendirilmiştir. Bu çalışmada, sıvılaşma potansiyeli değerlendirmesinde dikkate alınması gereken deprem büyüklüğünün tahminine yönelik bir yöntem önerilmektedir. Deprem büyüklüklerinin sıvılaşma için sismik talep üzerindeki etkisi, uniform kayma çevrimlerinin sayısı ile deprem büyüklükleri arasındaki bir ilişki ile temsil edilmektedir. Bu ilişki, Youd ve arkadaşları tarafından 2001 yılında önerilen ve daha sonra 2018 Türkiye Deprem Yönetmeliği'nde referans alınan deprem büyüklüğü düzeltme katsayısı kullanılarak geliştirilmiştir.

Sıvılaşma direnci ile çevrim sayısı arasındaki logaritmik bir model, 234 ivme zaman geçmişine uygulanarak bu ilişkinin regresyonu yapılmış ve model katsayılarının belirtilen referansla tutarlı bir koşullu ortalama sağladığı görülmüştür. Böylece,

deprem büyüklüğü için düzeltilmiş çevrimsel gerilme oranı tahmini için ampirik bir denklem geliştirilmiştir. Bu tahmin denklemi, Akkar ve Bommer (2010) tarafından önerilen fonksiyonel form temel alınarak oluşturulmuştur. Çalışma, genel faylar için geliştirilen yer hareketi tahmin denkleminin kullanıldığı bir sismik tehlike analizi ile sonuçlandırılmıştır. Bu analiz, belirli bir zaman diliminde belirli bir olasılıkla aşılacak sismik gerilme oranını hesaplamayı sağlamış ve deprem büyüklüğünün nihai etkisinin belirlenmesine olanak tanımıştır.

Anahtar Kelimeler: Deprem çalışmaları, deprem büyüklüğü düzeltme katsayısı, eşdeğer döngüsel yük sayısı, yer hareketi tahmin denklemi, sismik tehlike analizi

ACKNOWLEDGMENTS

I would like to express my gratitude to my supervisors Prof. Dr. Bahadır Sadık BAKIR and Assoc. Prof. Dr. Mustafa Tolga YILMAZ for their guidance and support. This work could not have been completed without their support.

I would also like to thank my family, Berna Aydoğan and Emin Aydoğan for their unconditional support and guidance in any aspect of my life.

TABLE OF CONTENTS

LIST OF TABLES

TABLES

LIST OF FIGURES

FIGURES

LIST OF SYMBOLS

SYMBOLS

AB10	GMPE model of Akkar and Bommer (2010)
a_{max}	Maximum acceleration in shearing direction
a_{peak}	Maximum acceleration between successive zero crossings.
b	Material coefficient for liquefaction resistance
CSR	Cyclic stress ratio
$CSR_{M7.5}$	Cyclic stress ratio corrected for M_w=7.5
CSR_N	CSR normalized by ignoring depth
CSR_M	CSR during earthquake magnitude M
g	Gravitational acceleration
GMPE	Ground motion prediction equation
MSF	Magnitude scaling factor
M_0	Threshold (or, lower limit) for magnitude
MS_N	GMPE for CSR_N
$MS_{M7.5}$	GMPE for $CSR_{M7.5}$
M_u	Maximum (or, upper limit) for expected magnitude
M_w	Moment magnitude
N_{160}	SPT blow-count corrected for overburden, energy, equipment and procedural factors
N_{eq}	Equivalent number of cycles
$N_{M7.5}$	Equivalent number of cycles at M_w=7.5
PGA	Peak (maximum) horizontal ground acceleration
PSHA	Probabilistic Seismic Hazard Analysis
R_{jb}	Joyner-Boore distance
V_{s30}	Shear wave velocity at top 30 m
λ_M	Magnitude recurrence rate
σ_{res}	Standard deviation of residuals

σ_v	Vertical total stress
σ_v'	Vertical effective stress

CHAPTER 1

INTRODUCTION

1.1 Research Statement

During seismic motion, cyclic-induced stresses lead to the accumulation of shear strains and the excess pore water pressure, which in turn results in a reduction of soil stiffness. This process can culminate in soil liquefaction, a phenomenon that has garnered significant attention due to its severe consequences.

The term liquefaction is defined as the loss of strength and/or rigidity in a soil that is partially or fully saturated with water due to the application of shear stress. As a result of the loss of strength and/or rigidity, the soil begins to behave as if it were a liquid. In general, liquefaction occurs in saturated cohesionless loose soils (predominantly sand) during seismic events. It has also been observed that non-plastic silts can be susceptible to liquefaction. The seismic demand on soils is expressed by the seismic stress ratio, initially referred to as cyclic stress ratio (Youd et. al. 2001).

The seismic opportunity for liquefaction is related to the cyclic stress ratio (CSR), defined as the amplitude of shear stresses normalized by effective normal stress. The seismic opportunity is also related to the earthquake magnitude, since the number of shearing reversals are dependent on the duration. To facilitate this adjustment, Seed and Idriss (1982) introduced correction factors, namely "magnitude scaling factors" (MSFs). However, the magnitude to be taken into consideration in assessment of liquefaction potential is not well defined in seismic codes, whereas this is usually not considered in the probabilistic seismic hazard analyses.

For instance, the Seismic Code of Türkiye (2018) provides a function for calculation of the magnitude scaling factors. This function is primarily proposed by Youd et al.

(1999). On the other hand, the seismic hazard on a specific site is related to the possibilities of a range of event magnitudes. Therefore, the selection of an average magnitude to estimate the magnitude scaling factor is not straightforward. Consequently, either the magnitude scaling factors shall be implemented in seismic hazard analysis, or a method to calculate the weighted average of magnitude shall be used. These two possibilities are related to each other, and they need empirical relationships yet to be developed.

1.2 Literature Survey

Basically, earthquake magnitudes are related to the number of equivalent uniform stress cycles to be considered in assessment of liquefaction assessments. The effect of magnitude can either be empirically estimated by data from case studies after earthquakes, or by relating the magnitudes to the number of uniform cyclic stress amplitudes that can be applied in laboratory tests on specimens. In the following, the empirical relationships for estimation of magnitude effect on liquefaction potential, and the methods that relate the cyclic shear stress ratio to earthquake magnitudes are presented.

1.2.1 Equivalent Number of Stress Cycles

The concept of the "equivalent number of cycles" is fundamental in the assessment of cyclic liquefaction, particularly in laboratory assessments. A uniform series of load cycles is described by an amplitude, frequency of load cycles and a number of cycles (Liu et al. 2001). The underlying idea is that the irregular motions generated by an earthquake can be modeled as an equivalent number of uniform stress cycles to simplify laboratory experiments. This number of cycles will be denoted as N_{eq}. The concept of equivalent number of cycles is critical, as it provides a practical metric for comparing the duration of seismic motions, and consequently it underpins MSFs used in field-based liquefaction evaluations.

Seed et al. (1975) principally drew a parallel between metal fatigue and soil liquefaction, adapting the Palmgren–Miner theory to compute the N_{eq} for earthquake-induced motions. In liquefaction assessments, these relationships are established experimentally and are commonly referred to as CSR-N_{liq} curves. Here, N_{liq} represents the number of loading cycles necessary to trigger the onset of liquefaction. A CSR-N_{liq} curve's shape and position are highly influenced by factors such as soil fabric, density, effective confining stress, and other soil properties. To generalize the relationship for sands, Seed et al. (1975) introduced a normalized version of the CSR-N_{liq} curve, ensuring it represented the typical behavior of sands under cyclic loading. The procedure proposed by Seed et al. (1975) for calculating N_{eq} involves computing a weighted average of the peaks in an acceleration time history, where the weighting function is defined by the normalized CSR-N_{liq} curve. The normalized curve proposed by Seed et. al. (1975), and later adapted by Lesley et. al. (2017) is illustrated in Figure 1. Any peak of irregular shearing history is normalized to the 65% of maximum value by adding its equivalent number of cycles to the N_{eq}.

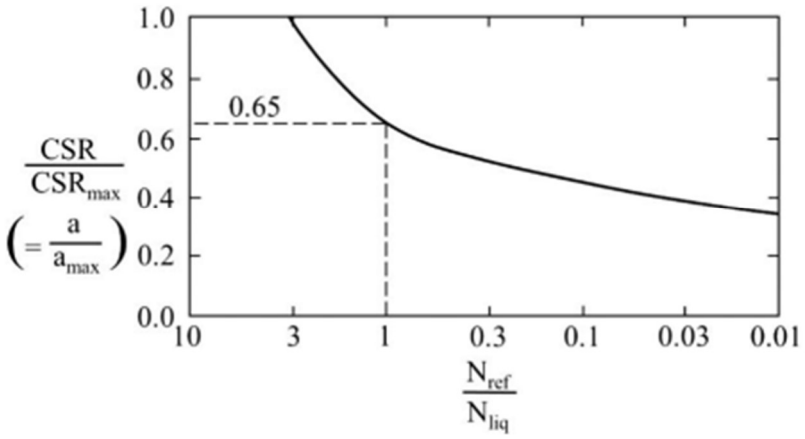

Figure 1. Normalized CSR-N_{liq} curve (Lasley et al., 2017).

It is important to highlight that this method is based on the assumption that the ratio of ground surface acceleration to the peak ground acceleration (a/a_{max}) is equivalent to the ratio of the cyclic stress ratio to the maximum cyclic stress ratio at any depth

in soil (CSR/CSR_{max}). The amplitude of each cycle is defined as the maximum value between successive zero crossings in the time history. Since earthquake acceleration peaks are seldom symmetrical about the zero axis, a peak above the axis represents only half a cycle of loading. To address this, Seed et al (1975) calculated the number of equivalent cycles separately for both the positive and negative peaks in time history. The average of these values was considered as the N_{eq} for the record. The average relationship is approximately

$$\ln(N_{eq}) = -1.405 + 0.547M_w \quad (1)$$

Liu et al. (2001) adapted the model of Seed et al. (1975) to develop an empirical relationship based on past earthquake events, such that;

$$\ln(N_{eq}) = \left(\frac{\left\{ \frac{\exp[1.53 + 1.51(M_w - 5.8)]}{10^{1.5M_w + 16.05}} \right\}^{-\frac{1}{3}}}{4.9.10^6 ß} + 0.75S + 0.095R \right) + \varepsilon \quad (2)$$

where β is shear wave velocity at the earthquake source (suggested as 3.2 km/s), S equals to 0 for rock sites or 1 otherwise, R is defined as the closest distance to the rupture plane from source in kilometers, and ε is normally distributed error term with a mean of zero and a standard deviation of 0.56.

Biondi et al. (2004) adapted the model of Seed et al. (1975) to develop a N_{eq} relationship from past earthquake events. They treated each ground motion component individually and used the weighting factor curve identical to Seed et al. (1975). Biondi et al. (2004) suggested several prediction models, whereas their simplest equation is

$$\ln(N_{eq}) = -4.995 - 0.4536 \ln(a_{\max}) + 3.204 \ln(M_w) + \varepsilon \quad (3)$$

where ε is the error term with zero mean and a standard deviation of 0.68.

Green and Terri (2005) established the relationship for N_{eq} through Palmgren-Miner theorem based on energy concepts. The suggested relationship for N_{eq} is

$$N_{eq} = \frac{\sum w G_\gamma}{2\pi D_\gamma \tau_{ref}^2} \tag{4}$$

for

$$\tau_{ref} = 0.65\sqrt{\max(|\tau_1|)\max(|\tau_2|)} \tag{5}$$

where τ_{ref} is reference amplitude, $max(|\tau_1|)$ and $max(|\tau_2|)$ are the maximum absolute values of the two components of shear stress induced in the soil profile at a given depth, w is the absorbed work (or dissipated energy), G_γ and D_γ are degraded shear modulus and damping ratio at shear strain (γ) corresponding to τ_{ref}.

Lee (2009) adapted the model of Green and Terri (2005), to the equivalent linear site response analyses of six soil profiles. The proposed N_{eq} relationship is

$$\ln(N_{eq}) = \exp(c_1 z) + c_2 R^{c_3} + c_4 M_w + c_5 + \varepsilon \tag{6}$$

where c_1 to c_5 are the model coefficients, z is depth below the ground surface, and ε is error term. Lee (2009) presented regression coefficients separately for each ground-motion database (i.e. WUS and CEUS) which are provided in Table 1.

Table 1. The regression coefficients for Lee's (2009) estimation equation for N_{eq}, adapted from Lasley et. al. (2017).

Motion database	c_1	c_2	c_3	c_4	c_5	σ_ε
WUS	−0.0101	1.664	0.131	0.122	−2.11	0.50
CEUS	−0.0190	1.857	0.136	0.050	−1.77	0.59

Lasley et al. (2017) used a number of models considered in literature to develop an empirical prediction relationship for MSF. However, they used a different database for ground motions and soil profiles. They implemented three different functional forms to account for multidirectional shaking. The functional forms are

$$ln(N_{eq}) = a_1 + a_2 \ln(a_{\max}) + a_3 M_w + \delta_{event} + \delta_{profile} + \delta_0 \tag{7}$$

$$\ln(N_{eq}) = b_1 + b_2 M_w + b_3 \ln(R) + \delta_{event} + \delta_{profile} + \delta_0 \quad (8)$$

where a_1 to a_3 and b_1 to b_3 are the regression coefficients, δ_{event} and $\delta_{profile}$ are the random effects terms that correspond to an average event residual and the average-profile residuals respectively, and δ_0 is also a residual term. In the third alternative, the equation proposed by Green and Terri (2005) is utilized. The amplitude of the equivalent cycle was consistently defined as 0.65 times the geometric mean of the maximum shear stresses encountered at a specific depth.

Hence, various correlations for N_{eq} to be considered in liquefaction assessments have been developed since Seed et. al. (1975) over the years. These correlations also justified the relationship between earthquake magnitude and N_{eq}. Therefore, for an empirical assessment of in-situ liquefaction potential without using more expensive cyclic testing opportunities in laboratory, several researchers suggested statistical analyses of past events to estimate the effect of event magnitude on liquefaction potential. These studies are summarized in the following section.

1.2.2 Magnitude Scaling Factors

Magnitude scaling factors (MSF) play a crucial role in liquefaction triggering analyses by accounting for the effects of irregular cyclic loading from earthquakes of varying magnitudes on liquefaction potential. These factors rely on both the characteristics of the applied seismic loading and the soil's response, reflecting the principles of fatigue behavior. The primary objective of MSF relationships is to capture the essential influencing factors while maintaining a level of simplicity suitable for practical use. Seed and Idriss (1982) investigated the cyclic shear strength of soils under varying confinement levels through laboratory testing and introduced magnitude scaling factors based on the laboratory tests. These factors were defined by dividing the cyclic stress ratio corresponding to the number of loading cycles for the earthquake magnitude, *Mw* 7.5, which corresponds to 15 loading cycles. Their analysis yielded a set of MSFs derived from the average

number of loading cycles associated with different earthquake magnitudes and the results of laboratory tests. These values are presented in Table 2.

$$\mathrm{MSF} = \frac{\mathrm{CSR_M}}{\mathrm{CSR_{M7.5}}} \tag{9}$$

Table 2. MSFs proposed by Seed and Idriss, 1982.

Earthquake Magnitude, M	No. of representative cycles at $0.65\,\tau_{max}$	$\left(\frac{\tau_{av}}{\sigma_o'}\right)_{\text{M}} = \text{M} \Big/ \left(\frac{\tau_{av}}{\sigma_o'}\right)_{\text{M}} = 7.5$
8½	26	0.89
7½	15	1.0
6¾	10	1.13
6	5–6	1.32
5¼	2–3	1.5

Idriss (1995) revisited the dataset originally used by Seed and Idriss (1982). In this reassessment, Idriss identified a significant outlier in the original analysis that had skewed the results, leading to a nonlinear trend and unrealistically low MSF values for M_w below 7.5. As a result of this reconsideration, Idriss proposed a revised set of MSFs, expressed through:

$$\mathrm{MSF} = \frac{10^{2.24}}{{M_w}^{2.56}} \tag{10}$$

Later, Idriss (1999) introduced a new set of MSFs as

$$\mathrm{MSF} = 6.9\exp\left(-\frac{M_w}{4}\right) - 0.058 \qquad MSF \leq 1.8 \tag{11}$$

This latest relationship of Idriss (1999) is constrained to a maximum value of 1.8 for small earthquake magnitudes, approximately corresponding to the range $M_w \leq 5.25$.

Ambraseys (1988) derived empirical exponential equations that express the CSR as a function of corrected SPT blow count, $(N_1)_{60}$ and M_w. By keeping the $(N_1)_{60}$ value

constant within the equations and calculating the ratio of CSR for different earthquake magnitudes relative to the CSR for magnitude 7.5 earthquakes, the MSF relationship could be built.

Arango (1996) developed two sets of MSFs. The first set is derived from the most distant observed liquefaction effects relative to the seismic energy source, the estimated average peak accelerations at these distant sites, and the amount of seismic energy necessary to induce liquefaction. This set of MSFs are shown in Table 3. The second set was derived from energy principles and the relationship established by Seed and Idriss (1982) between the number of equivalent stress cycles and earthquake magnitude. The second set of MSF is shown in Table 4, whereas the second can be calculated by

$$\mathrm{MSF} = \left(\frac{15}{N_{eq}}\right)^{\frac{1}{2}} \tag{12}$$

Table 3 MSFs derived by Arango (1996) built on consideration of distant liquefaction sites

Earthquake magnitude (1)	Equivalent uniform number of cycles (2)	Magnitude scaling factor (3)
8.25	38.4	0.63
8	26.7	0.75
7.5	15.0	1.00
7	9.6	1.25
6	3.8	2.00
5.5	1.7	3.00

Table 4. MSFs Derived by Arango (1996) built on Seed et. al. (1975) suggestions.

Earthquake magnitude (1)	Equivalent uniform number of cycles (2)	Magnitude scaling factors (3)
8.5	26	0.76
7.5	15	1.0
6.75	10	1.22
6	5–6	1.65
5.25	2–3	2.45

In their study on liquefaction resistance in relation to shear wave velocity (V_s), Andrus and Stokoe (1997) established bounding curves for sites where surface liquefaction either occurred or did not occur during earthquakes with magnitudes of 6.0, 6.5, and 7.0. MSFs were then calculated by employing Eq. (1). These MSFs can be expressed as

$$\mathrm{MSF} = \left(\frac{M_w}{7.5}\right)^{-2.56} \tag{13}$$

Youd and Noble (1997a, 1997b) conducted a probabilistic (logistic) analysis to evaluate case history data. This analysis led to the formulation of the estimation equation

$$Logit(P_L) = -7.0351 + 2.1738M_w - 0.2678)(N_1)_{60CS} + 3.0265\ln(\mathrm{CSR}) \tag{14}$$

where P_L is the probability that liquefaction occurred, and $(N_1)_{60cs}$ is the corrected equivalent clean-sand blow count in an SPT test. Consequently, Youd and Noble (1997a) proposed three sets of MSFs, corresponding to liquefaction occurrence probabilities of less than 20%, 32%, and 50%.

Table 5. Youd and Noble (1997a) recommendations for MSF.

Magnitude, M_w	**MSF**		
	P_L<20%	**P_L<32%**	**P_L<50%**
5.5	2.86	3.42	4.44
6.0	1.93	2.35	2.92
6.5	1.34	1.66	1.99
7.0	1.00	1.20	1.39
7.5	-	-	1.00

Kayen et al. (2013) employed shear wave velocity as a parameter to evaluate soil's seismic resistance to liquefaction. They used Bayesian regression and structural

reliability methods to apply a probabilistic approach to the dataset, leading to the MSF relationship:

$$\mathrm{MSF} = 15M_w^{-1.342} \tag{15}$$

Boulanger and Idriss (2014) developed a model linking the relationship between MSF and *b*. They revised the MSF relationship from Boulanger and Idriss (2008) to incorporate the influence of soil particle characteristics on MSF variation. This approach enables the generation of MSF curves for varying *b* values.

$$\mathrm{MSF} = 1 + \left(0.65\left(\frac{N_{M7.5}}{(3/4)\mathrm{cycle}}\right)^{\mathrm{b}} - 1\right)\left(8.64\exp\left(-\frac{M_w}{4}\right) - 1.325\right) \tag{16}$$

where 3/4 of a cycle stands for the equivalent uniform cyclic loading at peak stress in earthquakes dominated by a single strong shaking cycle, where the loading ranges from 1/2 to 1 cycle.

Kishida and Tsai (2014) introduced a MSF relationship that accounts for the soil parameter *b*, which represents the slope of the relationship between CSR and the number of uniform loading cycles required to reach failure. Consequently, the significant influence of soil properties on MSF relationships is evident in Figure 2. Figure 2 indicates that for soil sites which exhibit higher *b* values yield a larger MSF across magnitudes, M_w between 5.0-7.5. However, for magnitudes beyond 7.5, the situation is reversed. Magnitude M_w 7.5 is taken as the reference value.

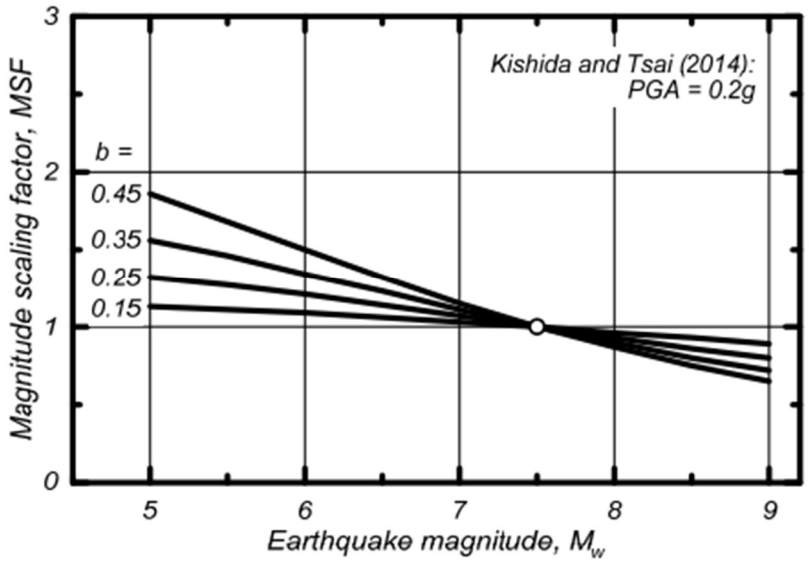

Figure 2. MSF relationships proposed by Kishida and Tsai (2014), adapted from Boulanger and Idriss (2014).

Boulanger and Idriss (2014), and Kishida and Tsai (2014) used 42 and 3500 ground motions respectively on category D (soil) sites to observe the effect of b on N_{eq} for M_w in the range 7.3 to 7.6 and for PGA in the range 0.11g to 0.51g. The analyses of Boulanger and Idriss (2014) shown in Figure 3 support that N_{eq} is stationary for b>0.25.

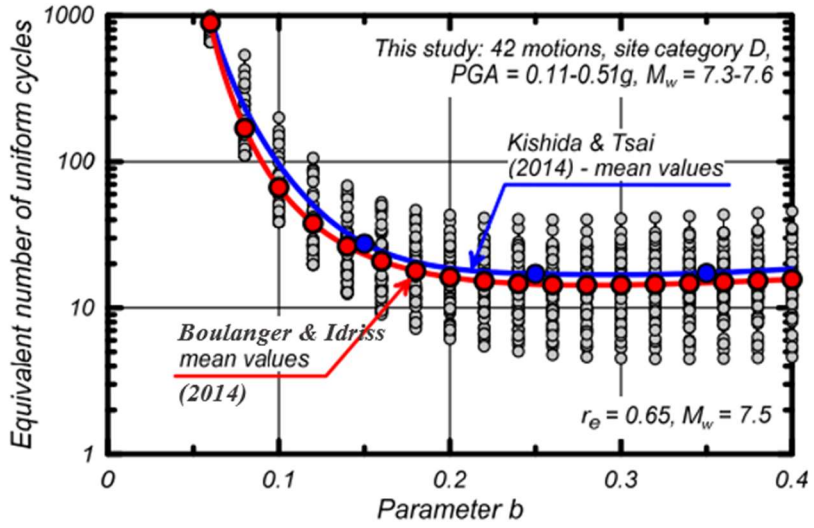

Figure 3. Variation in number of equivalent cycles with parameter *b*, adapted from Boulanger and Idriss (2014).

Cetin et al. (2018) developed liquefaction triggering correlations by using probabilistic regressions based on the maximum likelihood estimation (MLE) method. They proposed the following relationship for calculation of MSFs:

$$\text{MSF} = \left(\frac{M_w}{7.5}\right)^{-2.324} \quad \text{for } 5.5 < M_w < 8.4 \tag{17}$$

Finally, the MSF values defined by various researchers are presented in Figure 4 for magnitudes between 5.5-8.0. The relationship expressed by Seed and Idriss (1982) is overly conservative compared to other relationships. Youd et al. (2001) suggested MSF relationship of Idriss (1995) as the lower bound, and that of Andrus and Stokoe (1997) as the upper bound of MSF estimation. In general, these relationships can be attributed to parameter *b*, which is more specifically discussed in the following section.

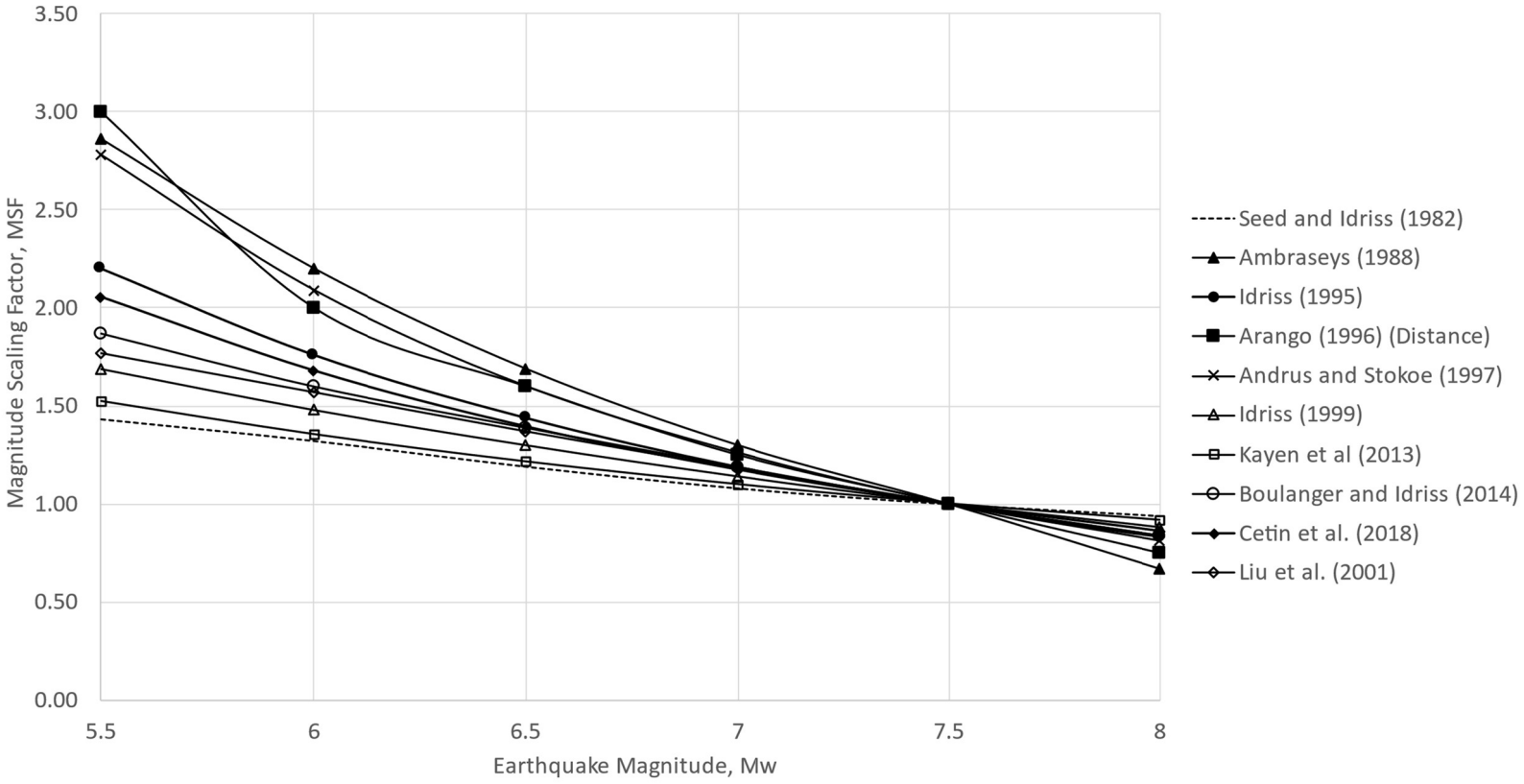

Figure 4 A comparison of MSFs suggested in the literature

1.2.3 Weighting of Irregular Loading Cycles

Material coefficient for liquefaction resistance, so called "*b*" value is basically described as

$$\log \mathrm{CSR} = \mathrm{a} + \mathrm{b}\log\left(N_{eq}\right) \tag{18}$$

This parameter determined usually by laboratory testing of specimens is substantial to convert an irregular time-history of ground motion to a uniform number of stress cycles to be considered in testing or analysis. Figure 5 shows an example for this relationship due to the cyclic tests on sands obtained by frozen sampling methods. Yoshimi et al. (1989) reported *b* as 0.34 for the densest site (curve D in Figure 5). For three sands of intermediate strength, *b* is reported as 0.41, 0.27, and 0.13 (curves C3, C1, and B). For the loosest soils, *b* is reported as 0.15 (curve A). Similarly, the sand from Duncan Dam (Pillai and Stewart 1994, Figure 5) yields the lowest *b* value of 0.08.

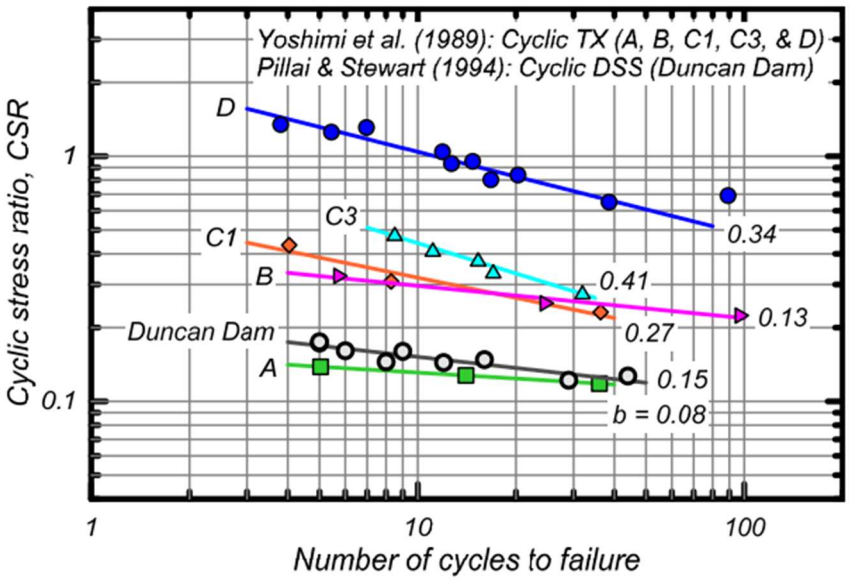

Figure 5. Cyclic tests on sands obtained by frozen sampling techniques (Boulanger and Idriss, 2014).

Liu et al. (2001) conducted a comprehensive review of the available data, considered the results of simple shear tests, and consequently recommended b as 0.37. Idriss and Boulanger (2004) conducted a similar analysis and proposed b as 0.34. Consequently, many researchers reached b values that are above the threshold where N_{eq} becomes insensitive to this parameter according to the study of Boulanger and Idriss (2014). Nevertheless, the representative range of b values consistent with MSF-M_w relationships shown in Figure 4 is yet to be estimated. This estimation is crucial for developing prediction methods for M_w to be used in the conditional assessment of liquefaction potential. The basic probabilistic method of seismic hazard analysis is presented in the following section.

1.2.4 Seismic Hazard Analysis

Liquefaction hazard mapping began in the early 1970s and has progressed over the decades. A significant milestone was the introduction of the "simplified procedure" by Seed and Idriss (1971). While this method was not specifically created for hazard mapping, it brought analytical rigor to the process. It also enabled a more quantitative evaluation of liquefaction-susceptibility zones.

As a preliminary understanding of the concepts “liquefaction opportunity” and “liquefaction susceptibility”, Youd and Perkins (1978) defined a geological criteria and enhanced mapping techniques. They introduced two component maps: one for liquefaction susceptibility, and the other for liquefaction opportunity. These maps were compared to create a "liquefaction potential" map. Youd et al. (1978) applied susceptibility and opportunity criteria to create maps for the San Fernando Valley. and extended across much of southern California.

Liquefaction opportunity measures the likelihood of ground shaking strong enough to cause liquefaction. Key factors include the distribution of earthquake source zones, expected seismic activity, wave attenuation with distance, and local soil amplification of motion. Regionally, it is assessed using three criteria: (1)

magnitude-maximum distance, (2) magnitude-liquefaction severity index, and (3) magnitude-peak acceleration (Youd, 1991). These metrics are easily integrated into probabilistic analyses. To create liquefaction opportunity maps from peak acceleration maps, both earthquake magnitude and acceleration must be accounted for (Youd, 1991). Opportunity maps are typically created using probabilistic methods, and they are expressed as probabilities of exceedance over a specified time period. Hence, this approach is related to the probabilistic seismic hazard analysis.

Seismic hazard analysis entails the calculations to develop a cumulative probability distribution function (CDF) for ground motion parameters at a specific location. The seismic hazard may be assessed either deterministically, where a specific earthquake event is assumed, or probabilistically, where uncertainties associated to the magnitude, location, and timing of an earthquake are factored explicitly. The probabilistic seismic hazard analysis (PSHA) offers a systematic framework through which the uncertainties can be identified, quantified, and integrated to yield a more comprehensive CDF for ground motion function. A PSHA for a given location involves calculating the probability that a certain earthquake characteristic, such as peak ground acceleration, will surpass a specified value (e.g., >0.1g) within a defined time frame (e.g., in the next 50 years).

The effective design of earthquake-resistant structures necessitates estimating the anticipated intensity of ground shaking, represented by ground motion parameters with physical or statistical relevance to the mechanisms of failure. The predictive relationships typically represent ground motion parameters as functions of earthquake magnitude, distance to seismic source, and various additional factors primarily including site conditions. Douglas (2011) summarized 289 GMPEs published between 1964 and 2010. Stewart (2013) created visual representations to illustrate the multi-dimensional space of predicted ground motions (including magnitude, source-to-site distance, structural period, etc.) to better understand GMPEs. These plots include pseudo-spectral acceleration (PSA) versus magnitude in Figure 6, and PSA versus distance in Figure 7.

Figure 6 demonstrates that the KEA06 and FEA10 models lack magnitude saturation. That means PSA acts linearly with moment magnitude. This characteristic makes them less suitable for selection, as it can result in unreasonably large or small ground motion predictions. Figure 7 reveals that certain models, such as BA08, CY08, MEA06, and ZEA06, exhibit steeper reduction for distances exceeding 70–100 km. This behavior is attributed to their inclusion of effective anelastic attenuation. Consequently, a possible prediction equation for CSR is expected to be sensitive to the functional form of equation. Some examples of these predictive equations, basically to be used in this study are presented in the following.

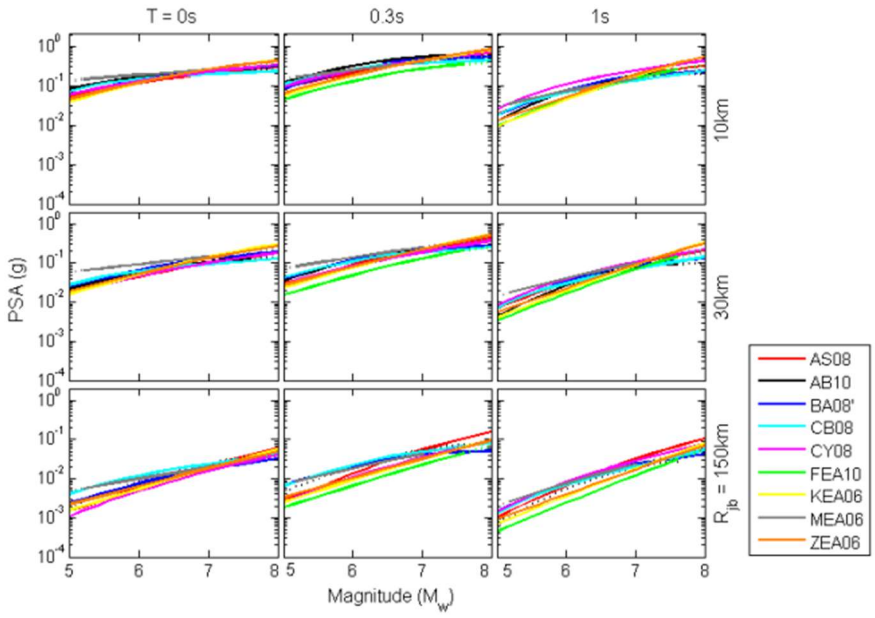

Figure 6. Magnitude scaling of predicted PSAs for pre-selected GMPEs for various structural periods and site to source distances for rock site conditions (AS08: Abraham and Silva, 2008, AB10: Akkar and Bommer, 2010, BA08': Boore and Atkinson, 2008, CB08: Campbell and Bozorgnia, 2008, CY08: Chiou and Youngs, 2008, FEA10: Faccioli et al., 2010, KEA06: Kanno et al., 2006, MEA06: McVerry et al., 2006, ZEA06: Zhao et al., 2006) (Stewart et. al., 2013).

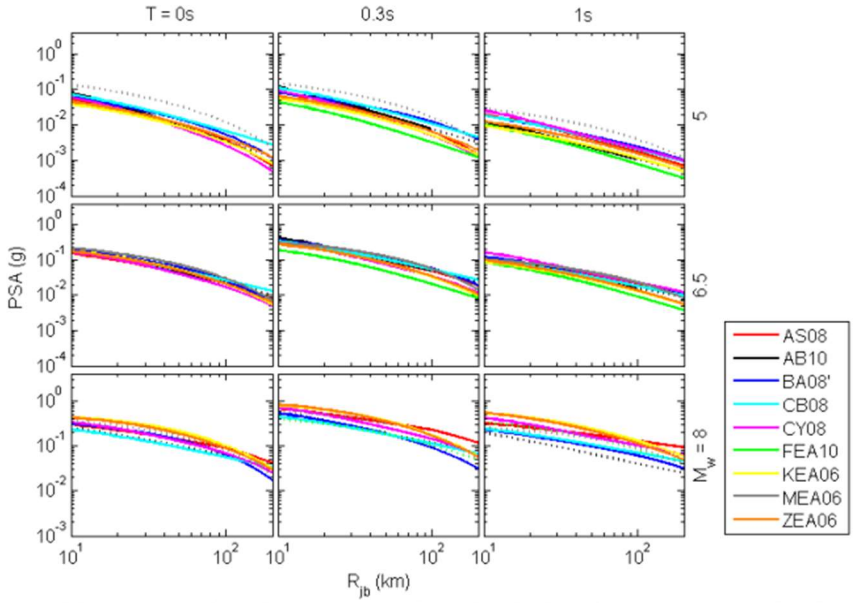

Figure 7. Distance decay of predicted PSAs for pre-selected GMPEs for various structural periods and magnitudes for rock site conditions (Stewart et. al. 2013).

As an example of functional forms, Akkar and Bommer (2010) estimated coefficients for prediction of pseudo-spectral acceleration (PSA) between periods of 0.00s – 3.00s by using the strong-motion data from Türkiye. The maximum likelihood method of Joyner and Boore (1993) was used for estimation of model coefficients. The functional form is

$$\log(\text{PSA}) = b_1 + b_2 M + b_3 M^2 + (b_4 + b_5 M)\log\sqrt{R_{jb}^2 + b_6^2} + b_7 S_s + b_8 S_A + b_9 F_N + b_{10} F_R + \varepsilon\sigma \quad (19)$$

where, S_S and S_A are set to 1 for soft (V_{s30}<360 m/s) and stiff soil sites, otherwise being zero; F_N and F_R are respectively set to 1 for "normal" and "reverse" fault types, otherwise being zero, ε is the multiplier for standard deviations of log(PSA), and σ is the total standard deviation. σ is equal to the square root of sum of squares of σ_1 and σ_2, where σ_1 is intra-event and σ_2 is inter-event components of ground motion parameters. The estimations of coefficients for this prediction model is given in Table 6 for T=0.01s (PGA).

Table 6. Coefficients of AB10 Model.

b_1	b_2	b_3	b_4	b_5	b_6
1.04159	0.91333	-0.0814	-2.9273	0.2812	7.86638
b_7	b_8	b_9	b_{10}	σ_1	σ_2
0.08753	0.01527	-0.0419	0.08015	0.261	0.0994

Kale et al. (2015) developed a ground-motion prediction equation for Türkiye and Iran between periods of 0.00s-4.00s by using strong motions from Middle East region. The model operates within a moment magnitude range of $4 \leq M_w \leq 8$, with the maximum R_{jb} being 200 km. It incorporates a functional form that accounts for three primary fault types: strike-slip, normal, and reverse. The nonlinear soil behavior, dependent on V_{s30}, is taken into consideration. The magnitude saturation is modeled by using a second power of magnitude term. Therefore, five terms were contributing to the prediction of geometric means of horizontal spectral accelerations and maximum ground velocity.

$$\ln(Y) = f_{mag} + f_{dis} + f_{Sof} + f_{aat} + f_{site} \tag{20}$$

The model involves factors for magnitude scaling (f_{mag}), geometric decay (f_{dis}), style of faulting (f_{sof}), site effects (f_{site}) and anelastic attenuation (f_{aat}) to predict the median of logarithm of ground motion parameter (ln(Y)).

Another component of seismic hazard analysis is the probabilistic function that expresses the likelihood of event magnitudes for a seismic source, namely the magnitude-recurrence relationship. Fundamental relationship was developed by Gutenberg and Richter (1944), conducting an extensive study on historical earthquakes in southern California. They categorized the data by the number of occurrences that surpassed various magnitudes. The annual rate of exceedance for a specific earthquake magnitude yielded a simple relationship. The Gutenberg-Richter law is represented schematically in Figure 8.

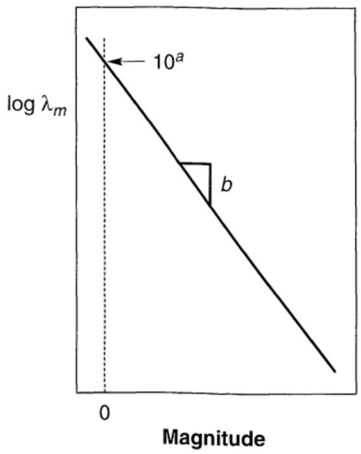

Figure 8. The schematic representation of Gutenberg - Richter law on mean annual rate of each earthquake magnitude (Kramer, 1996).

Youngs and Coppersmith (1985) formulated a magnitude-frequency density function that merges an exponential distribution for lower magnitudes with a uniform distribution around a characteristic earthquake magnitude. Recurrence relationships based on this function are provided in Figure 9. Other models incorporating characteristic earthquakes have been proposed by Wesnousky et al. (1984), and by Wu et al. (1995).

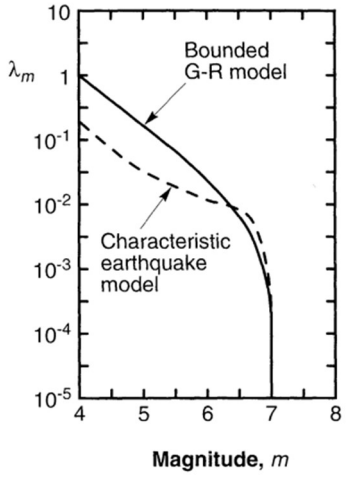

Figure 9. Comparison of Gutenberg Richter and Characteristic models (Youngs and Coppersmith 1985).

Several alternative recurrence models have also been proposed. Merz and Cornell (1973a) introduced a quadratic expression to represent the mean annual rate at which earthquakes of magnitudes between M_0 and M_u are exceeded. Shah et al. (1975) employed a bilinear recurrence model in a seismic risk assessment for Nicaragua. Additional methods involved modifying the Gutenberg-Richter law based on seismic moment and fault slip, as developed by Lomnitz-Adler and Lomnitz (1979).

As probabilistic seismic hazard analysis (PSHA) has evolved to become more detailed and realistic, it is now common practice to break down the relative contributions to the hazard from various random components of the problem. These components typically include the earthquake magnitude, the source-to-site distance, and often ε, which represents the variation of the ground motion from the predicted median value. This process, conducted separately for each fault and subsequently aggregated for all faults in the region, is referred to as the disaggregation of PSHA (Cornell and Bazzurro, 1999).

The idea of determining the mean magnitude ($\overline{M}$) and distance ($\overline{R}$) of seismic events contributing to ground-motion exceedance at a specified return period was first proposed by McGuire and Shedlock (1981). Similarly, Kameda and colleagues in Japan explored the concept of M and R within single-hypothesis PSHA, excluding input uncertainties (Ishikawa and Kameda, 1988, 1991, 1993). Additionally, various studies (e.g., Stepp et al., 1993; Chapman, 1995; McGuire, 1995) have disaggregated seismic hazard into components by magnitude, distance, and residual (ε), identifying events that most influence site-specific hazard levels. This involves summing the annual exceedance frequencies of the target ground-motion amplitude for each period (T) across M, R, and ε. These frequencies are then divided by the total hazard (overall annual frequency) to determine the probability that a specific combination of M, R, and ε caused the exceedance (McGuire, 1995). Consequently, the disaggregation technique can be used for identification of most likely event magnitude for maximum acceleration that is related to seismic (or, cyclic) stress ratio by Seed and Idriss (1975). Nonetheless, this approach is yet to be justified.

1.3 Scope

The scope of this study is an implementation of probabilistic hazard analysis for cyclic stress ratio, such that an average (or, most significant) magnitude to be used in liquefaction assessment can be retrieved. The calculations are primarily adjusted for the magnitude scaling factor presented in 2018 Seismic Code of Türkiye, which is widely used in engineering practice after Youd et al. (2001). This is a necessity, since the magnitude to be considered in liquefaction analyses is not shown on the country-scale seismic hazard map, whereas either the peak ground acceleration or the relevant spectral parameter is available. This limitation of hazard maps is also a shortcoming in other country maps for seismic hazard. For this purpose, a number of prediction equations for cyclic stress ratio are developed, and these equations are implemented in a generic seismic hazard analysis. However, certain constraints on the minimum peak ground acceleration and maximum average shear wave velocity were applied during the development of these equations. These constraints are essential to exclude ground motions that are insufficient to trigger liquefaction. Further details on these limitations are provided in Section 3.2. Then, the effect of magnitude-recurrence models on the hazard is also investigated. The method is examined by comparing the calculated average magnitude to be used for liquefaction potential assessments with those determined by alternative methods, such as the disaggregation technique.

CHAPTER 2

METHODOLOGY

2.1 Introduction

In this study, a method to estimate seismic demand through implementing cyclic stress ratio in seismic hazard analysis is proposed. However, the earthquake magnitude to be used for analysis of liquefaction potential on any given spatial coordinates is not specified in most seismic codes, including the 2018 Seismic Code of Türkiye. The seismic hazard on a specific site is related to the possibilities of a range of event magnitudes. Therefore, the selection of an average magnitude to estimate the scaling factor for liquefaction potential analysis is not straightforward.

To implement MSFs in seismic hazard analysis, empirical GMPEs are developed using the functional form of Akkar and Bommer (2010). To do that, regression techniques were applied on the strong-motion database, such that the cyclic stress ratio CSR standardized for top of the ground is considered as the estimated intensity parameter. The parameter b in Eq. (30) is applied on 234 acceleration time histories to count the number of equivalent uniform cycles at 65% of maximum CSR during a ground motion (see Section 3.3). The figures for b to fit the magnitude scaling factor (MSF) defined by Youd et al. (2001), which is later used by 2018 Seismic Code of Türkiye, is determined empirically. Thus, N_{eq} could be counted for each ground-motion record, and consequently CSRs could be standardized for the event magnitude of 7.5. Then, comparing the CSR standardized for earthquake magnitude, M_w of 7.5 and CSR that is not standardized for a specific hazard level, the predominant magnitude to be used in liquefaction assessment can be calculated by using MSF relationship. This approach is also compared with the result of disaggregation in seismic hazard analysis. Also, seismic hazard analyses are

performed by considering different magnitude recurrence laws to observe the effect of source modeling on the effect of predominant magnitude.

The methodology is briefly described by the following steps.

1- Determination of b that relates N_{eq} to M_w that fits to the MSF relationship of Youd et. al. (2001) in the mean,
2- Calculation of standardized and non-standardized CSR for each record to be used in development of empirical GMPEs,
3- Execution of probabilistic seismic hazard analysis based on these GMPEs to compute CSR with and without magnitude standardization,
4- Disaggregation of seismic hazard analysis to determine predominant magnitude for CSR, and comparison of this magnitude with that calculated by the ratio of two CSRs, with and without magnitude correction.

Details regarding the concepts used in the analysis are provided in the following sections.

2.2 Cyclic Stress Ratio

The seismic demand on soils to initiate liquefaction is represented by the parameter cyclic stress ratio (CSR). Seed and Idriss (1971) estimated the CSR generated by earthquake ground motions at a depth z below the ground surface as

$$\mathrm{CSR} = 0.65 \cdot \frac{\mathrm{PGA}}{g} \cdot \frac{\sigma_v}{\sigma'_v} \cdot r_d \tag{21}$$

where, σ_v is the vertical total stress, σ'_v is the vertical effective stress at depth z. The parameter r_d is a stress reduction coefficient that adjusts for the flexibility of the soil column. $r_d = 1$ indicates rigid body behavior, and it is valid at z equals 0.

Although CSR is dependent on ratio of normal and effective vertical stress and stress reduction factor, these depth-dependent parameters can be ignored to express this intensity measure on top of the ground for simplification. Hence, CSR on ground is

$$\mathrm{CSR_N} = 0.65 \cdot \frac{\mathrm{PGA}}{g} \tag{22}$$

2.3 Equivalent Number of Stress Cycles

The earthquake-induced non-uniform cyclic stress patterns are converted to an equivalent series of uniform stress cycles. The effect of each cycle of an irregular pattern is converted to another amplitude by using weighting factors (Boulanger and Idriss, 2004). For this purpose, a relationship between CSR and the number of uniform stress cycles is necessary.

$$\mathrm{CSR} = a * N_i^{-b} \tag{23}$$

Consequently, the number of cycles required to induce the same liquefaction opportunity at two different CSR levels are related as

$$\frac{N_A}{N_B} = \left(\frac{\mathrm{CSR_B}}{\mathrm{CSR_A}}\right)^{\frac{1}{b}} \tag{24}$$

The peak counting method of Seed et al. (1975) is implemented. The maximum amplitude between zero-crossings is defined as a peak amplitude and considered to represent one half cycle. Substituting $N_{M7.5}$ for N_A as the mean number of cycles for a magnitude M_w 7.5 event, $CSR_{\mathrm{M7.5}}$ for CSR_{A} as the scaled cyclic stress ratio for its magnitude, N_{eq} for N_B as the equivalent number of cycles for the ground motion for its cyclic stress ratio on ground, Eq. (24) improves to

$$\frac{N_{M7.5}}{N_{eq}} = \left(\frac{\mathrm{CSR_N}}{\mathrm{CSR_{M7.5}}}\right)^{\frac{1}{b}} \tag{25}$$

The mean number of cycles for a magnitude M_w 7.5 event is yet to be determined statistically. N_{eq} is to be counted for each acceleration history as explained in the following paragraphs. The magnitude scaling factor can be defined as

$$\mathrm{MSF} = \frac{\mathrm{CSR_N}}{\mathrm{CSR_{M7.5}}} \tag{26}$$

or, after Eq. (26)

$$\mathrm{MSF} = \left(\frac{N_{M7.5}}{N_{eq}}\right)^{b} \tag{27}$$

Eq. (27) shows the relationship between the parameter *b*, $N_{M7.5}$, and MSF. Consequently, this relation justifies the dependence of predominant magnitude to be considered in liquefaction potential assessment to the function defining MSF. Substituting Eq. (10) in Eq. (27);

$$\frac{10^{2.24}}{{M_w}^{2.56}} = \left(\frac{N_{M7.5}}{N_{eq}}\right)^{b} \tag{28.a}$$

or,

$$N_{eq} = N_{M7.5} \times 10^{\left(-\frac{2.24}{b}\right)} \times {M_w}^{\left(\frac{2.56}{b}\right)} \tag{28.b}$$

or,

$$\log\left(N_{eq}\right) = \frac{1}{b}\log\left(\frac{M_w^{2.56}}{10^{2.24}}\right) + \log(N_{M7.5}) \tag{28.c}$$

The parameter *b* that fits MSF proposed by Youd et al. (2001) can be determined by a regression analysis. However, the left side of Eq. (28.b), N_{eq}, is also dependent on *b*, so the relationship is nonlinear. An iterative procedure shall be followed to determine optimum *b*.

To explain the dependency of N_{eq} on *b*, and how this is calculated, Eq. (28.c) shall be reconsidered for counting equivalent number cycles. Due to Eq. (24), the equivalent number of uniform stress cycles at 65% of maximum acceleration shall be calculated. The substitution of $\mathrm{CSR_B} = 0.65{\cdot}a_{\max}$, and $\mathrm{CSR_A} = a_{\mathrm{peak}}$ yields

$$\frac{N_{\mathrm{A}}}{N_{\mathrm{B}}} = \left(\frac{0.65 \times a_{\max}}{a_{\mathrm{peak}}}\right)^{\frac{1}{b}} \tag{29}$$

where N_A is the equivalent number of stress cycle at 0.65 times $a_{\max}$, and N_B is taken as 1. As explained in Section 1.2.1, the equivalent number of cycles are calculated individually for the positive and negative stress amplitudes. Consequently, the average of cumulative number of cycles in two directions represents the equivalent number of cycles for the acceleration history. Therefore, the total number of uniform cycles for an acceleration history is

$$N_{eq} = \frac{1}{2}\sum\left(\left|\frac{0.65 \times a_{\max}}{a_{\mathrm{peak}}}\right|\right)^{\frac{1}{b}} \tag{30}$$

2.4 The Prediction Equation for CSR

Empirical prediction equations for the cyclic stress ratio, standardized for a specific number of cycles, are developed based on magnitude, distance, and site conditions. These equations use the functional form proposed by Akkar and Bommer (2010), which is abbreviated as AB10 in this study. The primary reason for utilizing AB10 is its simplicity and its incorporation of strong ground motions specific to Türkiye. This functional form was built to estimate the maximum ground motion acceleration PGA as the spectral acceleration at the period (T) of 0.01 s.

The AB10 model is simplified due to the limitations applied on the database used in this study. Since the records with V_{s30} < 300 m/s are considered, S_S and S_A in Eq. (19) are set to 1 and 0 respectively. Consequently, the prediction equation is reduced to the form:

$$\log(\mathrm{CSR_N}) = b_1 + b_2 M + b_3 M^2 + (b_4 + b_5 M) log\sqrt{R_{jb}^2 + b_6} + b_7 F_N + b_8 F_R + \varepsilon\sigma \tag{31}$$

The liquefaction potential of soil is dependent on the duration of shaking, which is related to the event magnitude. The average effect of magnitude is estimated by calculating the ratio of CSR_N to $CSR_{M7.5}$ defined in Eq. (9). To develop the empirical prediction equations for CSR_N and $CSR_{M7.5}$, simplified AB10 model in Eq. (31) is used. In other words, CSR is proportional to PGA ignoring duration effects, whereas $CSR_{M7.5}$ is the ratio corrected according to the number of cycles, taking magnitude M_w 7.5 as the reference. CSR and $CSR_{M7.5}$ are calculated for the strong-motion database in Section 3.2. With magnitude M_w, distance R_{jb} and factors for fault types are known, the coefficients of the prediction equations are calculated using *MATLAB* (*https://www.mathworks.com/*). The "*fitnlm*" function is used to fit the data to a nonlinear regression model, aligning with the functional form of Eq (31).

Prediction models for $CSR_{M7.5}$ can be directly utilized in hazard analysis since it is already weighted for magnitude. However, either MSFs have to be applied on predicted CSR, which is proportional to PGA, or a disaggregation of hazard technique has to be implemented to determine the predominant magnitude for magnitude correction. Accordingly, GMPEs are developed for CSR and $CSR_{M7.5}$ employing the same functional form, so that the effect of magnitude on liquefaction opportunity can be implicitly computed through the hazard integral.

2.5 Seismic Hazard Analysis

Probabilistic seismic hazard analysis (PSHA) of cyclic stress ratio is employed to develop a method in which the weighted average of magnitudes is calculated. A PSHA may be decomposed into four steps, as explained by Reiter (1990). The calculation steps are demonstrated in Figure 10.

1. The initial step involves specifying and characterizing the potential earthquake sources, along with determining the probability distribution for potential rupture locations within each source. Source characterization entails defining the geometry of each source zone and assessing its earthquake-generating potential.

2. The next task is to characterize the seismicity, or the temporal distribution of earthquake recurrence. A recurrence relationship, which defines the average frequency at which earthquakes of a particular magnitude or greater occur, is used to describe the seismic activity of each source zone.

3. The third step requires determining the ground motion at the site that could result from earthquakes within each source zone. This is achieved using predictive relationships. The uncertainty related with these predictive models is also factored into the PSHA.

4. Finally, all uncertainties regarding earthquake location, size, and the prediction of ground motion parameters are integrated to calculate the probability that a specific ground motion parameter will be exceeded within a given time frame.

McGuire (2004) presented the seismic hazard integral as

$$\gamma[C > c] = \sum v_j \int \int P_j[C > c|\bar{s}\ at\ l]P[\bar{s}\ at\ l]d\bar{s}dl \qquad (32)$$

Where γ is the frequency with which c is exceeded from earthquakes at source j, $\bar{s}$ is a vector of source properties, v_j is the rate of occurrence of earthquakes of interest at source j, $P_j[C > c|\bar{s}\ at\ l]$ is the probability that c is exceeded at the site, conditional on an earthquake at source j, with properties $\bar{s}$ at location l, $P[\bar{s}\ at\ l]$ is the probability that an earthquake with source properties $\bar{s}$ occurs at location l.

In most cases the quantities in $[\bar{s}\ at\ l]$ are magnitude and distance. Assuming both of them to be independent, the probability of exceedance function can be expressed as

$$\gamma[C > c] = \sum v_j \int \int P_j[C > c|m, r]f_m(m)f_R(r)dmdr \qquad (33)$$

where $f_m(m)$ and $f_R(r)$ are probability density functions for magnitude and distance.

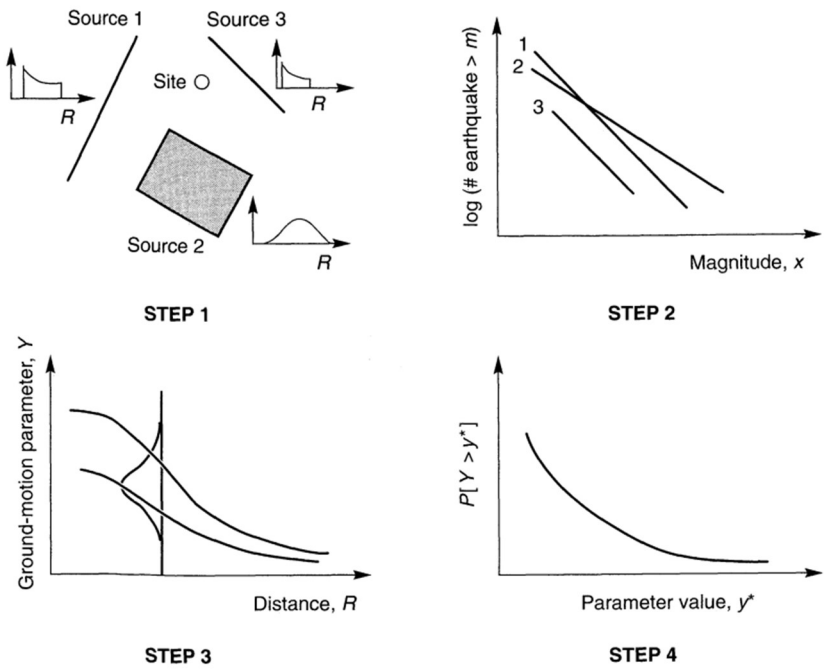

Figure 10. Four steps of PSHA (adapted from Kramer, 1996).

The computer program *R-Crisis* (*http://www.r-crisis.com/*) is used for PSHA. The seismic hazard of ground motion parameter (CSR_N) is then computed for 10% exceedance probability in 50 years, which corresponds to the return period of 475 years for CSR_N. The seismic analysis is conducted for three different prediction equations, which produce intensities of CSR_N, CSR_N/MSF and $CSR_{M7.5}$. The hazard for any specific parameter is then disaggregated to observe the dominant magnitudes.

2.5.1 The Ground Motion Prediction Equation

The prediction equations that are explained in Section 2.4 are used for analysis to calculate CSR conditional to magnitude, distance to fault, and V_{s30} of site. The variances of the prediction equations are also considered. Besides, the peak ground acceleration (PGA) prediction by the GMPE of AB10 is also considered for comparison purposes.

2.5.2 The Magnitude-Recurrence Relationship

Two alternative magnitude-recurrence relationships, the characteristic and the truncated exponential models are considered in this study.

In the implementation of the characteristic magnitude-recurrence relationship by Youngs and Coppersmith (1985) within the R-CRISIS software, the exceedance rate for a given earthquake magnitude on a seismic source is described mathematically as

$$\lambda(M) = \lambda_o \frac{\Phi\left[\frac{M_u - EM}{s}\right] - \Phi\left[\frac{M - EM}{s}\right]}{\Phi\left[\frac{M_u - EM}{s}\right] - \Phi\left[\frac{M_o - EM}{s}\right]}, M_0 \leq M \leq M_u \qquad (34)$$

Here, ϕ represents the standard normal cumulative distribution function, while M represents the earthquake magnitude. M_o and M_u correspond to the threshold (minimum) and maximum characteristic magnitudes, respectively. EM represents the expected value of the characteristic earthquake magnitude, while s corresponds to its standard deviation. The parameter λ_o indicates the exceedance rate associated with the threshold magnitude M_o and basically calculated by

$$\lambda_0 = \frac{1}{t_m} \qquad (35)$$

where t_m is the median value of the time between characteristic earthquakes.

In addition, a slip-predictable behavior can be modeled assuming that EM grows with the time elapsed since the last characteristic event ($T00$), formulated as

$$EM = D + Fln(T00) \qquad (36)$$

where parameters D and F are model coefficients. In this study, the effect of time is omitted. Therefore, F is set to 0. As a result, EM becomes equal to D regardless of the time elapsed. This is also equal to M_u.

For the truncated exponential magnitude recurrence model (or, modified Gutenberg – Richter model), earthquake magnitude recurrence is characterized based on Cornell and Vanmarke 1969.

$$\lambda(M) = \lambda_0 \frac{\exp(-ßM) - \exp(-ßM_U)}{\exp(-ßM_0) - \exp(-ßM_U)} \; where \; M_0 \leq M \leq M_U \qquad (37)$$

Here, β is $2.303b$, which describes the relative likelihood of large and small earthquakes. ß is determined as 2.07 corresponding to b value of 0.9, conventionally used in seismic hazard analyses. The coefficient of variation of β may be introduced to account for the uncertainty in β. However, it is considered as 0 due to lack of reasoning.

2.5.3 Disaggregation of Seismic Hazard

The methodology of PSHA facilitates the estimation of the mean annual exceedance rate at a given location by various magnitudes at different distances from the site. However, this exceedance rate is not directly linked to a specific magnitude or source-to-site distance. To address this, the disaggregation calculations are applied, allowing the exceedance rate to be represented as a distribution function for parameters such as magnitude or distance. Mathematically, this means detachment of terms from the integrals of Eq. (33). The results of disaggregation can be visualized to observe the dominant magnitudes at different distances. Figure 11 is presented to simplify disaggregation, visualizing the joint distribution of M, R, and ε for seismic events. (McGuire, 1995).

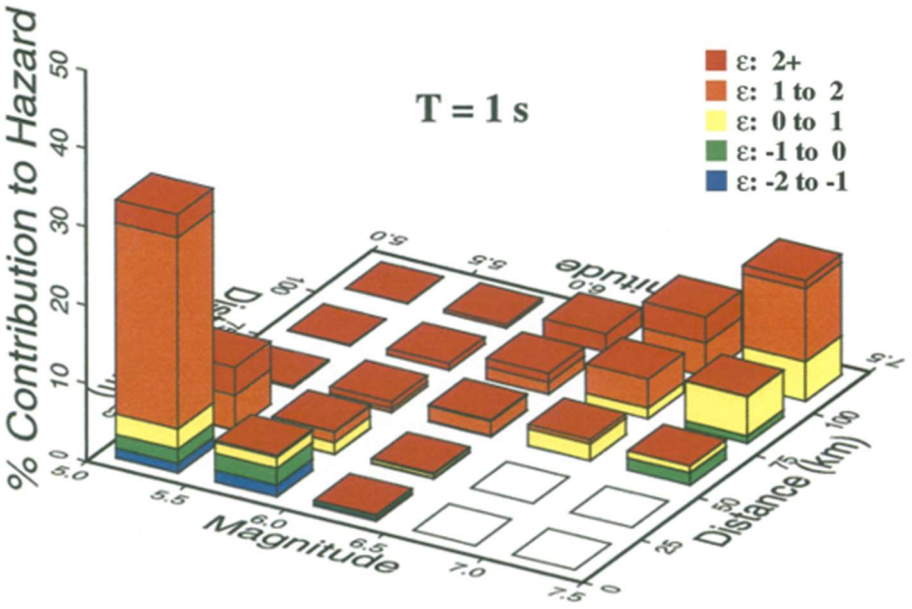

Figure 11. Contribution to hazard by magnitude, distance and standard deviation (McGuire, 1995).

2.6 Calculation of Predominant Magnitude for Liquefaction Assessments

In Section 4, seismic hazard analyses are performed using the ground motion prediction equations derived in Section 3.4. As a result, cyclic stress ratios are determined for models with and without magnitude correction. The ratio of these stress values yields the predominant magnitude scaling factor specific to a return period. The earthquake magnitude is back-calculated using Eq. (10). Additionally, disaggregation techniques are applied to the hazard analysis, and the results of different approaches for estimation of the predominant magnitude are compared.

CHAPTER 3

PREDICTION EQUATIONS FOR CSR

3.1 Introduction

In order to develop a relationship between $CSR_{M7.5}$, scaled due to magnitude effects, the strong-motion databases of PEER (*https://ngawest2.berkeley.edu/)* and AFAD (*https://tadas.afad.gov.tr/)* are used in this study. 234 time histories are investigated from 71 different earthquakes with moment magnitudes ranging from magnitude M_w 5.5 to 7.8, with maximum absolute accelerations a_{max} ranging from 0.05*g* to 0.86*g*, with maximum Joyner-Boore distances (R_{jb}) of 227 km, and with maximum V_{s30} of 300 m/s. In the following summary statistics for this acceleration histories are presented. All records were corrected either by PEER or by AFAD for the possible high and low frequency noise in the raw records.

3.2 The Strong Motion Database

The histograms for the distribution of M_w, a_{max}, V_{s30}, R_{jb}, fault mechanism and stations in the database are presented in Figure 12. The median value for M_w, a_{max}, V_{s30}, R_{jb} is 6.5, 0.14g, 257 m/s and 33 km respectively. a_{max} is greater than 0.05g for at least one of the components of each record. This minimum limit for a_{max} was necessary to avoid ground motions that are not severe enough to trigger liquefaction, and the limit was decided by considering the minimum CSR of 0.05 suggested by Youd et al. (2001), whereas the multiplier 0.65 for a_{max} is not taken into account. Another issue is to limit V_{s30}, since the sites with liquefaction susceptibility shall involve loose to medium dense sands. Usually, the upper limit for normalized S-wave velocity in susceptible sands is about 220 m/s according to Andrus and Stokoe (2000). Considering the limitations in sample size and the possibility of geological

formations like the sand deposits on very stiff layers, the maximum limit for V_{s30} was taken as 300 m/s. Nonetheless, at least half of the sites have a V_{s30} in the range 250 to 300 m/s, which may yield some bias in the results of this study. A reasonable distribution between larger and smaller magnitudes could be achieved. Another limitation of the sample is that the number of records for normal faults is very limited with respect to the number for reverse and strike-slip faults. Figure 12 illustrates the distribution of record numbers with respect to M_w, R_{jb}, PGA, V_{s30}, and fault mechanism. Figure 13 shows the scattering of data due to magnitude M_w, $a_{\max}$, and R_{jb}. Figure 14 shows the number of stations considered in each earthquake event.

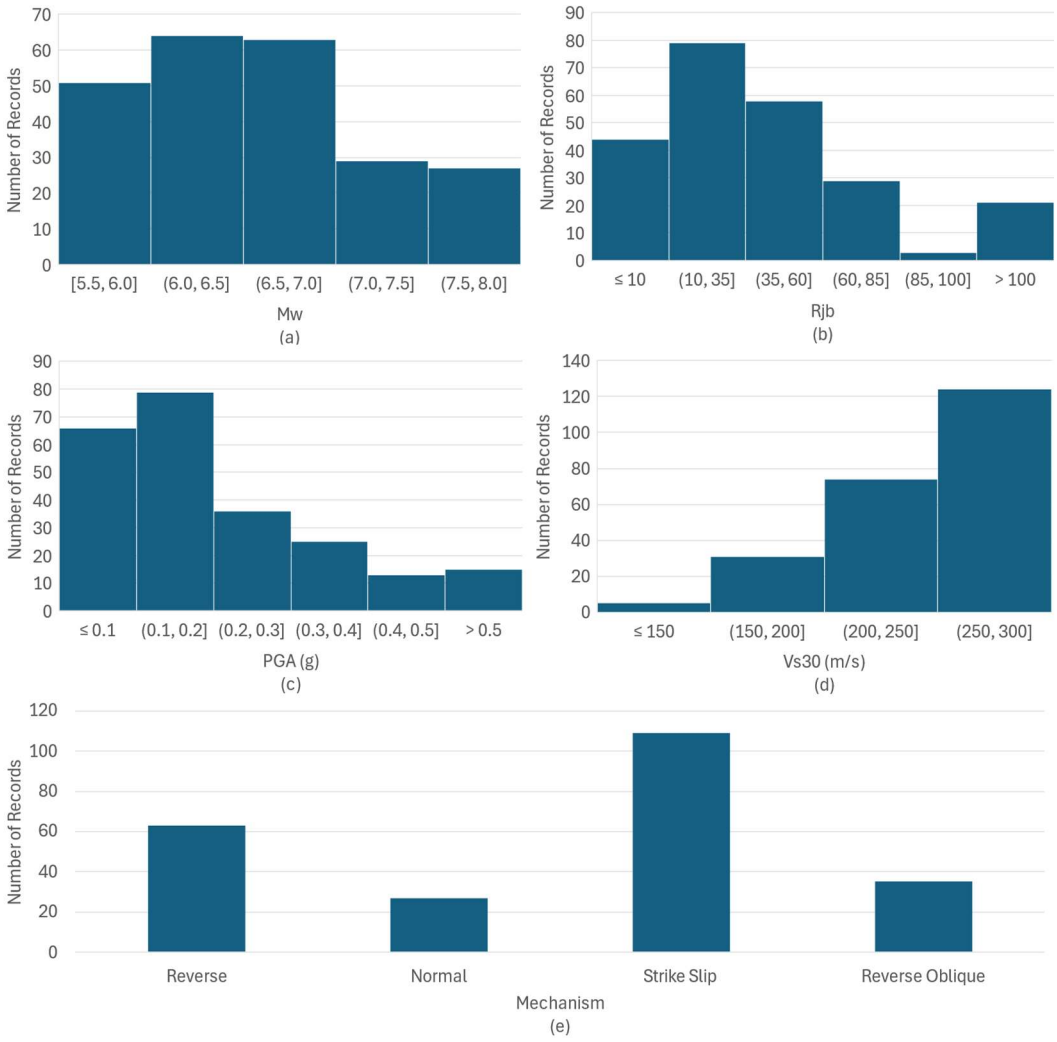

Figure 12. Histogram of seismicity parameters used in this study.

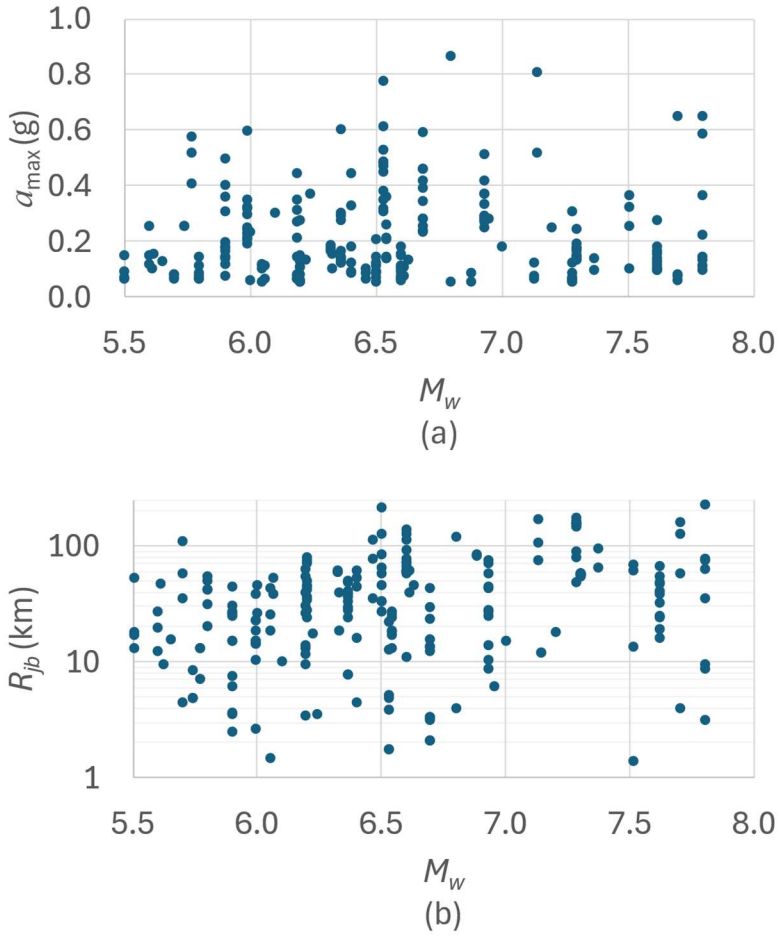

Figure 13. The distribution of strong-motion sample as (a) M_w versus a_{max}, and (b) M_w versus R_{jb}.

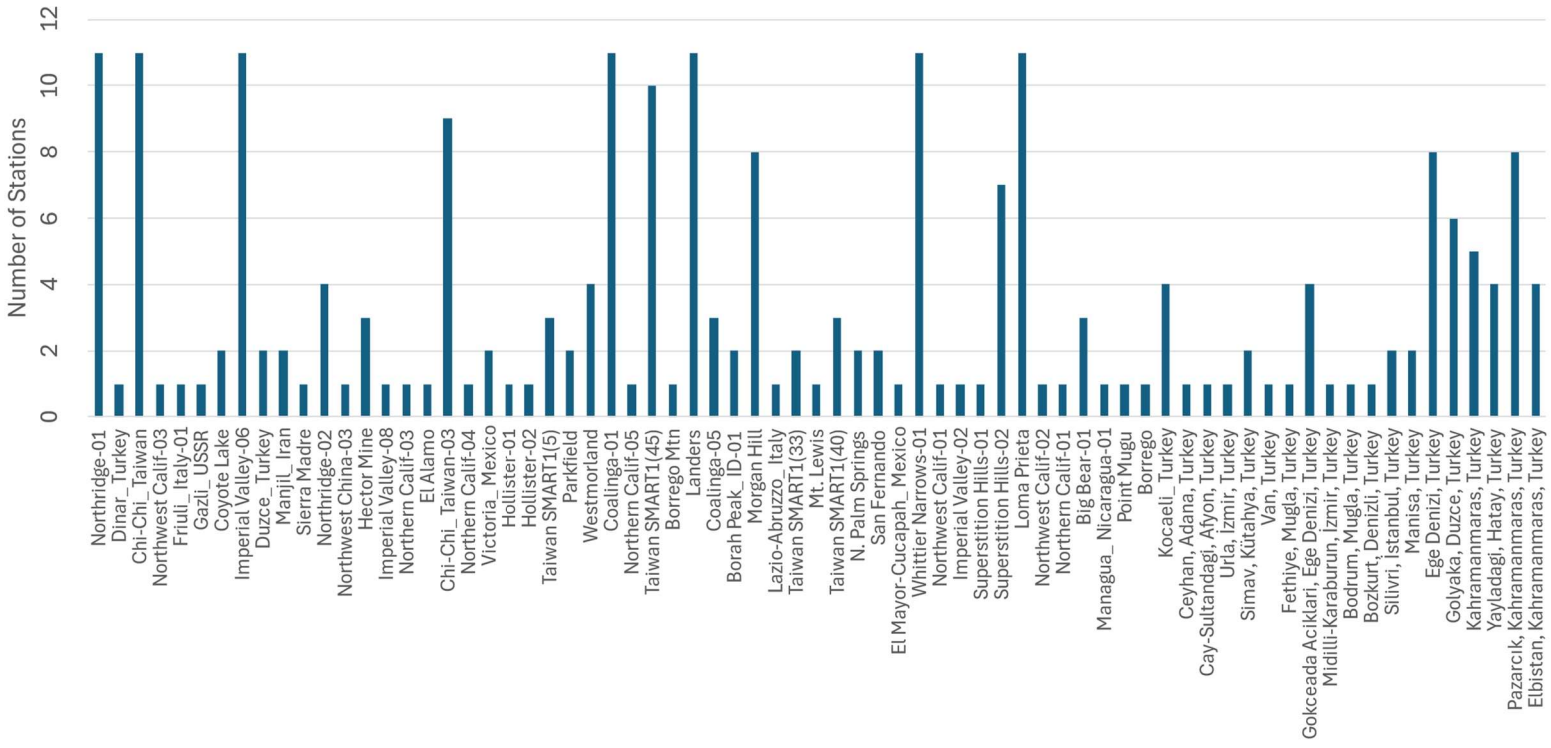

Figure 14. Number of stations considered in each earthquake event.

3.3 Calculation of CSRs

In this section, CSR_N and $CSR_{M7.5}$ for soil sites in Section 3.2 are calculated due to methodology provided in Section 2.2 and 2.3 respectively. CSR_N is simply calculated due to Eq. (22). In order to calculate $CSR_{M7.5}$, a trial-error procedure is used to simultaneously determine b value. First, a value for b is chosen, and consequently N_{eq} for the ground motion record is calculated by using Eq.(30). Then, the least-squares regression analysis is used for the coefficients of Eq. (28.c). The trials are continued until the presumed b is consistent with the value estimated by regression. Consequently, $N_{M7.5}$ is calculated for the final b in agreement between in two sides of the Eq. (28.c). These trials results are summarized in Table 7 indicating that two sides of Eq. (28.c) are consistent at the b value of 0.96, where $N_{M7.5}$ is calculated as 30. This final relationship is shown in Figure 15. This result can be strongly dependent on the sample of strong-motion records though.

Table 7. Iterative procedure for calculation of b and N_{eq} at M_w=7.5.

Presumed *b*	**1 / *b***	**log($N_{M7.5}$)**	***b***	$N_{M7.5}$
0.20	1.10	1.23	0.91	16.88
0.30	1.02	1.10	0.98	12.59
0.40	1.15	1.15	0.87	14.10
0.50	1.19	1.22	0.84	16.50
0.60	1.18	1.29	0.85	19.32
0.70	1.15	1.35	0.87	22.37
0.80	1.11	1.41	0.90	25.53
0.90	1.07	1.46	0.94	28.76
0.96	1.04	1.49	0.96	30.70
1.00	1.03	1.51	0.97	32.00
1.10	0.99	1.55	1.01	35.21
1.20	0.95	1.58	1.05	38.39
1.30	0.92	1.62	1.08	41.51

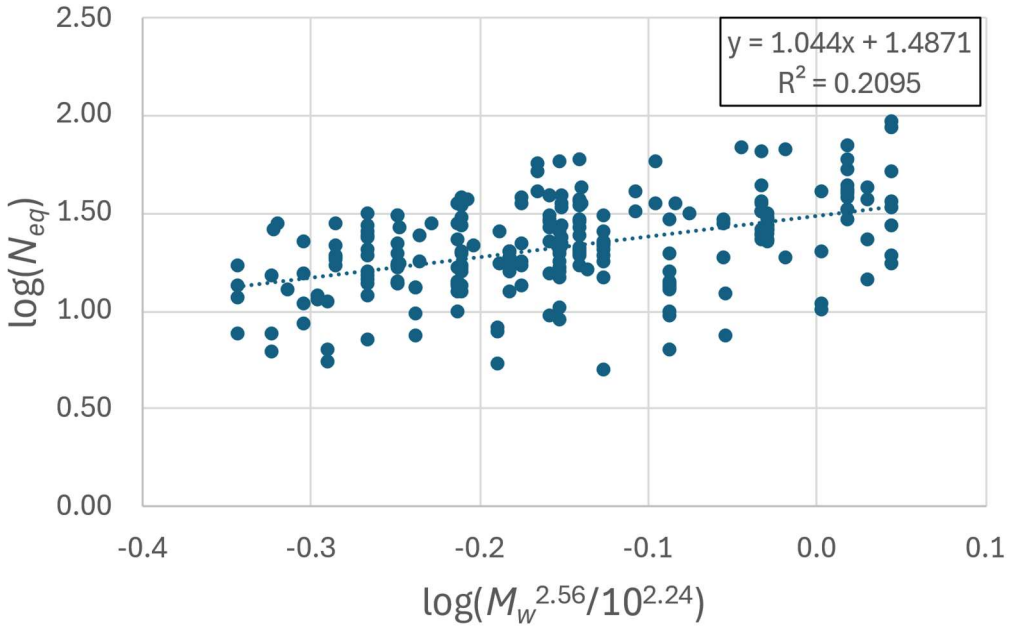

Figure 15. Linear relationship of $\log(N_{eq})$ and $\log(M_w^{2.56}/10^{2.24})$.

N_{eq} for different magnitudes are shown in Table 8 for b=0.20, 0.40 and 0.96. The first two values of b are typically consistent with the figures based on laboratory tests (Figure 5), whereas the last b is the one matching with Eq (10). As shown by these results, b does not have any significant effect on the relative number of cycles, taking M_w 7.5 as the reference. However, $N_{M7.5}$ is dependent on b.

Table 8. Equivalent number of uniform stress cycles for different magnitudes.

M_w	N_{eq} (b=0.20)	N_{eq} (b=0.40)	N_{eq} (b=0.96)
5.5	7 (42%)	6 (%40)	13 (44%)
6.0	9 (53%)	7 (%52)	17 (55%)
6.5	11 (67%)	9 (66%)	21 (68%)
7.0	14 (82%)	12 (82%)	26 (83%)
7.5	17 (100%)	14 (100%)	30 (100%)
8.0	20 (%120)	17 (%121)	36 (%119)

Seed et al. (1975) calculated N_{eq} as 4-5 and 15 for M_w equals to 5.5 and 7.5 respectively. This computation of N_{eq} is coherent for b equals to 0.3-0.4, as recommended by Yoshimi et. al. (1989), Liu et. al. (2001) and Boulanger and Idriss

(2014) as shown in Figure 3. It is observed that regressed b value and $N_{M7.5}$ for the benchmark relationship of Eq. (10) are significantly higher than those in previous studies as presented in Section 1.2.3. The variation in results is possibly due to earthquake records which influence the regression coefficients, or due to the conservatism of MSFs suggested by Youd et al. (2001) as a minimum limit. This issue is further investigated by using the MSFs of Seed and Idriss (1982), which is summarized in Section 1.2.1. The proposed MSFs are associated with the corresponding M_w by using a power regression equation, expressed by

$$MSF = \frac{9.53}{M_w^{1.112}} \tag{38}$$

Substituting Eq. (38) into Eq. (27);

$$log(N_{eq}) = \frac{1}{b} log\left(\frac{M_w^{1.112}}{9.53}\right) + log(N_{M7.5}) \tag{39}$$

Using the same procedure described above, b is calculated as 0.39, with $N_{M7.5}$ determined as 15. This aligns with the recommendation by Seed and Idriss (1982).

For comparison, $CSR_{M7.5}$ for each record is calculated using the logarithmic relationship between N_{eq} and CSR_N by setting b as 0.96 in Eq. (25). Then, this is compared by CSR_N/MSF, where MSF is determined according to Eq. (10). and CSR_N is calculated due to Eq. (22). CSR_N/MSF is compared with $CSR_{M7.5}$ in Figure 16. It is observed that both methods yield compatible results in the mean sense, but the variability is very significant as also depicted by the low coefficient of determination, R^2 in Figure 16. GMPEs are developed to estimate CSR_N and $CSR_{M7.5}$ based on both methods in Section 3.4.

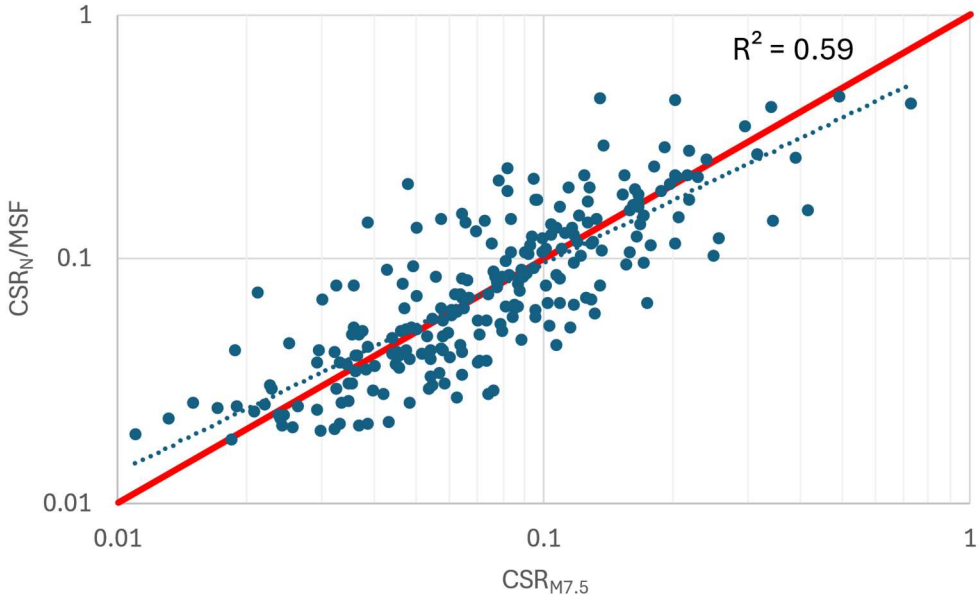

Figure 16. Comparison of magnitude corrected CSRs.

3.4 Predicting CSRs

In this section, empirical prediction equations for CSR_N and $CSR_{M7.5}$ are constructed. The functional form of AB10 model is simplified for use in the nonlinear regression fit in Eq. (31). Before constructing the prediction equations for CSR, the prediction of AB10 is compared with the actual a_{max} values from the records. The results are presented in Figure 17, categorized for earthquake magnitudes between 5.5–6.5, 6.5–7.5 and 7.5-7.8. The majority of the a_{max} values from the records fall within the prediction interval of AB10 model. This prediction range relies on the standard deviation for a_{max} at T=0.0s provided by Akkar and Bommer (2010). This observation is particularly valid for larger magnitudes and shorter distances. However, some data points are found to lie outside this range, particularly at R_{jb} > 10 km for moment magnitudes between 5.5-7.5. Therefore, AB10 predictions are rather biased for prediction of maximum ground accelerations of the sample, and tend to predict lower figures for lower ranges of a_{max}. Therefore, a simplified model, Eq.(31), based on the functional form of AB10, is regressed to obtain model coefficients that are more reasonably consistent with the data.

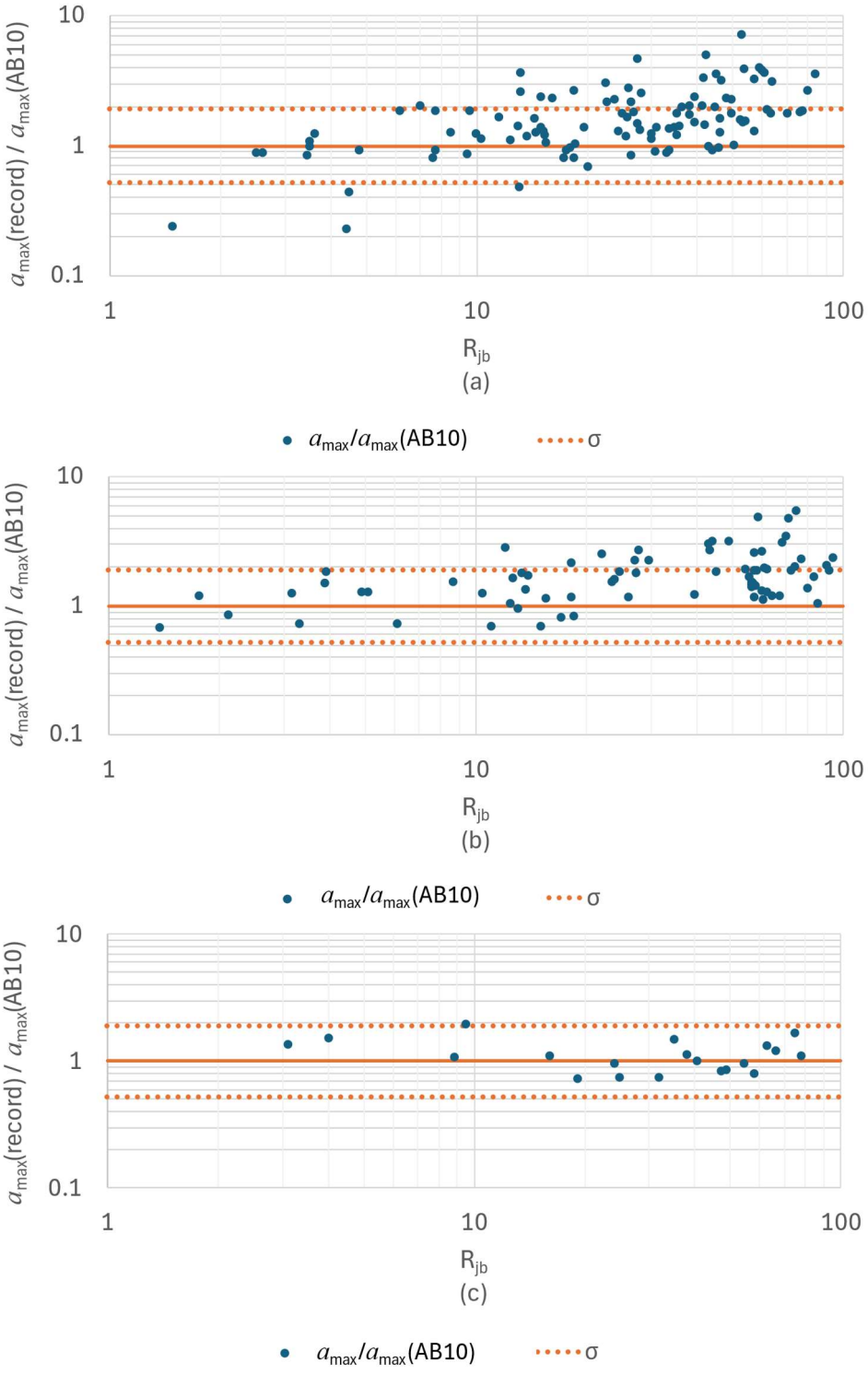

Figure 17. Comparison of actual and predicted a_{max} values based on AB10 model for moment-magnitude intervals (a) 5.5-6.5, (b) 6.5-7.5, and (c) 7.5-7.8.

Two GMPEs are developed by employing nonlinear regression on data to comply with the functional form Eq. (31) as previously explained in Section 2.4. These models estimate CSR_N and $CSR_{M7.5}$ and referred to as "MS_N" and "$MS_{M7.5}$" respectively. The coefficients for both GMPEs are presented in Table 9.

Table 9. Coefficients of GMPEs.

GMPE	$\mathbf{b_1}$	$\mathbf{b_2}$	$\mathbf{b_3}$	$\mathbf{b_4}$
MS_N	-6.2274	1.7016	-0.11294	-0.38859
$MS_{M7.5}$	-8.0836	2.0969	-0.13245	-0.5089
	$\mathbf{b_5}$	$\mathbf{b_6}$	$\mathbf{b_7}$	$\mathbf{b_8}$
MS_N	-0.04112	61.90	-0.15777	-0.023972
$MS_{M7.5}$	-0.023276	165.98	-0.069087	-0.085979
	$\boldsymbol{\sigma}$			
MS_N	0.185			
$MS_{M7.5}$	0.206			

The comparisons of calculated CSR_N and $CSR_{M7.5}$ values based on Eq. (22) and Eq. (25) with the predictions for strike slip faults are presented in Figure 18. It is observed that the majority of the CSR_N values lie within the prediction range of the model MS_N, but the scattering of $CSR_{M7.5}$ is wider. Hence, the variability of $CSR_{M7.5}$, which is related to both the variability of a_{max} and that of duration (or, number of acceleration cycles), is more significant than that of CSR_N. That is also showing the extreme simplicity in using techniques like disaggregation for determination of M_w to be used in liquefaction potential analysis.

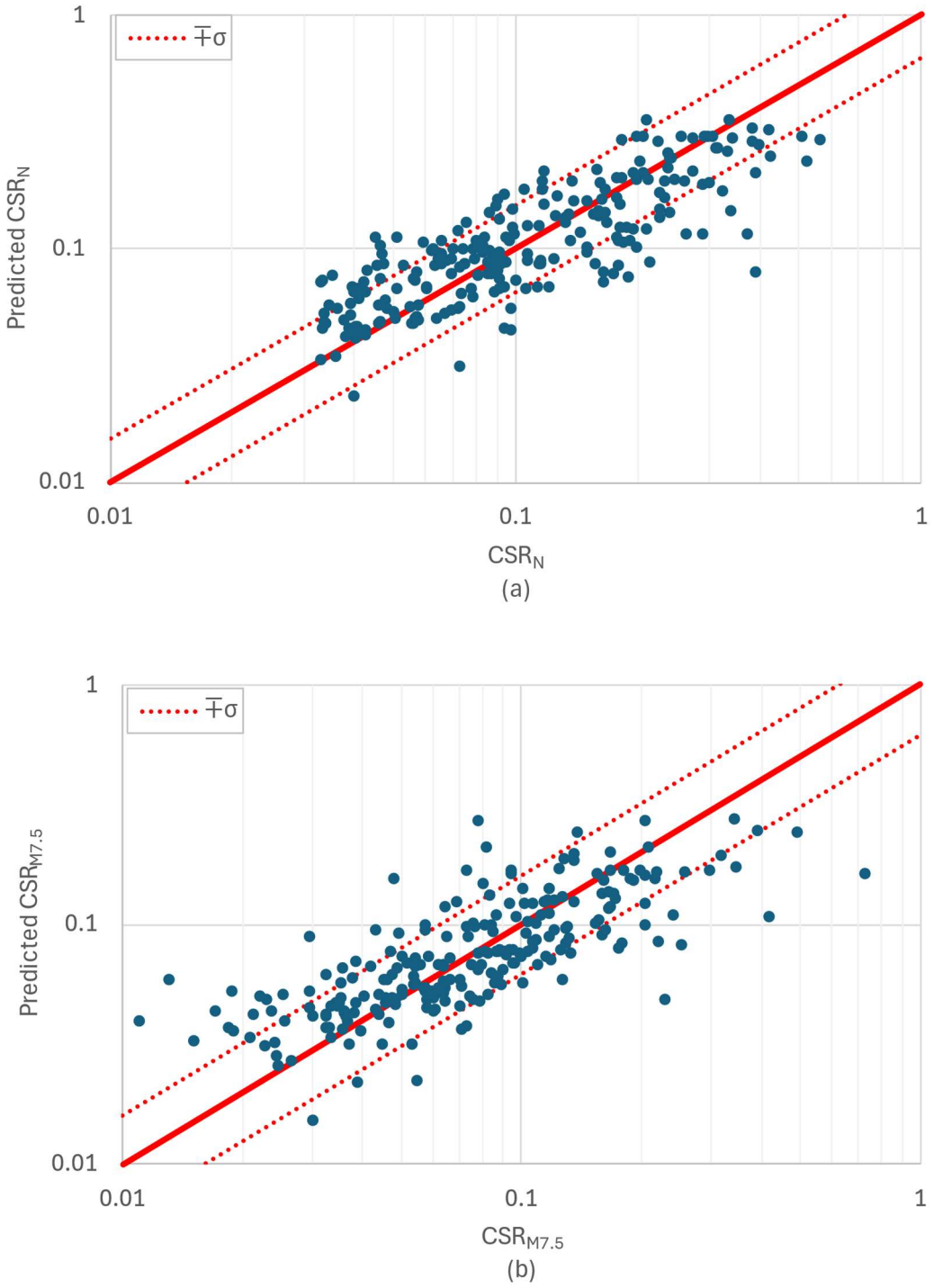

Figure 18. The comparison of calculated and predicted (a) CSR_N and (b) $CSR_{M7.5}$ values.

3.5 Effect of V_{s30} on Prediction Equations

As explained in Section 2.4, the functional form of Akkar and Bommer (2010) was utilized to develop prediction models. Due to the maximum limit for V_{s30} as 300 m/s, the coefficients associated with soil conditions in the prediction models were set to either 1 or 0 (Section 3.2). However, to examine the influence of V_{s30} on the conditional estimations of cyclic stress ratio, an additional term for V_{s30} was incorporated into the prediction model.

$$\log(\mathrm{CSR_N}) = b_1 + b_2 M + b_3 M^2 + (b_4 + b_5 M) log \sqrt{R_{jb}^2 + b_6} + b_7 F_N + b_8 F_R + b_9 \log(V_{s30}) + \varepsilon\sigma \quad (40)$$

The regressed coefficients of the prediction models for $\mathrm{CSR_N}$ and $\mathrm{CSR_{M7.5}}$ are respectively presented in Table 10.

Table 10. Coefficients of GMPEs including V_{s30}.

GMPE	**b1**	**b2**	**b3**	**b4**
$\mathrm{MS_N}$	-6.3907	1.7156	-0.11392	-0.38501
$\mathrm{MS_{M7.5}}$	-7.8956	2.0805	-0.13134	-0.51306
	b5	**b6**	**b7**	**b8**
$\mathrm{MS_N}$	-0.04185	63.049	-0.15767	-0.026007
$\mathrm{MS_{M7.5}}$	-0.022166	161.29	-0.069138	-0.083493
	b9	**σ**		
$\mathrm{MS_N}$	0.049099	0.185		
$\mathrm{MS_{M7.5}}$	-0.056869	0.206		

A comparison of the standard deviations in Table 10 with those in Table 9 reveals that there is no change in the standard deviation of prediction error (σ). This indicates that V_{s30} does not significantly affect the predictions. This is explained by the narrowness of the range of V_{s30} in the sample, such that median of V_{s30} is 257 m/s whereas its range is 116.3 m/s to 300 m/s (Section 3.2). Consequently, the majority

of V_{s30} values lie between 250–300 m/s, resulting in very narrow range of this parameter for the majority of the dataset. The standard deviation can be reduced if a more rigorous regression analysis for nonuniform sample is used.

3.6 The Comparisons of CSR Equations

The comparison of results between the MS_N/MSF and $MS_{M7.5}$ models at different earthquake magnitudes based on strike slip fault type are presented in Figure 19. Both the $MS_{M7.5}$ and MS_N models exhibit reasonably consistent median predictions at varying distances.

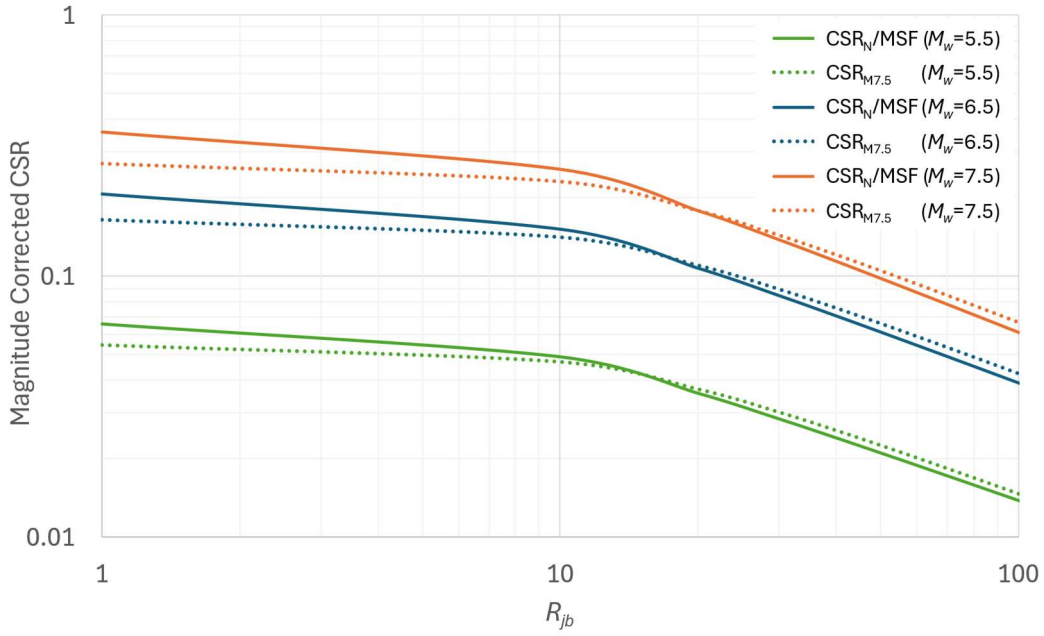

Figure 19. Comparison of median predictions for CSR_N/MSF and $CSR_{M7.5}$ by the models MS_N and $MS_{M7.5}$ respectively.

The estimated ground motion intensity in AB10 model, which is a_{max}, is replaced with CSR_N due to Eq.(31)(19). This modification does not affect any of the original coefficients of the AB10 model but the constant. Then, the modified AB10 model is

compared with the MS_N model with moment magnitudes equaling to 5.5, 6.5 and 7.5 for strike slip fault type. The results are presented in Figure 20.

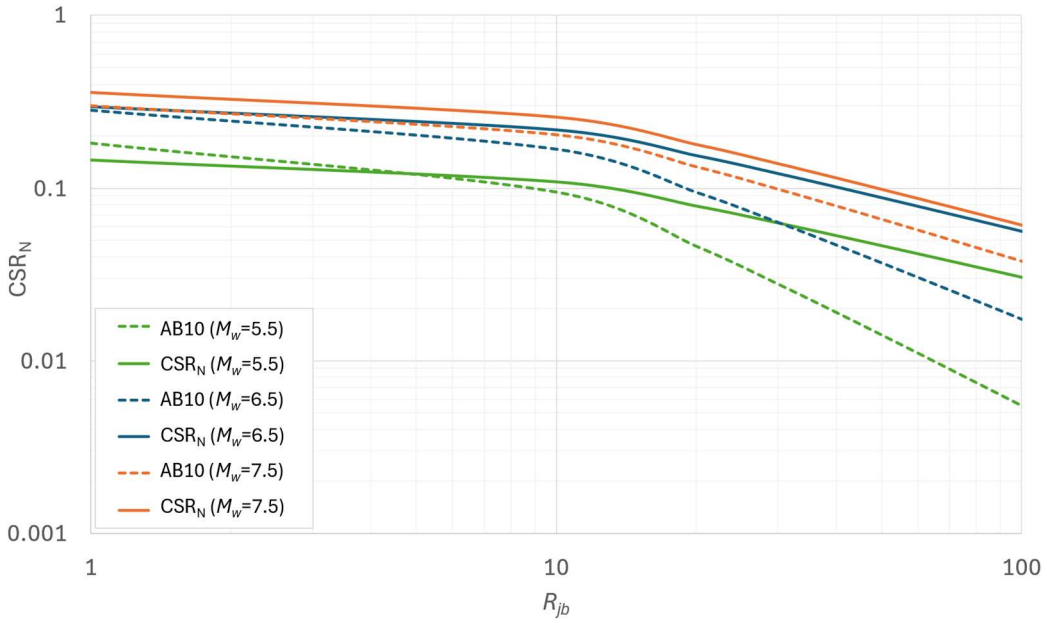

Figure 20. Comparison of median predictions for CSR_N by the models AB10 and MS_N respectively.

The predicted stress ratio values begin to diverge steeply after $R_{jb} > 10$ km. However, the rate of divergence decreases as the earthquake magnitude increases. It is also evident that MS_N model reveals higher CSR_N values for $R_{jb} > 10$ km distances. The disparity is mainly because of the difference in the sample, as shown in Figure 12. It is also supporting that consistent GMPE shall be used in calculation of significant MSF, or earthquake magnitude to be used in liquefaction analysis. The dependences of median predictions for CSR_N/MSF and that for $CSR_{M7.5}$ on earthquake magnitude are presented in Figure 21. Figure 21 also indicates that both prediction models MS_N and $MS_{M7.5}$ yield consistent results, except for large magnitude events (M_w>7) at short distances (R_{jb}<10 km). Since the effect of model variances are not included in this simple comparison, the hazard analyses can yield general conclusions about the agreement between two methods on the choice for average magnitude to be used in liquefaction potential assessment. These analyses are presented in Section 4.

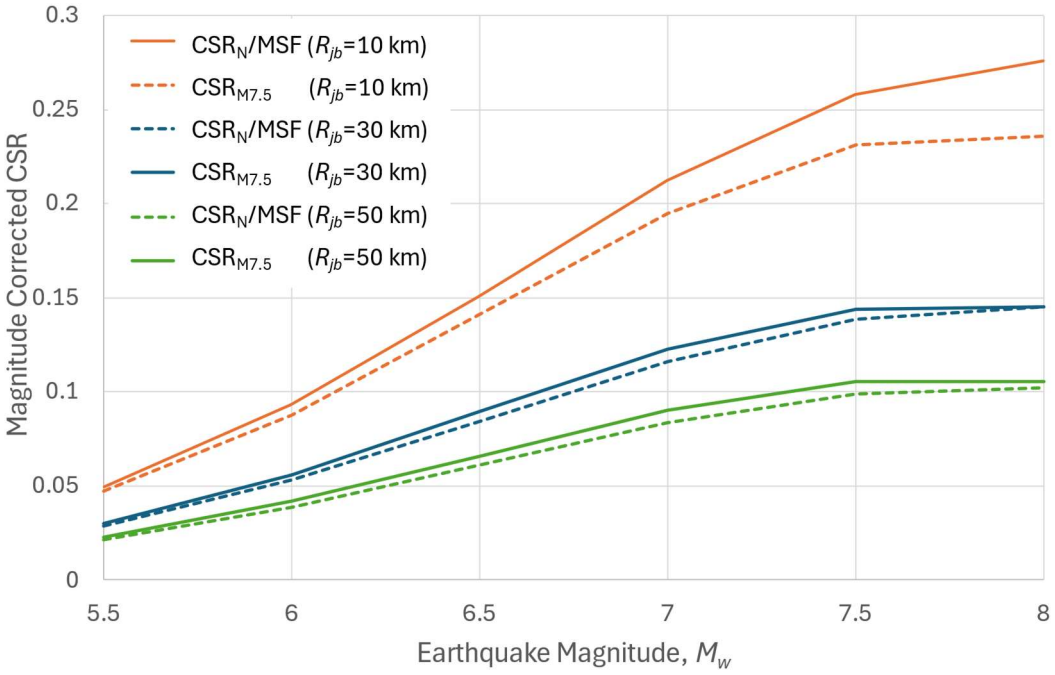

Figure 21. Comparison of median predictions for CSR_N/MSF and $CSR_{M7.5}$ by the models MS_N and $MS_{M7.5}$ respectively for M_w.

CHAPTER 4

SEISMIC HAZARD ANALYSIS

A probabilistic seismic hazard analysis is performed in the computer program R-Crisis (*http://www.r-crisis.com/*) by considering two generic faults as simple seismic sources. The sources 1 and 2 are fictitious line sources with 240 km and 60 km lengths respectively. These sources will be referred to as the long source (fault) or the short source (fault) respectively. Fault lengths were determined based on the relationships between fault length and earthquake magnitude proposed by Wells and Coppersmith (1994). Nevertheless, uniform seismicity along the faults is ensured during the analysis. These faults striking parallel to each other are 55 km away from each other. 7 calculation points are located between these faults as illustrated in Figure 22.

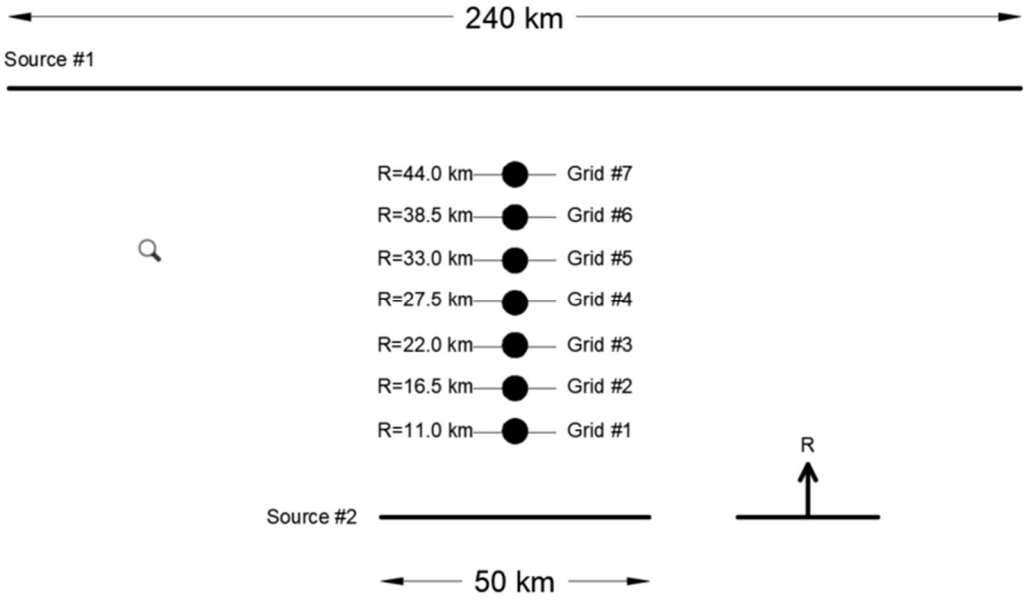

Figure 22. The generic faults and calculation (grid) points included in seismic hazard analysis.

Two different magnitude recurrence relationships that are explained in Section 2.5.2 are used in the analyses. Both sources are assigned with the same GMPE and magnitude-recurrence relationship in each analysis, except for the maximum magnitude of events on each source. The seismic hazard is computed for six combinations of different models, and for a practical set of probabilities of exceeding the intensity parameter in 50 years. The intensity parameter is CSR in general. In the following sections, a brief explanation of the analysis parameters is presented.

4.1 Intensity Parameters

The intensity parameters are chosen as CSR_N, $CSR_{M7.5}$, and CSR_N/MSF. The prediction equations MS_N and $MS_{M7.5}$ are used for the prediction of the first two intensity parameters respectively, whereas Eq. (10) is used for applying magnitude correction on CSR_N, such that the prediction by MS_N is divided by MSF for the respective seismic model. These prediction equations are presented in Section 3.4. A standard error is calculated for the prediction equations, as shown in Table 7. However, it is omitted in the hazard analysis for simplicity.

4.2 Magnitude-Recurrence Relationships

Seismic hazard analyses are performed by using the characteristic and the truncated exponential magnitude-recurrence relationships to see the significance of magnitude-recurrence model on average magnitude. The theoretical explanations of these models are presented in Section 1.2.4.

For the truncated exponential magnitude-recurrence relationship, the seismicity parameters assigned to each source within the computer program are presented in Table 11. These magnitude-recurrence relationships are graphically presented in Figure 23.

Table 11. Source seismicity parameters for truncated exponential magnitude-recurrence relationship.

Parameter	**Source 1 (240 km fault)**	**Source 2 (50 km fault)**
Threshold magnitude for the selected source, M_0	4.0	4.0
Average annual number of earthquakes with equal or higher magnitude than M_0, λ_o	6.5	0.26
Expected value of Beta, β	2.07	2.07
Coefficient of variation of Beta for the source, cov_β	0	0
Number of magnitudes to be used in the hazard integration process, n	50	50
Expected value of the maximum magnitude for the source, M_u	8.0	7.0
Uncertainty range (+/-)	0	0

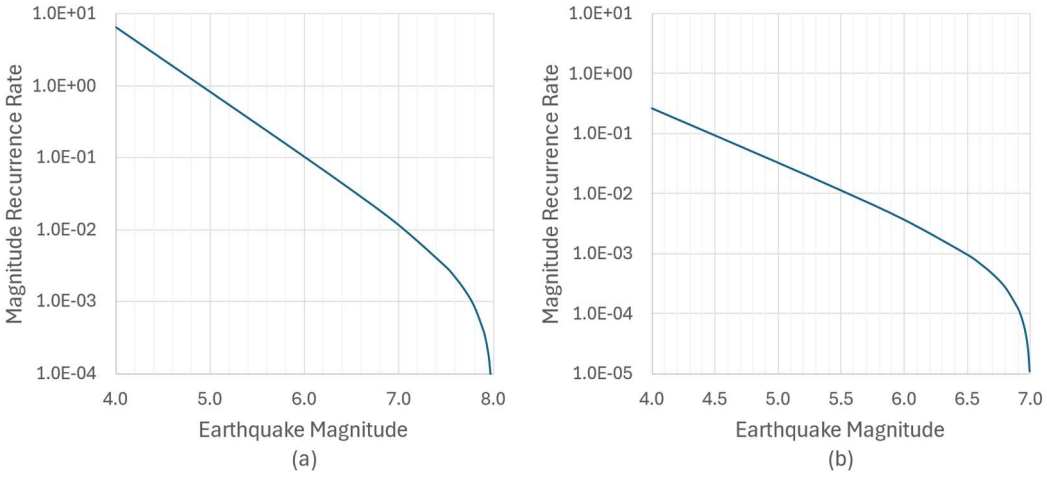

Figure 23. Exponential magnitude recurrence relationship for (a) the long source and (b) the short source.

For the characteristic magnitude-recurrence relationship, the seismicity parameters assigned to each source within the computer program are presented in Table 12. These magnitude-recurrence relationships are graphically presented in Figure 24.

Table 12. Source seismicity parameters for the characteristic magnitude-recurrence relationship.

Parameter	**Source 1 (240 km fault)**	**Source 2 (50 km fault)**
Median value of the time between characteristic earthquakes, t_m	125	400
Standard deviation of the magnitude of the characteristic earthquakes, s	1.0	1.0
Minimum possible magnitude of a characteristic earthquake, M_0	7.0	6.0
Maximum magnitude of the characteristic earthquake to be used in the integration process, M_u	8.0	7.0
Number of magnitudes to be used in the hazard integration process, n	9	9
D (EM when F is set to 0.)	8.0	7.0
F	0	0
Time elapsed, *T00*	1	1

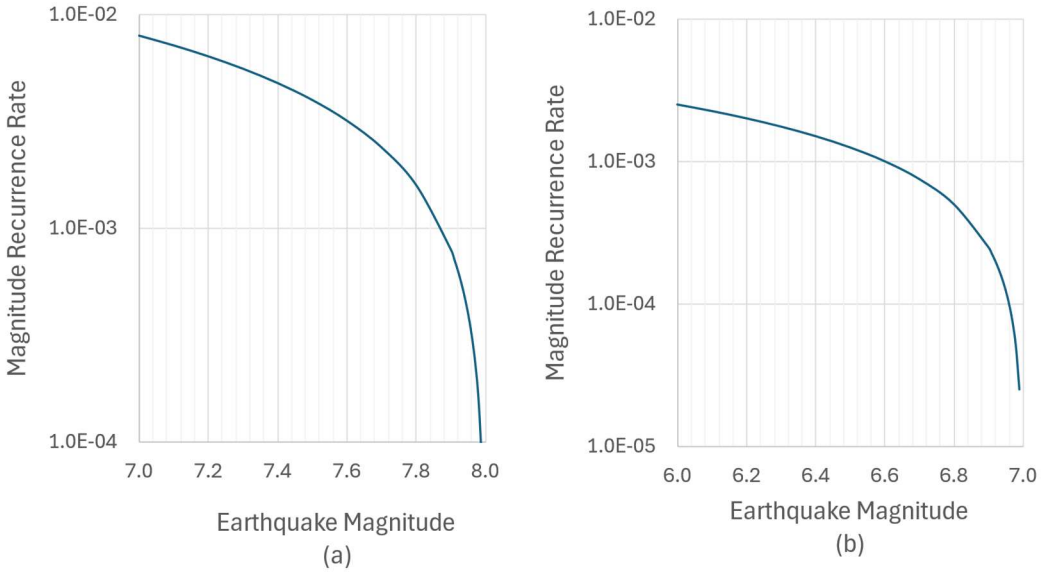

Figure 24. Magnitude recurrence for (a) long source and (b) short source due to the characteristic magnitude-recurrence relationship.

Figure 25 illustrates the use of truncated exponential magnitude-recurrence models, which are configured to generate a minimum earthquake magnitude M_w of 4.0 for

both sources. The maximum magnitudes are capped at 8.0 for the long source and 7.0 for the short source. For the case of characteristic magnitude-recurrence relationship, minimum magnitude is set 7.0 for the long source and 6.0 for the short source with maximum magnitudes similarly restricted to 8.0 and 7.0, respectively. The parameters of truncated exponential and characteristic magnitude-recurrence relationships are adjusted to ensure identical moment rates for each source.

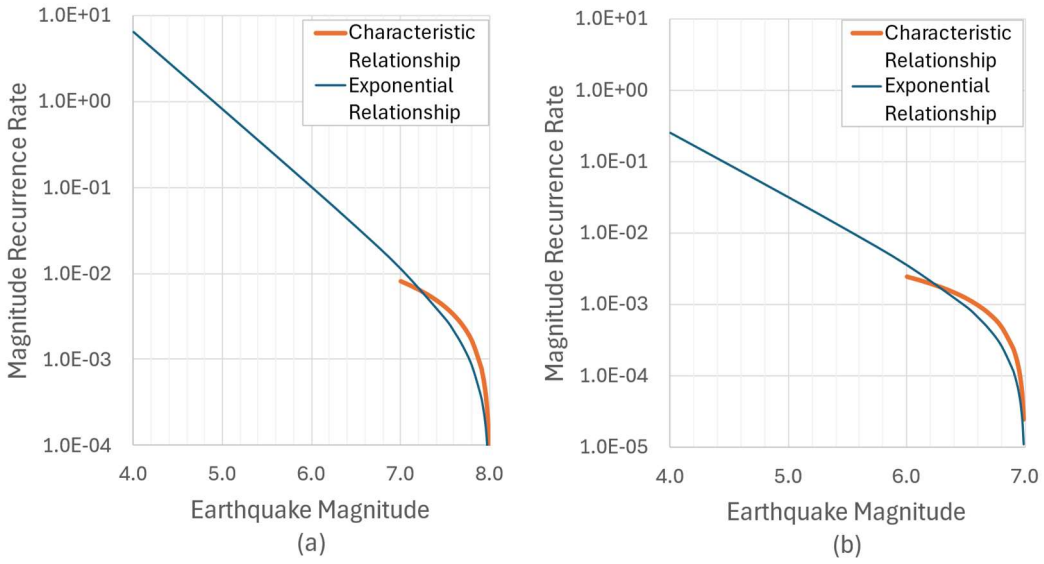

Figure 25. The comparison of magnitude recurrence rates for (a) long source and (b) short source.

4.3 The Results of Seismic Hazard Analysis

4.3.1 Truncated Exponential Magnitude-Recurrence Relationship

The hazard analysis is performed by using the MS_N, and $MS_{M7.5}$ models separately. Intensities of CSR_N, CSR_N/MSF and $CSR_{M7.5}$ for exceedance probability of 10% in 50 years at each calculation points are presented in Figure 26. The hazard curves for the intensity parameters CSR_N, CSR_N/MSF and $CSR_{M7.5}$ at the distances of 11.0, 27.5 and 44.0 km are shown in Figure 27. For a given exceedance probability, CSR_N

exceeds the magnitude-corrected intensities on all calculation points. For all the calculation points, the hazard curves for the $CSR_{M7.5}$ and CSR_N/MSF intensities align closely. This indicates that the *b* value derived in Eq. (10) to develop the GMPE for $CSR_{M7.5}$ has minimal influence on the exceedance probability for a given intensity. This suggests that the two different magnitude-correction methods for CSR would yield nearly identical magnitude effects at all calculation points.

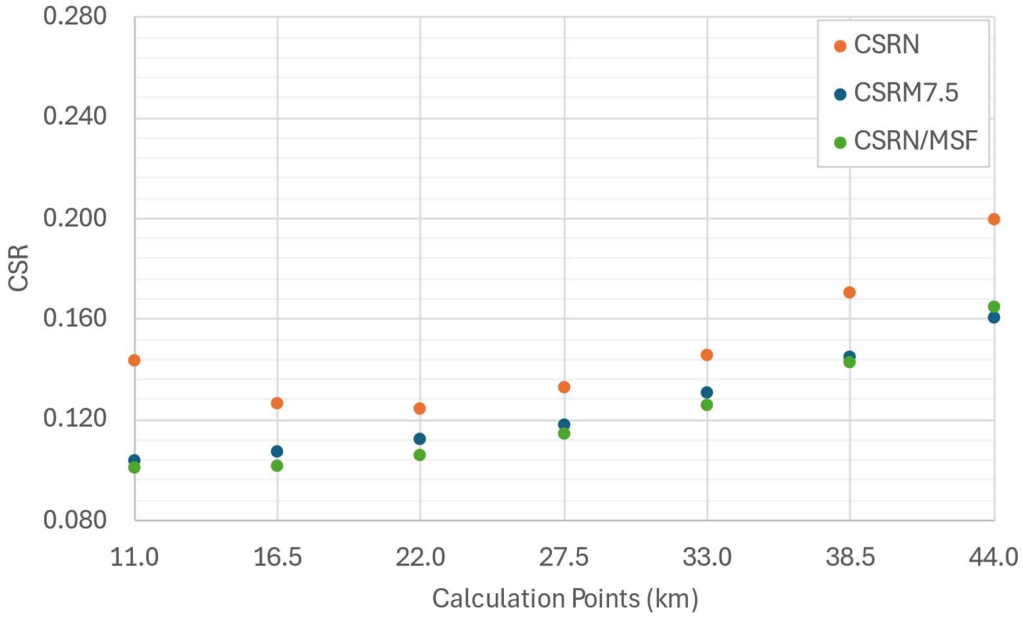

Figure 26. The variation of CSR_N, $CSR_{M7.5}$, and CSR_N/MSF between short and long fault in the case of truncated exponential magnitude-recurrence relationship.

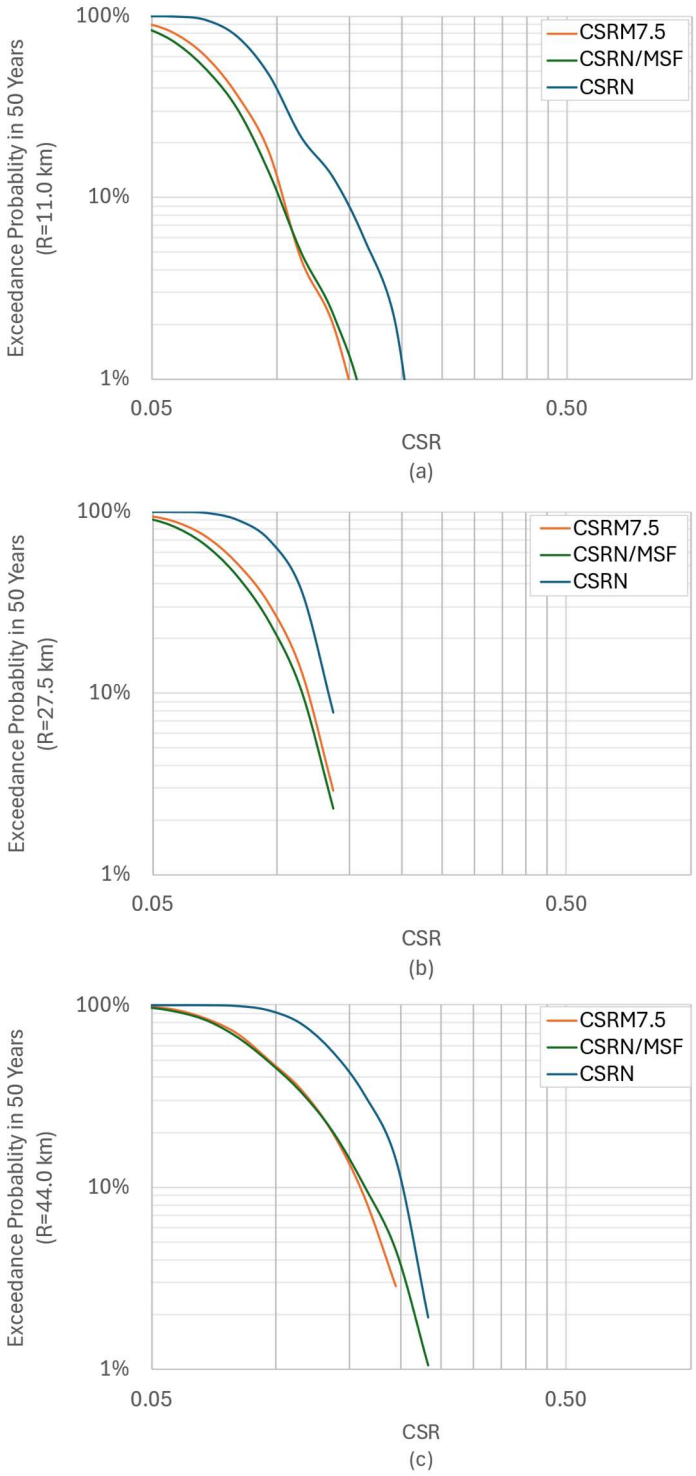

Figure 27. The hazard curves for the intensities CSR_N, CSR_N/MSF and $CSR_{M7.5}$ at the distances of (a) 11.0 km, (b) 27.5 km, and (c) 44.0 km from the short seismic source in the case of truncated exponential magnitude-recurrence model

4.3.2 Characteristic Magnitude-Recurrence Relationship

The hazard analysis is performed using MS_N and $MS_{M7.5}$ ground-motion models separately. The intensities of CSR_N, CSR_N/MSF and $CSR_{M7.5}$ for exceedance probability of 10% in 50 years at each calculation points are presented in Figure 28. The hazard curves for the intensity parameters CSR_N, CSR_N/MSF and $CSR_{M7.5}$ at the distances of 11.0, 27.5 and 44.0 km are shown in Figure 29. At shorter distances from the short seismic source, CSR_N yields higher exceedance probabilities when the intensities exceed 0.10. This disparity reduces as the calculation points approach the larger source, since the average magnitude for the longer fault is about 7.5, so that the magnitude correction becomes insignificant.

The curvature of the hazard is not smoothly changing particularly on the calculation point located at 11.0 km, and undulations in the hazard curve is very significant particularly for CSR_N. This is explained by the discontinuity in the magnitude-recurrence relationship, since a limited range of magnitudes can be generated by both sources.

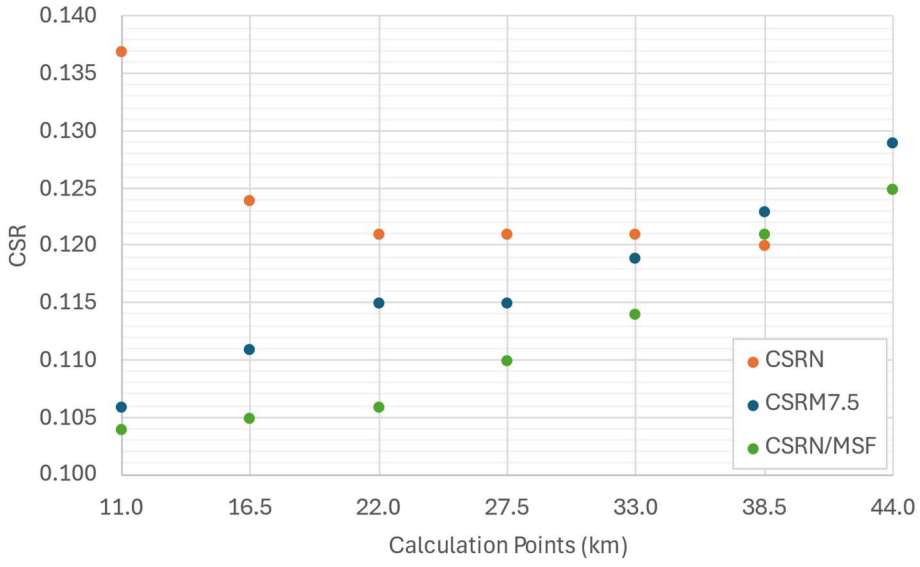

Figure 28. The variation of CSR_N, $CSR_{M7.5}$, and CRS_N/MSF between short and long fault in the case of characteristic magnitude-recurrence relationships.

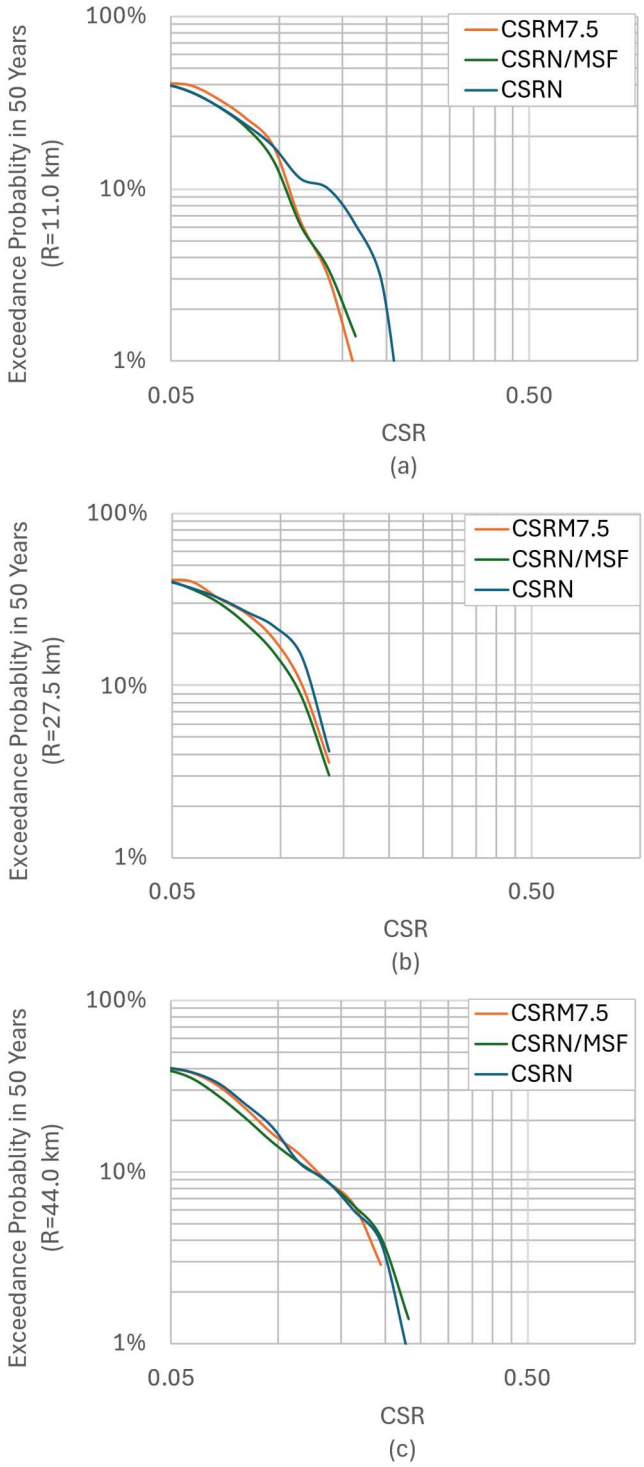

Figure 29. The hazard curves for the intensities CSR_N, CSR_N/MSF and $CSR_{M7.5}$ at the distances of (a) 11.0 km, (b) 27.5 km, and (c) 44.0 km from the short seismic source in the case of characteristic magnitude-recurrence relationship.

4.3.3 Comparison of Hazard among two Magnitude-Recurrence Models

The results of the seismic analysis performed by using characteristic and truncated exponential-recurrence relationships for $CSR_{M7.5}$ and CSR_N for exceedance probability of 10% in 50 years are presented in Figure 30. Both relationships yield similar results for distances shorter than 27.5 km from the short source, but the truncated exponential magnitude-recurrence model yields greater hazard on points close to longer fault.

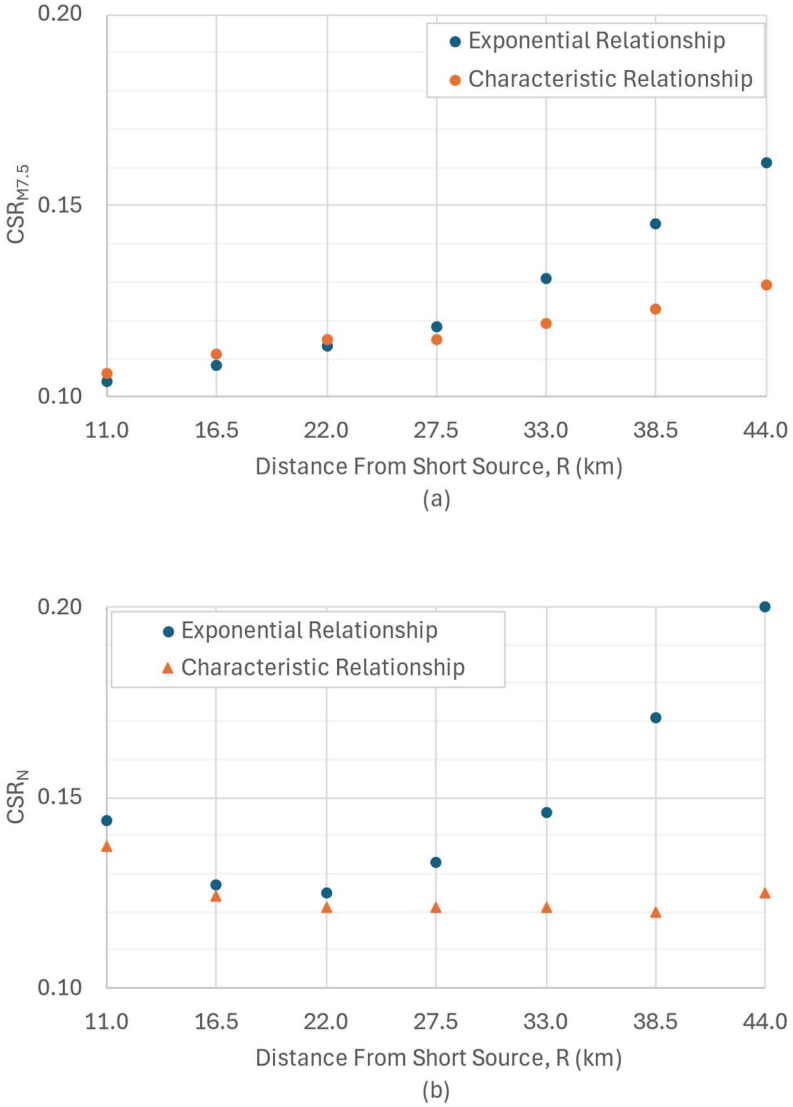

Figure 30 Hazard results for (a) $CSR_{M7.5}$ and (b) CSR_N

4.4 Disaggregation of Seismic Hazard

The seismic hazard is disaggregated to identify the dominant fault and earthquake magnitude contributing to the CSR_N at each grid. The program R-Crisis is capable of disaggregating the seismic hazard for the intensity parameter used. In Section 4.5, the average magnitude scaling factors are calculated for the 10% exceedance probability in 50 years. Then, the average scaling factor is converted to M_w by using Eq. (10). Finally, the magnitudes derived from the disaggregation technique in R-Crisis are compared with the average magnitude.

The disaggregation of hazard for CSR_N at 11.0 km distance from the short fault is presented in Figure 31 for the case of truncated exponential magnitude-recurrence relationship. The legend on the figure corresponds to exceedance probability rates for the magnitudes indicated in the chart in 50 years. This graphical presentation produced by the program shows the relative contributions of different magnitudes and distances to the seismic hazard at R=11.0 km. Figure 31 indicates that this calculation point is primarily influenced by magnitude M_w 6.4 earthquakes for R_{jb} between 0.0-20.0 km. Therefore, for this example, the short source is the predominant seismic source on this point.

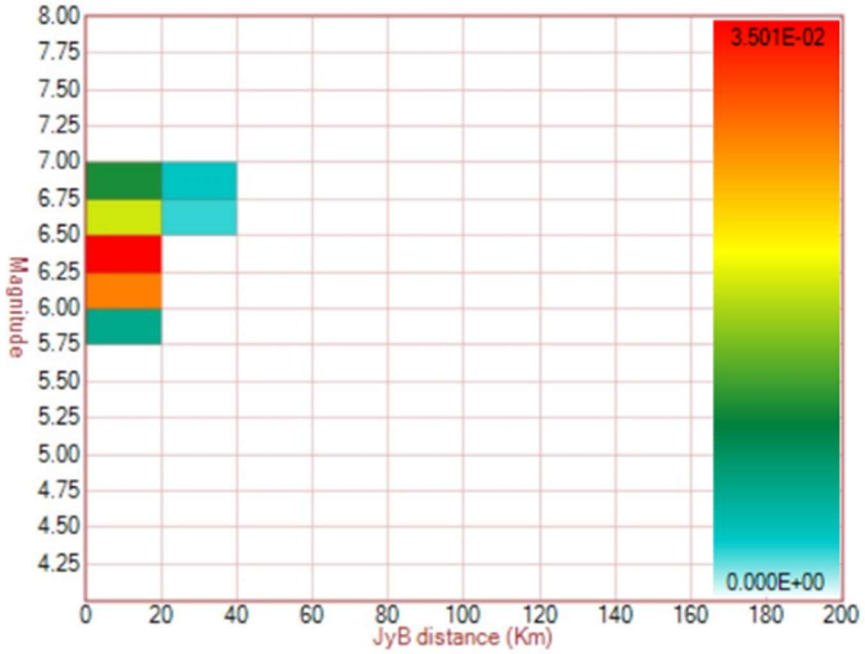

Figure 31. The disaggregation chart for CSR_N on the grid point at distance of 11.0 km in the case of truncated exponential magnitude-recurrence relationship.

The disaggregation of hazard for CSR_N at 11.0 km distance from the short fault is presented in Figure 32 for the case of characteristic magnitude-recurrence relationship. Figure 32 indicates that this calculation point is primarily influenced by magnitude M_w 6.6 earthquakes for R_{jb} between 0.0-20.0 km.

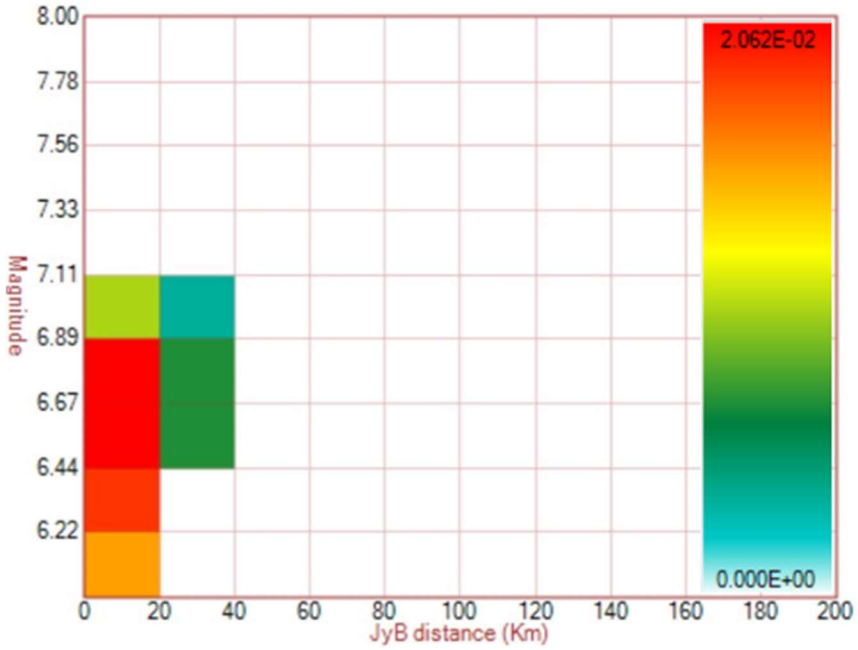

Figure 32. The disaggregation chart for CSR_N on the grid point at distance of 11.0 km in the case of characteristic magnitude-recurrence relationship.

The most significant magnitudes observed in the disaggregation of seismic hazard for both recurrence models in R-Crisis are presented in Figure 33. The results are provided for CSR_N having the probability of 10% being exceeded in 50 years. Noting that moment rates of sources are the same for both recurrence models, Figure 33 indicates that characteristic magnitude-recurrence relationship yields higher magnitudes, except for R=22.0 and R=27.5 km.

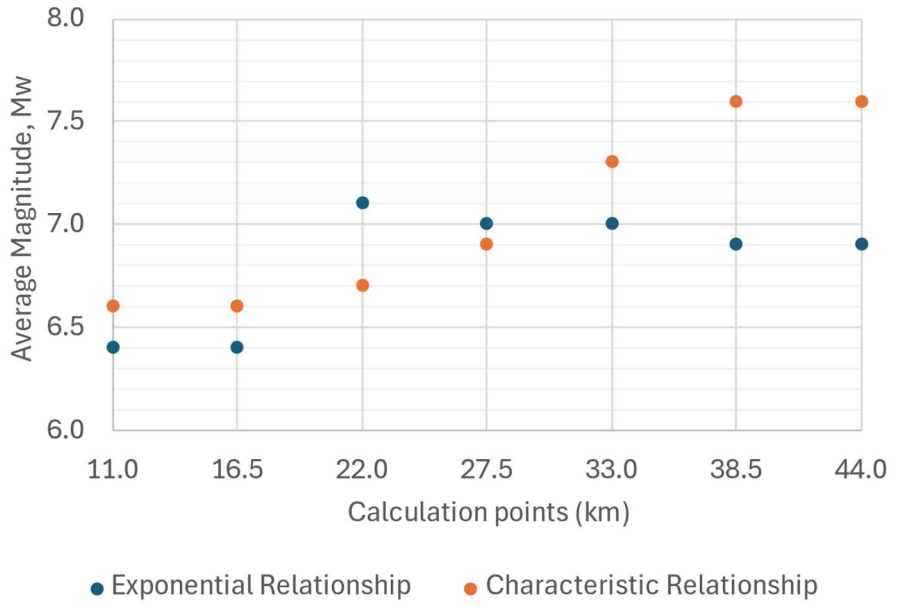

Figure 33. The most significant magnitudes due to disaggregation of hazard for CSR_N for the exceedance probability of 10% in 50 years.

4.5 Calculation of Average Magnitude

The intensities CSR_N, $CSR_{M7.5}$, and CSR_N/MSF corresponding to the 10% exceedance probability in 50 years are considered for calculation of the average magnitude scaling factors by using Eq. (9). In the use of CSR_N/MSF, this intensity parameter is substituted as $CSR_{M7.5}$ in Eq. (9). The calculated scaling factors are then converted to average M_w by Eq. (10) to determine the earthquake magnitude to be used in liquefaction potential assessment at this hazard level.

4.5.1 Truncated Exponential Magnitude-Recurrence Relationship

The magnitude scaling factors and corresponding magnitudes at each calculation points are presented in Figure 34 for the case of truncated exponential magnitude-recurrence relationship. Figure 34.b indicates that the uses of $CSR_{M7.5}$ and CSR_N/MSF for calculating average M_w yield reasonably consistent results with each

other. The maximum relative difference in M_w is 3%, observed at R = 22.0 km. Figure 34.b also presents the most significant M_w observed in disaggregation chart with the results obtained by the intensity ratios. The disaggregation results are reasonably consistent with average MSFs calculated by the two methods, except for R=16.5 km.

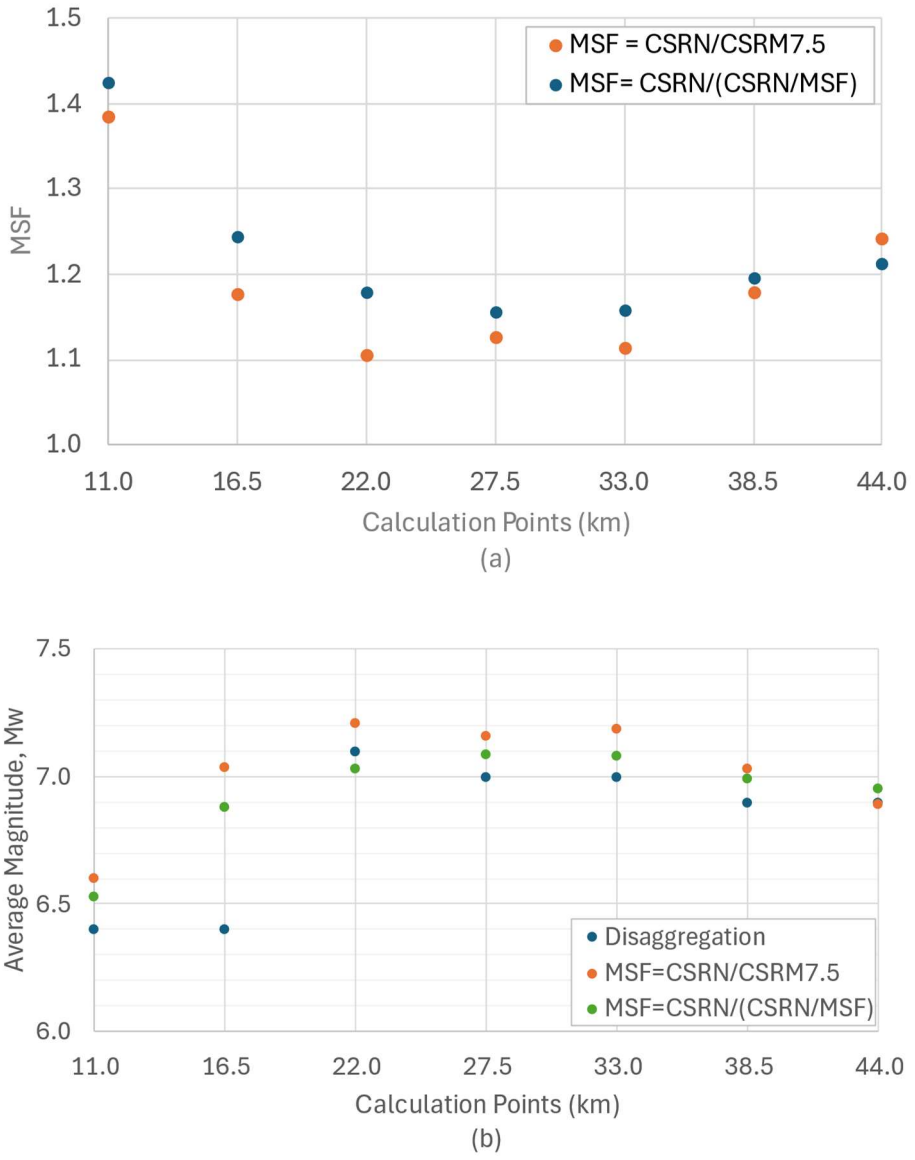

Figure 34. (a) MSFs and (b) corresponding average earthquake magnitudes on each calculation point for the case of truncated exponential magnitude-recurrence model.

4.5.2 Characteristic Magnitude-Recurrence Relationship

The magnitude scaling factors and corresponding magnitudes at each calculation points are presented in Figure 35 for the case of characteristic magnitude-recurrence relationship. Figure 35.b indicates that the uses of $CSR_{M7.5}$ and CSR_N/MSF for calculating average M_w yield reasonably consistent results with each other. The maximum relative difference in M_w is 3%, observed at R = 22.0 km. Figure 35.b also presents the most significant M_w observed in disaggregation chart with the results obtained by the intensity ratios. The disaggregation results are not consistent with average MSFs calculated by the two methods. This inconsistency occurs for distances from the short source between R=11.0 km and R= 27.5 km. There is a difference up to 9% between the M_w calculated from the disaggregation chart and average MSF calculated for $CSR_N/CSR_{M7.5}$ at R=22.0 km.

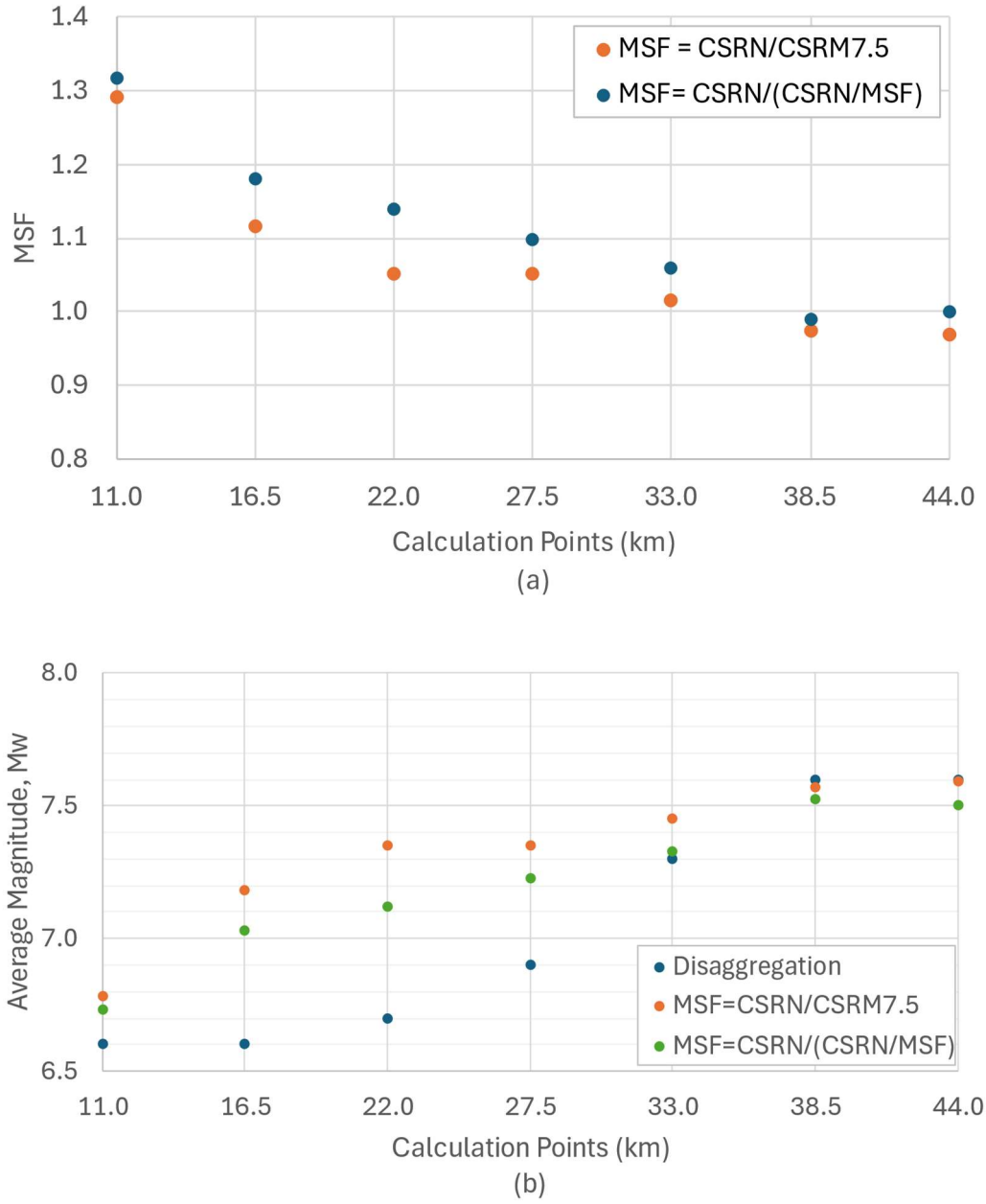

Figure 35. (a) MSFs and (b) corresponding average earthquake magnitudes on each calculation point for the case of characteristic magnitude-recurrence model.

4.5.3 Interpretation of the Effect of Magnitude-Recurrence Model

The comparison of M_w back-calculated by using Eq. (10) for both recurrence relationships are compared in Figure 36. It is observed that the characteristic magnitude-recurrence relationship results in higher magnitudes on each calculation point than those calculated due to the truncated exponential magnitude-recurrence relationship. This difference becomes more significant on points close to the long fault. This implies the magnitude-recurrence relationship has a significant effect on the average M_w for a specific hazard level.

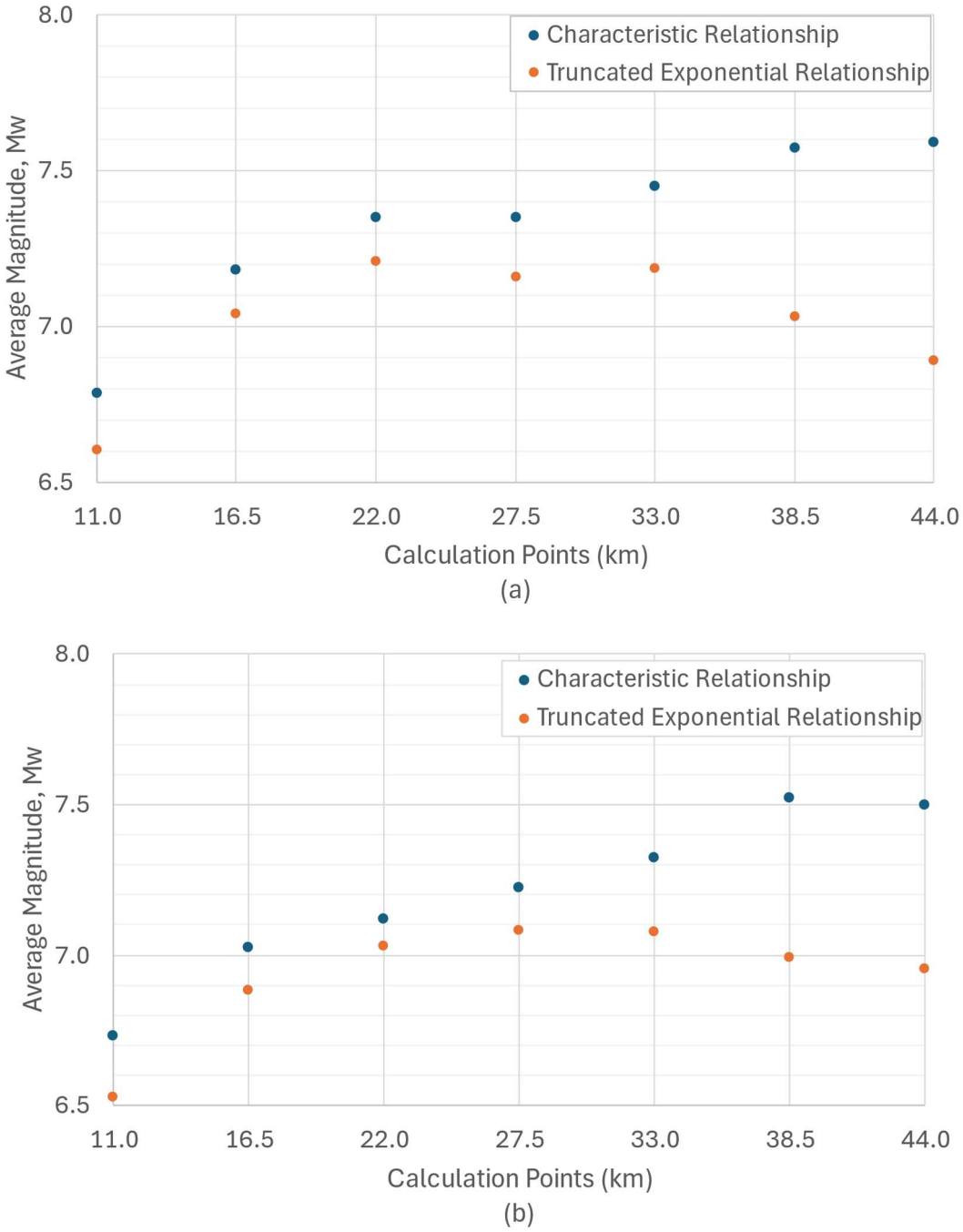

Figure 36. The comparison of average magnitudes calculated for (a) MSF = $CSR_N/CSR_{M7.5}$ and (b) MSF=$CSR_N/(CSR_N/MSF)$.

4.6 The Significance of the Choice for MSF Relationship

Alternative magnitude scaling factors proposed in literature may yield to different average magnitudes for liquefaction potential assessment. This is further investigated by using the MSFs of Seed and Idriss (1982), which is summarized in Section 1.2.2. Therefore, the relationship between the proposed MSFs and M_w in Eq. (38) is utilized for the same set of calculations. Consequently, another GMPE is developed based on the established relationship between the N_{eq} and M_w as defined in Eq. (39). Figure 37 presents a comparison of average M_w values due to Eq. (10) and due to Eq. (38) in the case of truncated exponential magnitude-recurrence model. The ratio of $CSR_N/CSR_{M7.5}$ is used to calculate MSF for the back-calculation of M_w.

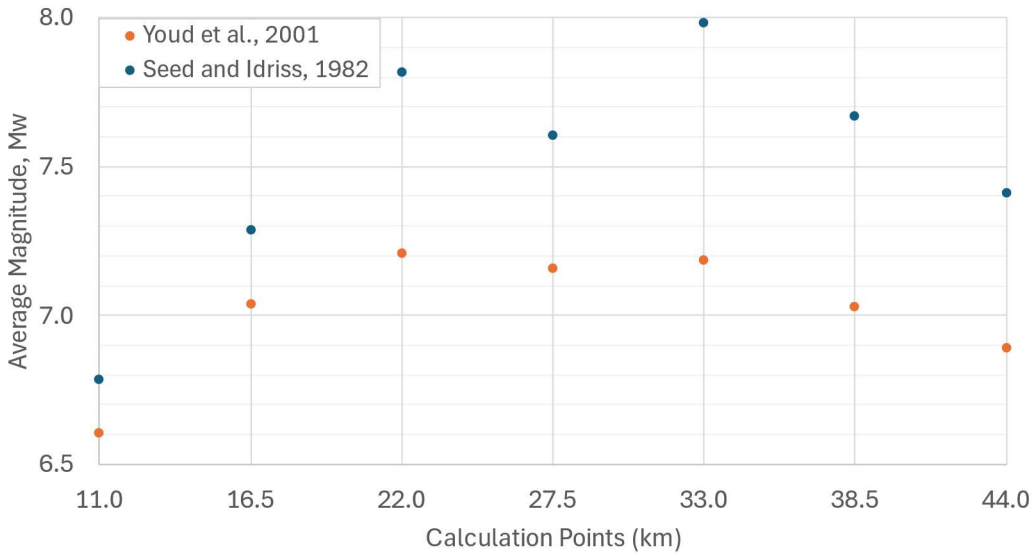

Figure 37. Average M_w due to MSFs of Youd et al. (2001), and that due to Seed and Idriss (1982).

Figure 37 illustrates that the averaged magnitudes derived by using MSF of Seed and Idriss (1982) are higher than those by MSF of Youd et al. (2001). An average magnitude of 8.0 is calculated at R = 33.0 km, which is the maximum magnitude the

long source can produce. Therefore, the magnitude to be used in liquefaction potential analysis is dependent on MSFs used.

4.7 The Effect of Exceedance Probability on Average Magnitude

To examine the effect of exceedance probability on average magnitude, the probability is changed from 10% in 50 years to 50% in 50 years. The analysis is redone using the $MS_{M7.5}$ prediction model for the truncated exponential magnitude-recurrence relationship. The comparison of MSFs calculated using Eq. (9) and the corresponding M_w derived from back-calculation using Eq. (10) are presented in Figure 38. It is observed that higher MSFs and, consequently, smaller magnitudes are calculated for an exceedance probability of 50% in 50 years. This result strongly suggests that average M_w to be used in liquefaction potential assessment depends on the hazard level, expressed as the probability of exceedance in a given period of time.

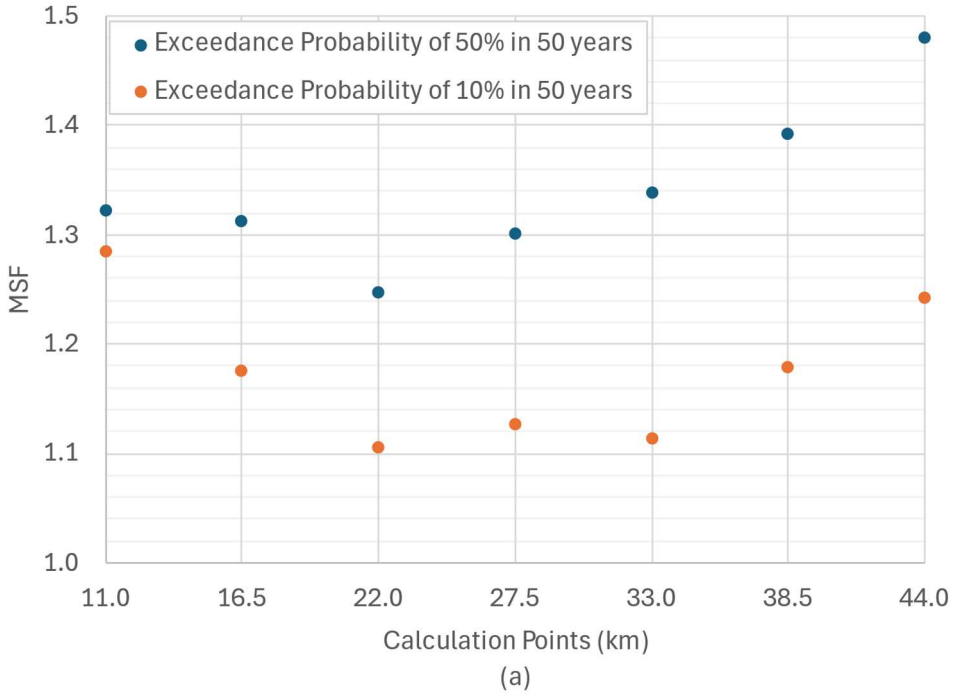

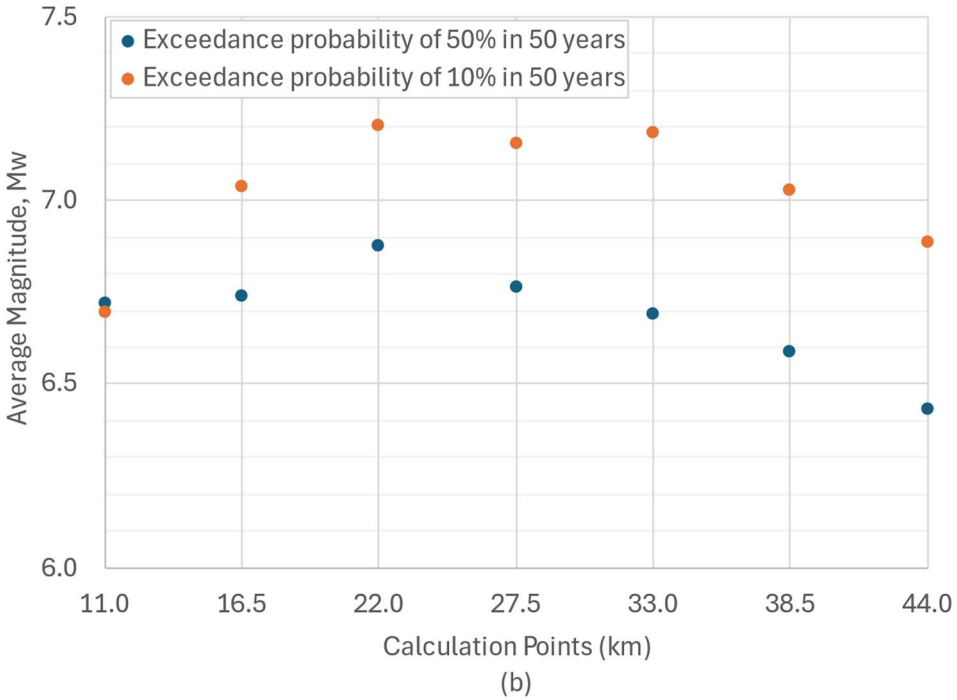

Figure 38. (a) MSFs and (b) corresponding magnitudes calculated for exceedance probability of 10% and %50 in 50 years for the truncated exponential magnitude-recurrence relationship.

CHAPTER 5

CONCLUSION

In this study, a method to estimate the magnitude to be considered in liquefaction potential assessment is suggested. The impact of earthquake magnitudes on seismic demand for liquefaction is represented by a relationship between the number of uniform shearing cycles and earthquake magnitudes. This relationship is developed by using the magnitude scaling factor suggested by Youd et al. in 2001, later implemented in 2018 Seismic Code of Türkiye. Then, prediction equations for cyclic stress ratio conditional to earthquake magnitude, distance to fault, fault type and seismic site condition were developed. These GMPEs are implemented in a probabilistic seismic hazard analysis involving two generic faults, such that one fault can produce much larger earthquake magnitudes. The hazard analysis resulted in the seismic stress ratio to be exceeded with a specific probability within a given time frame, so that the final effect of event magnitude can be calculated by comparing the results of two GMPEs. In this regard,

- The magnitude scaling factors, MSF, suggested as safe limits by Youd et al. (2001) yield to a relationship between equivalent number of uniform cycles and earthquake magnitude that is inconsistent with the experimental data in literature. On the other hand, the factors of Seed and Idriss (1982) are reasonably in agreement with the data.
- Two GMPEs are developed for predicting magnitude-corrected CSR. The predicted intensities are referred to as CSR_N/MSF and $CSR_{M7.5}$, respectively, where CSR_N denotes the uncorrected CSR value on ground. The equivalent number of uniform cycles is used in the prediction of $CSR_{M7.5}$, whereas CSR_N is adjusted using the MSF proposed by Youd et al. (2001) as an alternative to $CSR_{M7.5}$. Both models produce similar conditional estimations; however,

the variability is significant, as reflected by the low coefficient of determination (R^2=0.59).

- Comparing actual and predicted intensities for CSR_N and $CSR_{M7.5}$ reveals that $CSR_{M7.5}$ shows greater scatter due to variability in duration (or the number of stress cycles). This highlights the oversimplification involved in using techniques like disaggregation to determine M_w for liquefaction analysis.
- $CSR_{M7.5}$ and CSR_N/MSF predictions produce highly compatible results in hazard analysis. This indicates that *b*, which is used to calculate $CSR_{M7.5}$ has a negligible impact on the average magnitude. In other words, using MSF to adjust CSR_N after its prediction is just as effective as incorporating *b* for determining magnitude-corrected CSR. Therefore, the GMPEs developed for PGA predictions can be simply normalized by MSF to compute the seismic hazard for liquefaction potential assessment, and consequently for estimation of average magnitude.
- Back-calculating average magnitude from hazard results shows that the use of CSR_N/MSF or $CSR_{M7.5}$ predictions for average MSF yields similar results for both magnitude-recurrence models. The maximum difference was not greater than 3% for the generic hazard analysis.
- The characteristic magnitude-recurrence relationship produces higher average magnitudes than the truncated exponential relationship for both MSF calculations as expected. The difference becomes more pronounced at calculation points close to the long source. This can be explained by the lack of contribution of smaller magnitude events in seismic hazard in the case of characteristic magnitude-recurrence relationships. Therefore, the magnitude-recurrence relationships modeling the seismic activity significantly affect the average magnitude to be used liquefaction assessments.
- Using the MSFs proposed by Seed and Idriss (1982) as an alternative for calculating average magnitude results in figures greater than those calculated

due to MSFs suggested by Youd et al. (2001). Therefore, the magnitude to be used in liquefaction potential analysis is dependent on MSFs used.

- The seismic hazard analyses of CSR justified that an increase in the exceedance probability leads to smaller average magnitudes to be considered in liquefaction potential assessments.

For future works, it is recommended to enhance CSR estimates and their variances through the application of advanced GMPE techniques. Following this, the effect of variance should be incorporated into the hazard analysis. Finally, the study can be conducted on a national scale for Türkiye, such that the analysis of Seismic Hazard Map of Türkiye can involve the calculation of average magnitude for liquefaction analysis through calculating $CSR_{M7.5}/CSR_N$ ratios, since the available seismic hazard map can only suggest the cyclic stress ratio on ground without any magnitude correction.

REFERENCES

Akkar S., & Bommer JJ. (2014). Empirical Equations for the Prediction of PGA, PGV, and Spectral Accelerations in Europe, the Mediterranean Region, and the Middle East. Seismological Research Letters

Andrus, R. D., and Stokoe, K. H., II. (2000). ‘‘Liquefaction resistance of soils from shear-wave velocity.’’ J. Geotech. and Geoenvir. Engrg., ASCE, 126(11), 1015–1025.

Annaki M. et al. (1977) Equivalent Uniform Cycle Concept for Soil Dynamics, Journal Of The Geotechnical Engineering Division

Arango, I. (1996). Magnitude scaling factors for soil liquefaction evaluations, J. Geotech. Eng., ASCE, 122(11), 929–936

Boulanger RW, Idriss IM (2004). Semi-Empirical Procedures for Evaluating Liquefaction Potential During Earthquakes, Department of Civil and Environmental Engineering, University of California

Boulanger RW, Idriss IM (2014). CPT and SPT based liquefaction triggering procedures. (Report No. UCD/CGM-14/01). Davis, CA: Center for Geotechnical Modeling, Department of Civil and Environmental Engineering, University of California

Cetin, K. O., et al. (2004). SPT-based probabilistic and deterministic assessment of seismic soil liquefaction potential. J. Geotech. Geoenviron. Eng., 130(12), 1314– 1340

Green, R. A., & Terri, G. A. (2005). Number of equivalent cycles concept for liquefaction evaluations—Revisited. J. Geotech. Geoenviron. Eng., 131(4), 477–488.

Idriss, I.M., & Boulanger RW (2008). Soil Liquefaction During Earthquakes, Earthquake Engineering Research Institute, MNO-12

Kale, Özkan & Akkar, Sinan & Ansari, Anooshiravan & Hamzehloo, Hosseyn. (2015). A Ground-Motion Predictive Model for Iran and Türkiye for Horizontal PGA, PGV, and 5% Damped Response Spectrum: Investigation of Possible Regional Effects. Bulletin of the Seismological Society of America.

Kayen R. et al. (2013) Shear-Wave Velocity–Based Probabilistic and Deterministic Assessment of Seismic Soil Liquefaction Potential, Journal of Geotechnical and Geoenvironmental Engineering

Kramer S. L. (1996). Geotechnical earthquake engineering, Prentice-Hall, Englewood Cliffs, N. J., 653.

Lasley, Sam & Green, Russell & Rodriguez-Marek, Adrian. (2017). Number of Equivalent Stress Cycles for Liquefaction Evaluations in Active Tectonic and Stable Continental Regimes. Journal of Geotechnical and Geoenvironmental Engineering.

Liu, A. H. (2001). Equivalent number of uniform stress cycles for soil liquefaction analysis. MS thesis, Dept. Of Civ. Engrg., University of California, Los Angeles

Liu, A. H., Stewart, J. P., Abrahamson, N. A., & Moriwaki, Y. (2001). Equivalent number of uniform stress cycles for soil liquefaction analysis. J. Geotech. Geoenviron. Eng., 127(12), 1017–1026.

McGuire R (2004) Seismic hazard and risk analysis, Earthquake Engineering Research Institute

Ordaz M and Salgado-Galvez M A (2019) R-CRISIS Validation and Verification Document, Mexico City: ERN Technical Report

Pillai, V. S., and Stewart, R. A. (1994). "Evaluation of liquefaction potential of foundation soils at Duncan Dam." Canadian Geotechnical Journal, 31, 951-966.

Seed, H. B., & Idriss, I. M. (1971). Simplified procedure for evaluating soil liquefaction potential. J. Soil Mech. Found. Div., 97(9), 1249–1273.

Seed, H. B., Idriss, I. M., Makdisi, F., & Banerjee, N. (1975). Representation of irregular stress time histories by equivalent uniform stress series in liquefaction analysis. Rep. No. EERC75-29, Earthquake Engineering Research Center, College of Engineering, Univ. of CA, Berkeley, CA.

Seed, H. B., & Idriss, I. M. (1982). Ground motion and soil liquefaction during earthquakes. Earthquake Engineering Res. Institute Monograph, Oakland, CA

Yoshimi, Y., Tokimatsu, K., and Hosaka, Y. (1989). "Evaluation of liquefaction resistance of clean sands based on high-quality undisturbed samples." Soils and Foundations, 29(1), 93-104.

Stewart, Jonathan & Douglas, John & Javanbarg, Mohammad & Bozorgnia, Yousef & Boore, David & Campbell, Kenneth & Delavaud, Elise & Erdik, Mustafa & Stafford, Peter. (2013). Selection of Ground Motion Prediction Equations for the Global Earthquake Model.

Wells, Donald & Coppersmith, K. (1994). New Empirical Relationships among Magnitude, Rupture Length, Rupture Width, Rupture Area, and Surface Displacement. Bulletin of the Seismological Society of America. 84. 974-1002. 10.1785/BSSA0840040974.

Youd, T. (1991). Mapping of earthquake-induced liquefaction for seismic zonation. Proceedings of the 4th International Conference on Seismic Zonation. 1. 111-147.

Youd, T. & Idriss, I. & Andrus, Ronald & Arango, Ignacio & Castro, Gonzalo & Christian, John & Dobry, Richardo & Finn, Liam & Jr, Leslie & Koester, Joseph & Liao, Sam & Marcuson, William. (2001). Liquefaction Resistance of Soils: Summary Report from the 1996 NCEER and 1998 NCEER/NSF Workshops on Evaluation of Liquefaction Resistance of Soils. Journal of Geotechnical and Geoenvironmental Engineering.

Youd, T.L. and Noble, S.K. (1997) Magnitude Scaling Factors. NCEER Workshop on Evaluation of Liquefaction Resistance of Soils, National Center for Earthquake Engineering Research, State University of New York at Buffalo, 149-165

Youd, T. & Perkins, David. (1978). Mapping Liquefaction-Induced Ground Failure Potential. ASCE J Geotech Eng Div. 104. 433-446. 10.1061/AJGEB6.0000612.

Youngs, R.R., & Coppersmith K.J. (1985). Implications of fault slip rates and earthquake recurrence models to probabilistic seismic hazard estimates. Bulletin of the Seismological Society of America, Vol. 75, No. 4, pp. 939-964

Ziotopoulou, K., and Boulanger, R. W. (2012). "Constitutive modeling of duration and overburden effects in liquefaction evaluations." 2nd International Conference on Performance-Based Design in Earthquake Geotechnical Engineering, ISSMGE, Taormina, Italy, May 28-30, paper no. 03.10, 467-482.

APPENDICES

A. Calculation of CSRs

The steps to calculate the CSR_N and $CSR_{M7.5}$ for a fictious ground motion record are outlined by the following steps, followed by an example.

Step 1. Calculation of CSR on ground surface by

$$CSR_N = \frac{0.65 a_{max}}{g}$$

Step 2. Calculation of equivalent number of cycles by using the peak counting method of Seed et al. (1975), such that

$$N_{eq} = \frac{1}{2}\sum\left(\left|\frac{0.65 \times a_{max}}{a_{peak}}\right|\right)^{\frac{1}{b}}$$

Step 3. Formation of a logarithmic relationship between N_{eq} and M_w by equating the MSF relationship recommended by Youd et al. (2001) for estimation of b that is consistent with the data, such that

$$N_{eq} = N_{M7.5} \times 10^{\left(\frac{-2.24}{b}\right)} \times M_w^{\left(\frac{2.56}{b}\right)}$$

or, for regression

$$log\left(N_{eq}\right) = \frac{1}{b} log\left(\frac{M_w^{2.56}}{10^{2.24}}\right) + log(N_{M7.5})$$

Consequently, b and $N_{M7.5}$ are estimated by using least-squares regression. In case the regressed b is not consistent with that used in Step 2, Step 2 followed by Step 3 are recalculated. The iterations are finalized when b presumed in Step 2 is consistent with that calculated in Step 3.

Step 4. For each record, $CSR_{M7.5}$ is calculated by multiplying CSR_N of the record with the number of cycles (N_{eq}) normalized by $N_{M7.5}$. $CSR_{M7.5}$ is later used in developing magnitude corrected GMPEs. The correction is done by the equation

$$CSR_{M7.5} = CSR_N \left(\frac{N_{eq}}{N_{M7.5}}\right)^b$$

which is Eq. (25).

Example: Consider the following simple artificial accelerogram with M_w=5.5 and a_{max}=1.5g in which the peak accelerations are identified according to Seed et al. (1975) as shown in Figure B1.

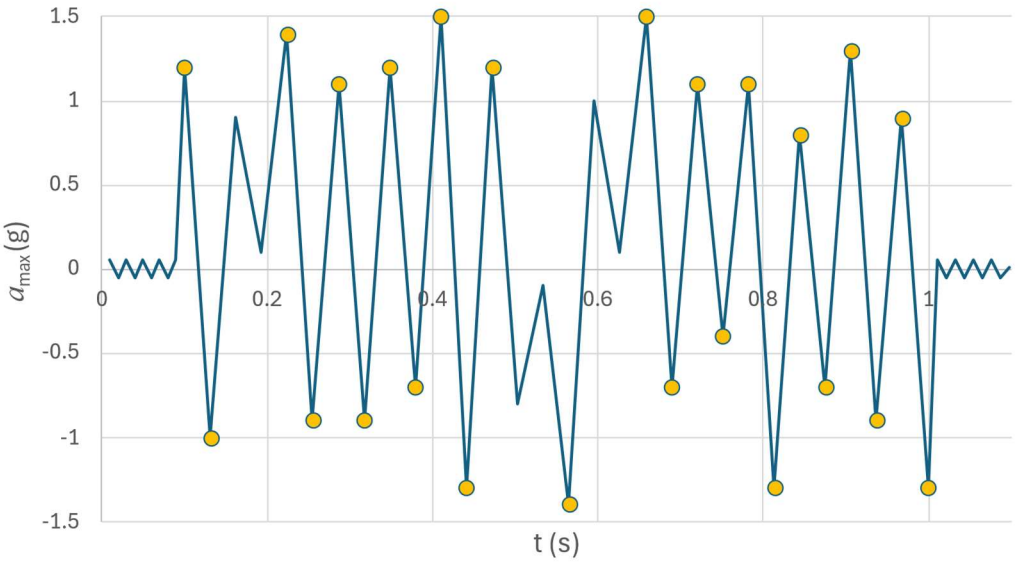

Figure B1. Fictious accelerogram.

1) CSR_N is calculated as 0.65 ·a_{max} / g = 0.975
2) The peak accelerations are used for counting the equivalent number of cycles at 65% of the maximum acceleration for presumed b of 0.2 as shown in Table B1. Consequently N_{eq} is calculated for all available records for b=0.2.

Table B1. N_{eq} calculations for the artificial record (b=0.2) in Step 1.

t (s)	a_{peak} (g) for each half cycle	N_{eq}
0.10	1.20	2.82
0.13	1.00	1.13
0.22	1.40	6.10
0.26	0.90	0.67
0.29	1.10	1.83
0.32	0.90	0.67
0.35	1.20	2.82
0.38	0.70	0.19
0.41	1.50	8.62
0.44	1.30	4.21
0.47	1.20	2.82
0.57	1.40	6.10
0.66	1.50	8.62
0.69	0.70	0.19
0.72	1.10	1.83
0.75	0.40	0.01
0.78	1.10	1.83
0.81	1.30	4.21
0.84	0.80	0.37
0.88	0.70	0.19
0.91	1.30	4.21
0.94	0.90	0.67
0.97	0.90	0.67
1.00	1.30	4.21
Sum:		**65.03**
N_{eq} for the record:		**32.51**

3) A logarithmic relationship between N_{eq} and M_w for b=0.2 is regressed as shown in Figure B2 for all N_{eq} sample. The estimated model coefficients are presented on the first data row in Table B2. Since b=0.91 is not equal to the presumed value of b=0.2, iterations continued until an agreement at b=0.96 between two steps is found. This agreement is shown in Table B2. The final calculations for N_{eq} are presented in Table B3 for this artificial record.

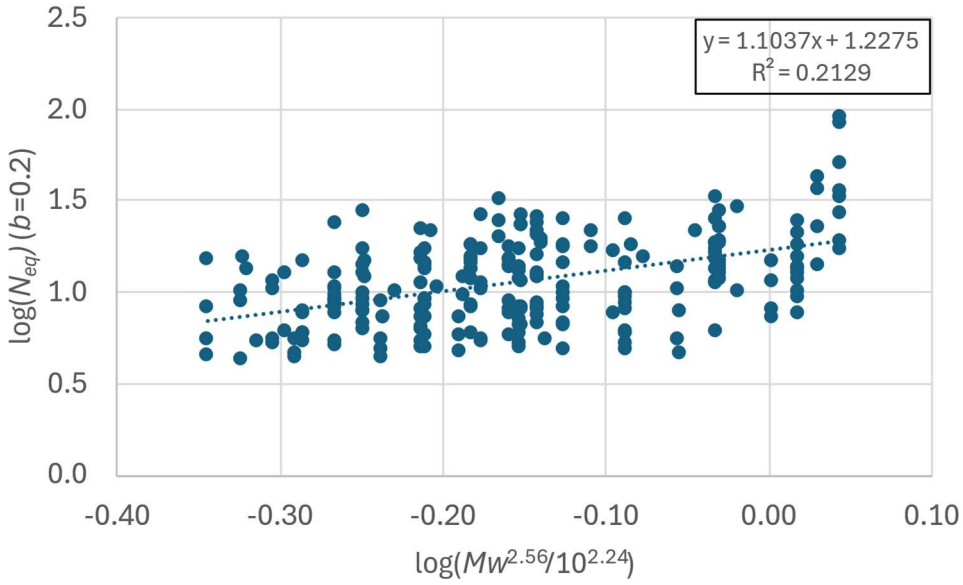

Figure B2. Least squares regression on the data due to b=0.2.

Table B2. Iteration table for b and $N_{M7.5}$.

Presumed b	1 / b	log($N_{M7.5}$)	b	$N_{M7.5}$
0.20	1.1	1.23	0.91	16.88
0.90	1.07	1.46	0.94	28.76
0.96	1.04	1.49	**0.96**	**30.70**

Table B3. N_{eq} calculations for the fictious record (b=0.96).

t (s)	a_{peak} (g) for each half cycle	N_{eq}
0.10	1.20	1.24
0.13	1.00	1.03
0.22	1.40	1.46
0.26	0.90	0.92
0.29	1.10	1.13
0.32	0.90	0.92
0.35	1.20	1.24
0.38	0.70	0.71
0.41	1.50	1.57
0.44	1.30	1.35
0.47	1.20	1.24
0.57	1.40	1.46
0.66	1.50	1.57
0.69	0.70	0.71
0.72	1.10	1.13
0.75	0.40	0.40
0.78	1.10	1.13
0.81	1.30	1.35
0.84	0.80	0.81
0.88	0.70	0.71
0.91	1.30	1.35
0.94	0.90	0.92
0.97	0.90	0.92
1.00	1.30	1.35
Sum:		**26.61**
N_{eq} for the record:		**13.31**

4) The magnitude-corrected CSR for the artificial record is calculated by

$$CSR_{M7.5} = 0.975\left(\frac{13.31}{30.70}\right)^{0.96} = 0.437$$

This calculation is applied to all accelerograms in the sample, so that prediction equations for $CSR_{M7.5}$ can be statistically constructed.

B. Earthquake Records

#	Earthquake Name	Station	M_w	*Vs30* (m/s)	PGA (g)	R_{jb} (km)	Mechanism
1	Northridge-01	LA - S Grand Ave	6.69	285.28	0.279	29.52	Reverse
2	Northridge-01	Newhall - Fire Sta	6.69	269.14	0.590	3.16	Reverse
3	Northridge-01	Newhall - W Pico Canyon Rd.	6.69	285.93	0.419	2.11	Reverse
4	Northridge-01	Northridge - 17645 Saticoy St	6.69	280.86	0.459	0.00	Reverse
5	Northridge-01	Pacific Palisades - Sunset	6.69	191.06	0.461	13.34	Reverse
6	Dinar_ Türkiye	Dinar	6.40	219.75	0.326	0.00	Normal
7	Kocaeli_ Türkiye	Ambarli	7.51	175	0.253	68.09	strike slip
8	Kocaeli_ Türkiye	Bursa Tofas	7.51	289.69	0.101	60.43	strike slip
9	Kocaeli_ Türkiye	Duzce	7.51	281.86	0.364	13.60	strike slip
10	Kocaeli_ Türkiye	Yarimca	7.51	297	0.322	1.38	strike slip
11	Chi-Chi_ Taiwan	CHY002	7.62	235.13	0.137	24.96	Reverse Oblique
12	Chi-Chi_ Taiwan	CHY004	7.62	271.3	0.097	47.32	Reverse Oblique
13	Chi-Chi_ Taiwan	CHY008	7.62	210.73	0.129	40.43	Reverse Oblique
14	Chi-Chi_ Taiwan	CHY015	7.62	228.66	0.152	38.13	Reverse Oblique
15	Chi-Chi_ Taiwan	CHY016	7.62	200.86	0.107	66.64	Reverse Oblique
16	Chi-Chi_ Taiwan	CHY025	7.62	277.5	0.162	19.07	Reverse Oblique
17	Northwest Calif-03	Ferndale City Hall	5.80	219.31	0.111	53.73	strike slip
18	Chi-Chi_ Taiwan	CHY036	7.62	233.14	0.273	16.04	Reverse Oblique
19	Chi-Chi_ Taiwan	CHY039	7.62	201.21	0.116	31.87	Reverse Oblique
20	Chi-Chi_ Taiwan	CHY047	7.62	169.52	0.181	24.13	Reverse Oblique
21	Chi-Chi_ Taiwan	CHY054	7.62	172.1	0.096	48.49	Reverse Oblique
22	Chi-Chi_ Taiwan	CHY055	7.62	225.77	0.099	54.30	Reverse Oblique
23	Friuli_ Italy-01	Codroipo	6.50	249.28	0.091	33.32	Reverse
24	Gazli_ USSR	Karakyr	6.80	259.59	0.864	3.92	Reverse
25	Coyote Lake	Gilroy Array #2	5.74	270.84	0.256	8.47	strike slip

26	Coyote Lake	Gilroy Array #4	5.74	221.78	0.252	4.79	strike slip
27	Imperial Valley-06	Aeropuerto Mexicali	6.53	259.86	0.307	0.00	strike slip
28	Duzce_ Türkiye	Bolu	7.14	293.57	0.806	12.02	strike slip
29	Duzce_ Türkiye	Duzce	7.14	281.86	0.515	0.00	strike slip
30	Imperial Valley-06	Bonds Corner	6.53	223.03	0.777	0.44	strike slip
31	Manjil_ Iran	Rudsar	7.37	242.05	0.097	63.96	strike slip
32	Manjil_ Iran	Tonekabun	7.37	289.69	0.137	93.30	strike slip
33	Sierra Madre	Tarzana - Cedar Hill A	5.61	257.21	0.098	46.45	Reverse
34	Northridge-02	Arleta - Nordhoff Fire Sta	6.05	297.71	0.101	1.48	Reverse
35	Northridge-02	Downey - Co Maint Bldg	6.05	271.9	0.051	42.80	Reverse
36	Northridge-02	LA - Baldwin Hills	6.05	297.07	0.114	25.57	Reverse
37	Northridge-02	LA - Century City CC North	6.05	277.98	0.111	18.34	Reverse
38	Imperial Valley-06	Delta	6.53	242.05	0.350	22.03	strike slip
39	Imperial Valley-06	El Centro - Meloland Geot. Array	6.53	264.57	0.317	0.07	strike slip
40	Imperial Valley-06	El Centro Array #11	6.53	196.25	0.379	12.56	strike slip
41	Northwest China-03	Jiashi	6.10	240.09	0.300	9.98	Normal
42	Hector Mine	Indio - Riverside Co Fair Grnds	7.13	282.14	0.124	74.00	strike slip
43	Imperial Valley-06	El Centro Array #4	6.53	208.91	0.484	4.90	strike slip
44	Imperial Valley-06	El Centro Array #5	6.53	205.63	0.529	1.76	strike slip
45	Imperial Valley-06	El Centro Array #6	6.53	203.22	0.449	0.00	strike slip
46	Hector Mine	San Bernardino - E & Hospitality	7.13	296.97	0.073	105.20	strike slip
47	Imperial Valley-06	El Centro Array #7	6.53	210.51	0.469	0.56	strike slip
48	Imperial Valley-06	El Centro Array #8	6.53	206.08	0.610	3.86	strike slip
49	Hector Mine	Whittier Narrows Dam downstream	7.13	298.68	0.061	169.83	strike slip
50	Imperial Valley-06	El Centro Differential Array	6.53	202.26	0.481	5.09	strike slip
51	Imperial Valley-08	Westmorland Fire Sta	5.62	193.67	0.151	9.39	strike slip
52	Northern Calif-03	Ferndale City Hall	6.50	219.31	0.203	26.72	strike slip
53	El Alamo	El Centro Array #9	6.80	213.44	0.052	121.00	strike slip
54	Chi-Chi_ Taiwan-03	CHY025	6.20	277.5	0.128	27.88	Reverse
55	Chi-Chi_ Taiwan-03	CHY036	6.20	233.14	0.104	35.78	Reverse
56	Chi-Chi_ Taiwan-03	CHY047	6.20	169.52	0.054	45.69	Reverse
57	Chi-Chi_ Taiwan-03	CHY054	6.20	172.1	0.060	70.11	Reverse
58	Chi-Chi_ Taiwan-03	CHY055	6.20	225.77	0.056	75.92	Reverse

59	Chi-Chi_ Taiwan-03	CHY082	6.20	193.69	0.051	50.08	Reverse
60	Chi-Chi_ Taiwan-03	CHY090	6.20	180.33	0.077	80.06	Reverse
61	Chi-Chi_ Taiwan-03	CHY101	6.20	258.89	0.146	24.40	Reverse
62	Chi-Chi_ Taiwan-03	CHY104	6.20	223.24	0.107	34.40	Reverse
63	Northern Calif-04	Ferndale City Hall	5.70	219.31	0.078	56.94	strike slip
64	Victoria_ Mexico	Chihuahua	6.33	242.05	0.151	18.53	strike slip
65	Victoria_ Mexico	SAHOP Casa Flores	6.33	259.59	0.101	39.10	strike slip
66	Hollister-01	Hollister City Hall	5.60	198.77	0.115	19.55	strike slip
67	Hollister-02	Hollister City Hall	5.50	198.77	0.070	17.20	strike slip
68	Taiwan SMART1(5)	SMART1 I12	5.90	275.82	0.139	25.70	Reverse
69	Taiwan SMART1(5)	SMART1 M01	5.90	268.37	0.177	26.31	Reverse
70	Parkfield	Cholame - Shandon Array #5	6.19	289.56	0.444	9.58	strike slip
71	Taiwan SMART1(5)	SMART1 O01	5.90	267.67	0.115	27.30	Reverse
72	Westmorland	Brawley Airport	5.90	208.71	0.165	15.28	strike slip
73	Westmorland	Niland Fire Station	5.90	212	0.176	15.16	strike slip
74	Westmorland	Salton Sea Wildlife Refuge	5.90	191.14	0.195	7.57	strike slip
75	Westmorland	Westmorland Fire Sta	5.90	193.67	0.499	6.18	strike slip
76	Parkfield	Cholame - Shandon Array #8	6.19	256.82	0.272	12.90	strike slip
77	Coalinga-01	Cantua Creek School	6.36	274.73	0.288	23.78	Reverse
78	Coalinga-01	Parkfield - Cholame 5W	6.36	236.59	0.139	47.88	Reverse
79	Coalinga-01	Parkfield - Cholame 6W	6.36	251.57	0.133	49.40	Reverse
80	Coalinga-01	Parkfield - Fault Zone 1	6.36	178.27	0.143	41.04	Reverse
81	Coalinga-01	Parkfield - Fault Zone 14	6.36	246.07	0.274	28.11	Reverse
82	Coalinga-01	Parkfield - Fault Zone 2	6.36	294.26	0.135	37.92	Reverse
83	Coalinga-01	Parkfield - Fault Zone 3	6.36	211.74	0.164	36.14	Reverse
84	Coalinga-01	Parkfield - Fault Zone 4	6.36	220.75	0.121	33.42	Reverse
85	Coalinga-01	Parkfield - Fault Zone 7	6.36	297.46	0.123	29.91	Reverse
86	Northern Calif-05	Ferndale City Hall	5.60	219.31	0.253	27.36	strike slip
87	Taiwan SMART1(45)	SMART1 I12	7.30	275.82	0.132	56.20	Reverse

88	Coalinga-01	Pleasant Valley P.P. - bldg	6.36	257.38	0.300	7.69	Reverse
89	Taiwan SMART1(45)	SMART1 M12	7.30	275.82	0.176	57.00	Reverse
90	Taiwan SMART1(45)	SMART1 O03	7.30	278.32	0.145	56.16	Reverse
91	Taiwan SMART1(45)	SMART1 O11	7.30	295.17	0.134	57.64	Reverse
92	Coalinga-01	Pleasant Valley P.P. - yard	6.36	257.38	0.602	7.69	Reverse
93	Borrego Mtn	El Centro Array #9	6.63	213.44	0.133	45.12	strike slip
94	Landers	Indio - Jackson Road	7.28	292.12	0.307	48.84	strike slip
95	Coalinga-05	Coalinga-14th & Elm (Old CHP)	5.77	286.41	0.519	7.02	Reverse
96	Coalinga-05	Pleasant Valley P.P. - FF	5.77	257.38	0.406	13.16	Reverse
97	Coalinga-05	Pleasant Valley P.P. - yard	5.77	257.38	0.575	13.16	Reverse
98	Borah Peak_ ID-01	CPP-610	6.88	279.97	0.085	83.00	Normal
99	Borah Peak_ ID-01	TAN-719	6.88	279.97	0.052	84.80	Normal
100	Morgan Hill	Capitola	6.19	288.62	0.142	39.08	strike slip
101	Morgan Hill	Foster City - APEEL 1	6.19	116.35	0.065	53.89	strike slip
102	Morgan Hill	Gilroy Array #2	6.19	270.84	0.213	13.68	strike slip
103	Morgan Hill	Gilroy Array #4	6.19	221.78	0.349	11.53	strike slip
104	Morgan Hill	Halls Valley	6.19	281.61	0.312	3.45	strike slip
105	Morgan Hill	Hollister City Hall	6.19	198.77	0.071	30.76	strike slip
106	Morgan Hill	Hollister Differential Array #3	6.19	215.54	0.079	26.42	strike slip
107	Morgan Hill	Los Banos	6.19	262.05	0.062	63.16	strike slip
108	Lazio-Abruzzo_ Italy	Garigliano-Centrale Nucleare	5.80	266.41	0.062	49.33	Normal
109	Taiwan SMART1(33)	SMART1 I01	5.80	275.82	0.144	41.54	Normal
110	Taiwan SMART1(33)	SMART1 O01	5.80	267.67	0.062	41.79	Normal
111	Mt. Lewis	Halls Valley	5.60	281.61	0.149	12.37	strike slip
112	Taiwan SMART1(40)	SMART1 I01	6.32	275.82	0.185	58.88	Reverse
113	Taiwan SMART1(40)	SMART1 M01	6.32	268.37	0.174	59.64	Reverse
114	Taiwan SMART1(40)	SMART1 O01	6.32	267.67	0.163	60.77	Reverse
115	N. Palm Springs	Colton Interchange - Vault	6.06	274.98	0.061	52.26	Reverse Oblique
116	N. Palm Springs	Winchester Page Bros R	6.06	287.87	0.112	38.01	Reverse Oblique
117	San Fernando	Carbon Canyon Dam	6.61	235	0.071	61.79	Reverse
118	Taiwan SMART1(45)	SMART1 I01	7.30	275.82	0.140	56.18	Reverse
119	Taiwan SMART1(45)	SMART1 M01	7.30	268.37	0.142	56.87	Reverse

120	Taiwan SMART1(45)	SMART1 O01	7.30	267.67	0.175	57.90	Reverse
121	Taiwan SMART1(45)	SMART1 O02	7.30	285.09	0.242	57.13	Reverse
122	Taiwan SMART1(45)	SMART1 O04	7.30	288.24	0.164	55.18	Reverse
123	Taiwan SMART1(45)	SMART1 O06	7.30	293.46	0.190	53.99	Reverse
124	El Mayor-Cucapah_ Mexico	Chihuahua	7.20	242.05	0.248	18.21	strike slip
125	Whittier Narrows-01	Bell Gardens - Jaboneria	5.99	267.13	0.229	10.31	Reverse Oblique
126	Northwest Calif-01	Ferndale City Hall	5.50	219.31	0.150	52.73	strike slip
127	Whittier Narrows-01	Carbon Canyon Dam	5.99	235	0.209	22.57	Reverse Oblique
128	Whittier Narrows-01	Compton - Castlegate St	5.99	266.9	0.322	18.32	Reverse Oblique
129	Whittier Narrows-01	Downey - Birchdale	5.99	245.06	0.348	14.90	Reverse Oblique
130	Whittier Narrows-01	Downey - Co Maint Bldg	5.99	271.9	0.205	14.95	Reverse Oblique
131	Whittier Narrows-01	El Monte - Fairview Av	5.99	290.63	0.245	0.75	Reverse Oblique
132	Whittier Narrows-01	LA - S Grand Ave	5.99	285.28	0.192	14.46	Reverse Oblique
133	Whittier Narrows-01	Lakewood - Del Amo Blvd	5.99	267.35	0.295	22.40	Reverse Oblique
134	Whittier Narrows-01	Norwalk - Imp Hwy_ S Grnd	5.99	279.46	0.247	14.37	Reverse Oblique
135	Imperial Valley-02	El Centro Array #9	6.95	213.44	0.281	6.09	strike slip
136	Whittier Narrows-01	Tarzana - Cedar Hill	5.99	257.21	0.599	38.24	Reverse Oblique
137	Whittier Narrows-01	Whittier Narrows Dam upstream	5.99	298.68	0.317	2.60	Reverse Oblique
138	Superstition Hills-01	Imperial Valley Wildlife Liquefaction Array	6.22	179	0.133	17.59	strike slip
139	Superstition Hills-02	Brawley Airport	6.54	208.71	0.144	17.03	strike slip
140	Superstition Hills-02	Calipatria Fire Station	6.54	205.78	0.259	27.00	strike slip
141	Superstition Hills-02	El Centro Imp. Co. Cent	6.54	192.05	0.357	18.20	strike slip
142	Superstition Hills-02	Kornbloom Road (temp)	6.54	266.01	0.139	18.48	strike slip
143	Superstition Hills-02	Salton Sea Wildlife Refuge	6.54	191.14	0.140	25.88	strike slip

144	Superstition Hills-02	Westmorland Fire Sta	6.54	193.67	0.211	13.03	strike slip
145	Superstition Hills-02	Imperial Valley Wildlife Liquefaction Array	6.54	179	0.208	23.85	strike slip
146	Loma Prieta	APEEL 2 - Redwood City	6.93	133.11	0.274	43.06	Reverse Oblique
147	Loma Prieta	Alameda Naval Air Stn Hanger	6.93	190	0.268	70.90	Reverse Oblique
148	Loma Prieta	Capitola	6.93	288.62	0.511	8.65	Reverse Oblique
149	Loma Prieta	Foster City - APEEL 1	6.93	116.35	0.284	43.77	Reverse Oblique
150	Loma Prieta	Gilroy Array #2	6.93	270.84	0.370	10.38	Reverse Oblique
151	Loma Prieta	Gilroy Array #4	6.93	221.78	0.419	13.81	Reverse Oblique
152	Loma Prieta	Hollister - South & Pine	6.93	282.14	0.370	27.67	Reverse Oblique
153	Loma Prieta	Hollister City Hall	6.93	198.77	0.246	27.33	Reverse Oblique
154	Loma Prieta	Hollister Differential Array	6.93	215.54	0.279	24.52	Reverse Oblique
155	Loma Prieta	Oakland - Outer Harbor Wharf	6.93	248.62	0.290	74.16	Reverse Oblique
156	Loma Prieta	SF Intern. Airport	6.93	190.14	0.330	58.52	Reverse Oblique
157	Northwest Calif-02	Ferndale City Hall	6.60	219.31	0.063	91.15	strike slip
158	Landers	Anaheim - W Ball Rd	7.28	269.29	0.052	144.90	strike slip
159	Landers	Boron Fire Station	7.28	291.03	0.119	89.69	strike slip
160	Landers	Compton - Castlegate St	7.28	266.9	0.066	161.23	strike slip
161	Landers	Downey - Co Maint Bldg	7.28	271.9	0.052	157.46	strike slip
162	Landers	Fountain Valley - Euclid	7.28	270.54	0.071	146.89	strike slip
163	Landers	Huntington Bch - Waikiki	7.28	270.54	0.062	156.00	strike slip
164	Landers	LA - W 70th St	7.28	241.41	0.063	163.96	strike slip
165	Landers	Lakewood - Del Amo Blvd	7.28	267.35	0.060	157.41	strike slip
166	Landers	San Bernardino - E & Hospitality	7.28	296.97	0.087	79.76	strike slip

167	Landers	Tarzana - Cedar Hill	7.28	257.21	0.066	175.65	strike slip
168	Northern Calif-01	Ferndale City Hall	6.40	219.31	0.122	44.52	strike slip
169	Big Bear-01	Indio - Riverside Co Fair Grnds	6.46	282.14	0.065	77.33	strike slip
170	Big Bear-01	North Shore - Salton Sea Pk HQ	6.46	265.16	0.087	113.58	strike slip
171	Big Bear-01	San Bernardino - E & Hospitality	6.46	296.97	0.101	34.98	strike slip
172	San Fernando	Whittier Narrows Dam	6.61	298.68	0.108	39.45	Reverse
173	Northridge-01	Arleta - Nordhoff Fire Sta	6.69	297.71	0.345	3.30	Reverse
174	Northridge-01	Canoga Park - Topanga Can	6.69	267.49	0.392	0.00	Reverse
175	Managua_ Nicaragua-01	Managua_ ESSO	6.24	288.77	0.372	3.51	strike slip
176	Northridge-01	Downey - Co Maint Bldg	6.69	271.9	0.230	43.20	Reverse
177	Point Mugu	Port Hueneme	5.65	248.98	0.128	15.48	Reverse
178	Northridge-01	LA - Baldwin Hills	6.69	297.07	0.239	23.50	Reverse
179	Northridge-01	LA - Century City CC North	6.69	277.98	0.256	15.53	Reverse
180	Northridge-01	LA - N Faring Rd	6.69	255	0.280	12.42	Reverse
181	Borrego	El Centro Array #9	6.50	213.44	0.066	56.88	strike slip
182	Ceyhan, Adana, Türkiye	NA	6.20	263	0.276	42.00	strike slip
183	Cay-Sultandagi, Afyon, Türkiye	NA	6.50	226	0.113	46.00	Normal
184	Urla, İzmir, Türkiye	NA	5.70	270	0.079	35.00	strike slip
185	Simav, Kütahya, Türkiye	NA	5.70	265	0.062	111.00	Normal
186	Simav, Kütahya, Türkiye	NA	5.70	259	0.069	4.40	Normal

187	Van, Türkiye	NA	7.00	292	0.178	15.00	Reverse
188	Fethiye, Mugla, Türkiye	NA	6.00	248	0.230	26.00	strike slip
189	Gokceada Aciklari, Ege Denizi, Türkiye	NA	6.50	293	0.051	216.00	strike slip
190	Gokceada Aciklari, Ege Denizi, Türkiye	NA	6.50	192	0.140	64.00	strike slip
191	Gokceada Aciklari, Ege Denizi, Türkiye	NA	6.50	286	0.120	84.00	strike slip
192	Gokceada Aciklari, Ege Denizi, Türkiye	NA	6.50	225	0.086	126.00	strike slip
193	Midilli-Karaburun, İzmir, Türkiye	NA	6.20	193	0.053	44.00	Normal
194	Bodrum, Mugla, Türkiye	NA	6.50	219	0.087	33.00	Normal
195	Bozkurt, Denizli, Türkiye	NA	6.00	294	0.058	46.00	Normal
196	Silivri, İstanbul, Türkiye	NA	5.80	247	0.086	31.00	Reverse
197	Silivri, İstanbul, Türkiye	NA	5.80	224	0.072	20.00	Reverse
198	Manisa, Türkiye	NA	5.50	292	0.063	13.00	Normal
199	Manisa, Türkiye	NA	5.50	229	0.089	18.00	Normal
200	Ege Denizi, Türkiye	NA	6.60	252	0.071	57.00	Normal
201	Ege Denizi, Türkiye	NA	6.60	205	0.060	67.00	Normal
202	Ege Denizi, Türkiye	NA	6.60	193	0.056	126.00	Normal
203	Ege Denizi, Türkiye	NA	6.60	195	0.106	62.00	Normal
204	Ege Denizi, Türkiye	NA	6.60	131	0.150	60.00	Normal
205	Ege Denizi, Türkiye	NA	6.60	145	0.111	61.00	Normal
206	Ege Denizi, Türkiye	NA	6.60	249	0.074	60.00	Normal
207	Ege Denizi, Türkiye	NA	6.60	198	0.089	72.00	Normal
208	Golyaka, Duzce, Türkiye	NA	5.90	273	0.140	25.00	strike slip
209	Golyaka, Duzce, Türkiye	NA	5.90	229	0.141	45.00	strike slip
210	Golyaka, Duzce, Türkiye	NA	5.90	271	0.073	30.00	strike slip
211	Golyaka, Duzce, Türkiye	NA	5.90	282	0.306	2.50	strike slip
212	Golyaka, Duzce, Türkiye	NA	5.90	242	0.403	3.60	strike slip
213	Golyaka, Duzce, Türkiye	NA	5.90	183	0.357	3.50	strike slip
214	Kahramanmaras, Türkiye	NA	6.60	283	0.103	114.00	strike slip

215	Kahramanmaras, Türkiye	NA	6.60	271	0.154	70.00	strike slip
216	Kahramanmaras, Türkiye	NA	6.60	210	0.063	139.00	strike slip
217	Kahramanmaras, Türkiye	NA	6.60	246	0.093	77.00	strike slip
218	Kahramanmaras, Türkiye	NA	6.60	280	0.181	11.00	strike slip
219	Yayladagi, Hatay, Türkiye	NA	6.40	233	0.084	53.00	Normal
220	Yayladagi, Hatay, Türkiye	NA	6.40	271	0.088	62.00	Normal
221	Yayladagi, Hatay, Türkiye	NA	6.40	283	0.445	16.00	Normal
222	Yayladagi, Hatay, Türkiye	NA	6.40	210	0.180	4.50	Normal
223	Pazarcık, Kahramanmaras, Türkiye	Hatay, Samandağ	7.80	210	0.223	35.00	strike slip
224	Pazarcık, Kahramanmaras, Türkiye	Adana, Ceyhan	7.80	208	0.131	63.00	strike slip
225	Pazarcık, Kahramanmaras, Türkiye	Erzincan, Otlukbeli	7.80	284	0.112	227.00	strike slip
226	Pazarcık, Kahramanmaras, Türkiye	Hatay, Antakya	7.80	283	0.650	9.50	strike slip
227	Pazarcık, Kahramanmaras, Türkiye	Hatay, Kırıkhan	7.80	271	0.588	3.10	strike slip
228	Pazarcık, Kahramanmaras, Türkiye	Kahramanmaraş, Göksun	7.80	246	0.144	75.00	strike slip
229	Pazarcık, Kahramanmaras, Türkiye	Kahramanmaraş, Onikişubar	7.80	280	0.364	8.80	strike slip
230	Pazarcık, Kahramanmaras, Türkiye	Kahramanmaraş, Afşin	7.80	186	0.093	78.00	strike slip
231	Elbistan, Kahramanmaras, Türkiye	Adana, Ceyhan	7.70	208	0.071	128.00	strike slip

232	Elbistan, Kahramanmaras, Türkiye	Hatay, Kırıkhan	7.70	271	0.059	158.00	strike slip
233	Elbistan, Kahramanmaras, Türkiye	Kahramanmaraş, Göksun	7.70	246	0.648	4.00	strike slip
234	Elbistan, Kahramanmaras, Türkiye	Kahramanmaraş, Onikişubat	7.70	280	0.081	58.00	strike slip